
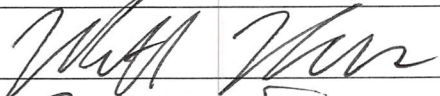
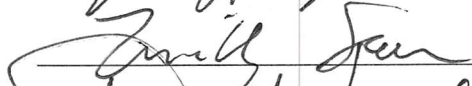

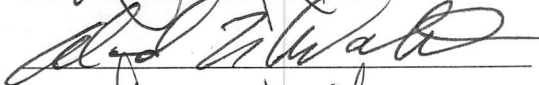
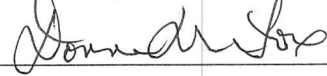
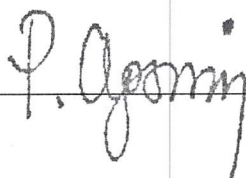


TOPOLOGICAL METHODS FOR EVOLUTION EQUATIONS

by

Thomas Stephens  
A Dissertation  
Submitted to the  
Graduate Faculty  
of  
George Mason University  
In Partial fulfillment of  
The Requirements for the Degree  
of  
Doctor of Philosophy  
Mathematics

Committee:

	Dr. Thomas Wanner, Dissertation Director
	Dr. Matthew Holzer, Committee Member
	Dr. Timothy Sauer, Committee Member
	Dr. David Nordstrom, Committee Member
	Dr. David Walnut, Department Chair
	Dr. Donna Fox, Associate Dean for Student Affairs, College of Science
	Dr. Peggy Agouris, Dean, College of Science

Date:

April 27, 2016

Spring Semester 2016  
George Mason University  
Fairfax, VA

# Table of Contents

	Page
List of Figures . . . . .	iv
Abstract . . . . .	v
Introduction . . . . .	1
2 Homotopy Equivalent Approximation of Superlevel Sets . . . . .	7
2.1 Sublevel and Superlevel Sets in Context . . . . .	7
2.1.1 Regular Values and the Topology of Superlevel Sets (briefly) . . . . .	12
2.2 Current State of the Art . . . . .	16
2.3 Rigorously Computing Homotopy Equivalent Approximations to Superlevel Sets . . . . .	17
2.3.1 Interval Arithmetic . . . . .	18
2.3.2 Automatic Differentiation . . . . .	20
2.3.3 Rectangular Cell Complexes: A Realization of Regular CW Complexes	23
2.3.4 Rigorous Validation Algorithm . . . . .	26
Algorithm . . . . .	29
2.4 Establishing the Homotopy Equivalence Between $N^{\geq \alpha}(\Omega, u)$ and <code>cmplx+</code> . .	34
2.4.1 The $\delta$ -collar on which Monotonicity is Guaranteed . . . . .	35
2.4.2 Rescaling Rectangular Cells $R^n$ to $[0, 1]^n$ , and Reordering the Stan- dard Basis . . . . .	36
2.4.3 The Collapsing Vector Field $\xi : \mathbb{R}^n \rightarrow \mathbb{R}^n$ . . . . .	36
2.4.4 Computer-assisted Proof that $N^{\geq \alpha}(\Omega, u)$ is Homotopy Equivalent to <code>cmplx+</code> . . . . .	39
2.5 Examples . . . . .	48
2.5.1 A Random Trigonometric Polynomial . . . . .	48
2.5.2 An Atoll-like Superlevel Set . . . . .	50
2.5.3 The Double-torus, a Three-dimensional Example . . . . .	52
3 Rigorous Isolating Blocks for Flows and their Conley Indices . . . . .	54
3.1 Flows and Bounded Invariant Sets . . . . .	54
3.1.1 Qualitative Perspective . . . . .	54



3.1.2	Remarks about the Quantitative Perspective . . . . .	59
3.2	Isolated Invariant Sets, Isolating Blocks, and the Conley Index . . . . .	60
3.3	Properties of, and Perspectives on, the Conley Index . . . . .	64
3.3.1	(Property) Isolating Blocks Exist . . . . .	65
3.3.2	(Perspective) Isolating Blocks as Ważwesi Sets . . . . .	65
3.3.3	(Property) Ważwesi: If the Index of $\mathcal{S}$ is Nontrivial, then so is $\mathcal{S}$ . . . . .	66
3.3.4	(Property) Summation Formula . . . . .	67
3.3.5	(Perspective) Usefulness of the Conley Index . . . . .	67
3.4	Current State of the Art . . . . .	70
3.5	Characterization of Isolating Blocks via Superlevel Sets . . . . .	71
3.5.1	A Worked Example . . . . .	79
3.5.2	Local Charts and Piecewise-smooth Boundaries . . . . .	87
3.6	Rigorous, Algorithmic Validation of Candidate Isolating Blocks . . . . .	88
3.7	Applications: Computer-assisted Proofs of Dynamical Behavior using the Conley Index . . . . .	93
3.7.1	A Simple Gradient System . . . . .	94
3.7.2	Asymptotic Behavior of Ground States . . . . .	111
3.7.3	A Planar Hopf Bifurcation . . . . .	120
	Concluding Remarks . . . . .	130
	Index . . . . .	133
	Bibliography . . . . .	136

## List of Figures

Figure	Page
1.1 Homotopy equivalent approximations to superlevel sets for real valued functions. . . . .	3
1.2 Geometric characterization of isolating blocks. . . . .	6
2.1 Approximations to superlevel sets of the function $u(x) = -(x_1^2 - 1)^2 - x_2^2 + 4$ on $\Omega \subset \mathbb{R}^2$ . . . . .	8
2.2 Superlevel sets in the context of materials science. . . . .	9
2.3 Simple contours drawn for $u(x_1, x_2) = -(x_1^2 - 1)^2 - x_2^2 + 4$ . . . . .	11
2.4 Result of Algorithm (V) applied to $u$ near a critical value. . . . .	15
2.5 Illustration of validation steps which lead to the validation of a single 2-cell in <code>cmplx</code> . . . . .	33
2.6 Illustration of vector field applied to monotone cells. . . . .	46
2.7 Illustration of strong deformation retraction constructed using information obtained from Algorithm (V). . . . .	47
2.8 Rectangular cell complex approximation to parabaloid. . . . .	48
2.9 Rectangular cell complex approximation to random trigonometric polynomial. . . . .	50
2.10 Rectangular cell complex approximation of atoll-like superlevel set. . . . .	51
2.11 Rectangular cell complex approximation to double torus. . . . .	53
3.1 Potential surface defining a vector field on the plane. . . . .	55
3.2 Phase portrait for Equation (3.2). . . . .	58
3.3 Phase portrait for $\dot{x} = (x_2, -x_1)$ . . . . .	61
3.4 Isolating block for a hyperbolic equilibrium and its Conley index. . . . .	64
3.5 Bifurcation diagram for Equation (3.9). . . . .	68
3.6 Selected trajectories of the system defined by Equation (3.18). . . . .	85
3.7 Parametric domain for an isolating block. . . . .	86
3.8 Cubical set representing the isolating block $\mathcal{B}$ , together with its exit set $\mathcal{B}^- \subset \partial\mathcal{B}$ . . . . .	87
3.9 Several trajectories of Equation (3.29). . . . .	96

3.10	The candidate block $\mathcal{A}_{01}$ is an isolating block. . . . .	98
3.11	Cubical representation of $\mathcal{A}_{01} \subset \mathbb{R}^3$ , along with its exit set $\mathcal{A}_{01}^- \subset \partial\mathcal{A}_{01}$ . . .	99
3.12	Several trajectories of Equation (3.29), along with the isolating block $\mathcal{A}_{012}$ surrounding $p_0$ , $p_1$ , and $p_2$ . Red trajectories are leaving their respective equilibria, and orange, green, and blue trajectories are traveling toward their respective equilibria. . . . .	100
3.13	Trajectories of Equation (3.29), along with the isolating blocks $\mathcal{A}_0$ , $\mathcal{A}_1$ , and $\mathcal{A}_2$ individually surrounding $p_0$ , $p_1$ , and $p_2$ , respectively. Red trajectories are leaving their respective equilibria, and orange, green, and blue trajectories are traveling toward their respective equilibria. . . . .	101
3.14	Trajectories of Equation (3.29), along with the isolating block $\mathcal{A}_{02}$ (left) around $p_0$ and $p_2$ , and $\mathcal{A}_{12}$ (right) around $p_1$ and $p_2$ . . . . .	104
3.15	The candidate block $\mathcal{A}_2$ is an isolating block. . . . .	106
3.16	The candidate block $\mathcal{A}_{012}$ is an isolating block. . . . .	107
3.17	The candidate block $\mathcal{A}_{02}$ is an isolating block. . . . .	108
3.18	The candidate block $\mathcal{A}_0$ is an isolating block. . . . .	109
3.19	The candidate block $\mathcal{A}_1$ is an isolating block. . . . .	110
3.20	The candidate block $\mathcal{A}_{12}$ is an isolating block. . . . .	111
3.21	Trajectories of Equation (3.31), along with the isolating blocks $\mathcal{B}_0$ and $\mathcal{B}_1$ . Red trajectories are leaving their respective equilibria in forward time, and green trajectories are traveling toward their respective equilibria. . . . .	113
3.22	The tubular neighborhood $\mathcal{B}_{01}$ . The boundary of this closed tube is parameterized as three smooth manifolds made up of the two spherical caps described by $\gamma_+$ and $\gamma_-$ above, and the parabolic section given by $\gamma_0$ . . . .	116
3.23	The top panel shows filled contour plots for the exit set and the tangency test function for a tubular neighborhood of the parabolic space curve (3.32) with $h = 1$ , $c = 0$ and thickness $\rho = 1/4$ . Since the boundary of the exit set intersects with the yellow region, there are internal tangencies — and this neighborhood is not an isolating block. The middle row shows a corrected tubular neighborhood, with $h = 1$ and $c = 0$ and thickness $\rho = 1/5$ . The bottom row illustrates a successful application of the validation algorithm (IB) applied to $\partial\mathcal{B}_{01}$ , defined piecewise over the domains $\Omega_- = [0, 2\pi] \times (-1.5, 0)$ , $\Omega_0 = [0, 2\pi] \times (0, 1)$ , and $\Omega_+ = [0, 2\pi] \times (1, 1.5)$ . . . . .	118

3.24	The candidate block $\mathcal{B}_0$ is an isolating block. . . . .	119
3.25	The candidate block $\mathcal{B}_1$ is an isolating block. . . . .	120
3.26	Trajectories of Equation (3.33) for $\lambda = -1/10$ (left), and $\lambda = 1/10$ (right). Red lines are moving away from the origin, and green lines are moving toward the origin. The small sphere $\mathcal{C}_1$ around the origin is a valid isolating block for (3.33) with $\lambda = -1/10$ . The same sphere is a valid isolating block for (3.33) with $\lambda = 1/10$ , however it must fail to be in isolating neighborhood at some value $\lambda \in (-1/10, 1/10)$ due to the different topological type of $\mathcal{C}_1^-$ for $\lambda = \pm 1/10$ . . . . .	122
3.27	Trajectories of Equation (3.33) for $\lambda = -1/10$ (left), and $\lambda = 1/10$ (right). Red lines are moving away from the origin, and green lines are moving toward the origin. The sphere $\mathcal{C}_2$ around the origin is larger than $\mathcal{C}_1$ in Figure 3.26, and $\mathcal{C}_2$ is a valid isolating block for (3.33) with $\lambda = -1/10$ . The same sphere is a valid isolating block for (3.33) with $\lambda = 1/10$ , and in fact, the topological type of the exit set $\mathcal{C}_2^-$ is the same for both parameter values. . . . .	123
3.28	The candidate block $\mathcal{C}_1$ is an isolating block. . . . .	126
3.29	The candidate block $\mathcal{C}_2$ is an isolating block. . . . .	127
3.30	The candidate block $\mathcal{C}_1$ is an isolating block. . . . .	128
3.31	The candidate block $\mathcal{C}_2$ is an isolating block. . . . .	129

# Abstract

## TOPOLOGICAL METHODS FOR EVOLUTION EQUATIONS

Thomas Stephens, PhD

George Mason University, 2016

Dissertation Director: Dr. Thomas Wanner

In this dissertation we develop a framework for rigorously computing the Conley index of isolated invariant sets for flows generated by finite-dimensional systems of ordinary differential equations  $\dot{x} = f(x)$ , where  $f : \mathbb{R}^n \rightarrow \mathbb{R}^n$ . Our main contribution in this area is the characterization of isolating blocks in terms of the level sets and superlevel sets of two real-valued functions,  $u, v : \mathbb{R}^n \rightarrow \mathbb{R}$ . The functions  $u$  and  $v$  incorporate geometric quantities computed on the boundary of proposed isolating blocks and relate them to local behavior of the vector field  $f$ . In order to obtain numerically rigorous results in this area, we have developed a new tool for computing superlevel sets of real-valued functions  $u : \mathbb{R}^n \rightarrow \mathbb{R}$  that guarantees our superlevel set approximations are homotopy equivalent to the actual superlevel sets we are interested in. This new tool is presented as the first logical half of this document, as it is a significant advance in its own right.

Our work makes use of basic differential geometry on piecewise smooth manifolds, exploits the interplay between flows and the topology of the underlying phase space (provided by the Ważewski theorem), and employs interval arithmetic and automatic differentiation. We provide full details for a collection of algorithms which enable the practitioner to easily apply our framework to a wide variety of problems in the theory of dynamical systems.

Several examples are provided showing the relative simplicity of our approach over earlier

efforts.

## Introduction

In this dissertation we provide computational tools to address questions that are usually only investigated in an abstract setting. Our algorithms use rigorous numerics to provide rapid and reliable results for a broad range of practical applications. In Chapter 2 we correctly determine topological features of  $\alpha$ -superlevel sets  $N^{\geq \alpha}(\Omega, u) := \{x \in \Omega : u(x) \geq \alpha\}$ , for differentiable functions  $u : \Omega \subset \mathbb{R}^n \rightarrow \mathbb{R}$ , and values  $\alpha \in \mathbb{R}$  which are regular for  $u$ . In Chapter 3 we piece together a start-to-finish workflow for computing the Conley index for isolated invariant sets for flows. A common strategy in both chapters is the use of indirect methods to achieve qualitative results. For example, rather than directly computing local metric information about superlevel sets, we use first derivative information to compute monotonicity behavior on entire regions  $R \subset \Omega$  and relate that to topological features of  $N^{\geq \alpha}(R, u)$ . We leverage this algorithm in Chapter 3 where we characterize isolating blocks  $\mathcal{B} \subset \mathbb{R}^n$  through level sets and superlevel sets of smooth functions  $u, v : \partial\mathcal{B} \rightarrow \mathbb{R}$ . Isolating blocks are compact sets in the phase space of a system of ordinary differential equations  $\dot{x} = f(x)$  which hold interesting behavior of the system strictly within their interior,  $\text{int } \mathcal{B}$ . As a result, we obtain computer-assisted proofs of dynamical behavior within  $\mathcal{B}$  using the Conley index, while never actually directly computing solutions of the system.

The work in Chapter 2 culminates in a stand-alone tool that provides a numerically rigorous approximation to sublevel and superlevel sets of differentiable functions  $u : \mathbb{R}^n \rightarrow \mathbb{R}$ , using a CW complex as the underlying data structure. We present the tool as Algorithm (V) in §2.3.4, and use much of Chapter 2 to develop strategies to avoid several limitations that are found in previous attempts at this task. In §2.2 we review recent work that is closely related to our current effort, and point out where we have extended previous work



or departed from what have been persistent limitations. In Chapter 2 we are able to: (1) Use interval range enclosures to obtain homotopically equivalent approximations to  $N^{\geq \alpha}(\Omega, u)$ , (2) Avoid nearly all grid alignment failures by employing a non-uniform subdivision strategy in the construction of the approximating CW complex (see §2.3.4), (3) Obtain the most general collapsibility conditions that we are aware of, resulting in fewer required subdivisions and ultimately a lower computational cost (see §2.4.3), and (4) Lower the burden on the user by using automatic differentiation for all derivatives required by the procedure at runtime (see §2.3.2), which means that while Algorithm (V) makes repeated use of  $\nabla u$ , the user only needs to provide a callable expression for  $u$  (see Equation (2.6) in §2.5.1 for an example where providing a callable expression for  $\nabla u$  could easily introduce a transcription error).

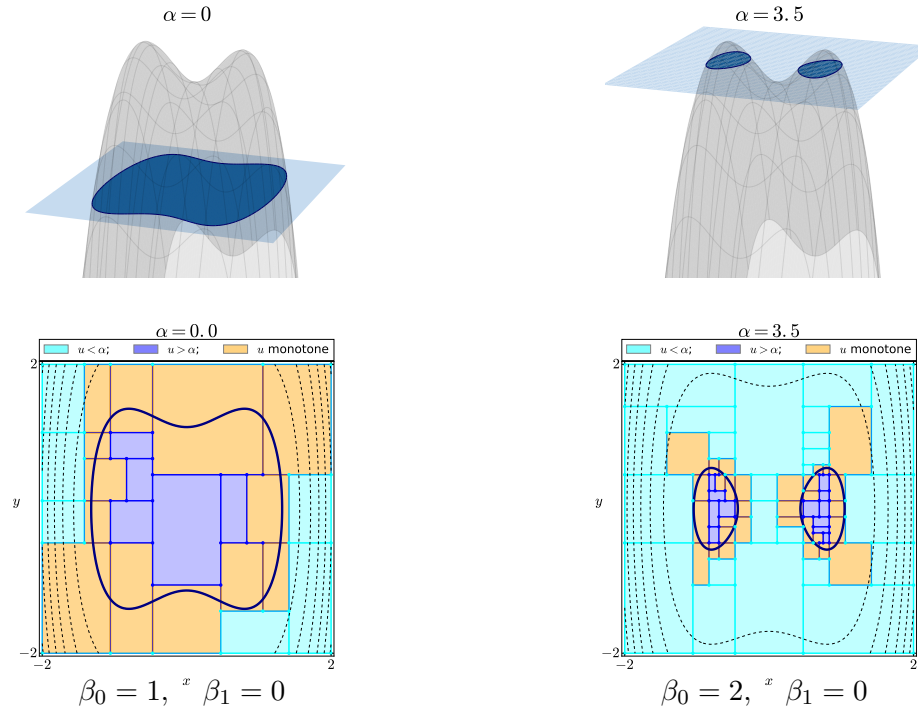


Figure 1.1: Homotopy equivalent approximations to superlevel sets for real valued functions. The top figures show the output from common level set approximation tools, such as `contourf()` found in MatLab or Python’s numerical libraries. The bottom figures show our homotopy equivalent approximations to these superlevel sets. We use rectangular, nonuniform subdivisions of the domain and homotopy invariants are easily computable from the resulting data structure.

The goal of constructing Algorithm (V) in Chapter 2 has been to accurately and conveniently compute the topological features of superlevel sets of real-valued functions  $u$  which arise in applications ranging from partial differential equation models for pattern formation in materials science, to computing persistent homology in data analysis. We show the output of the algorithm run on several benchmark examples in §2.5, along with corresponding Betti numbers computed directly from the resulting data structures as an example of the type of topological information that is immediately computable upon successful completion of the algorithm.

Chapter 3 assembles a convenient and numerically rigorous computational framework for

obtaining the Conley index of isolated invariant sets for flows on  $\mathbb{R}^n$ . The basics of Conley index theory were developed in an abstract setting over several years during the 1970's (see [13], [12]), and only recently have there been serious computational attempts at realizing its most practical object – the isolating block. An isolating block is a compact neighborhood  $\mathcal{B} \subset \mathbb{R}^n$  that satisfies conditions relating how the flow behaves on the boundary of the block. In particular, the set  $\mathcal{B}^- \subset \partial\mathcal{B}$  where the flow immediately exits  $\mathcal{B}$  in forward time, must be closed, and at points  $p \in \partial\mathcal{B}$  for which a section of some orbit is tangent to  $\mathcal{B}$ , that orbit section must be exterior to the block, except at  $p \in \partial\mathcal{B}$ . If a particular compact set  $\mathcal{B}$  can be shown to be an isolating block for a flow, then Conley index theory allows coarse statements to be made regarding bounded invariant sets for the flow which are contained strictly within the interior of the block. We use the homological definition of the Conley index in this work as it is relatively simple to compute and is often strong enough to deliver the results we seek. The (homological) Conley index is the relative homology group sequence  $H_*(\mathcal{B}, \mathcal{B}^-)$ . In all of our examples this can simply be thought of as a topological description of the quotient space  $\mathcal{B}/\mathcal{B}^-$ .

Isolating blocks have analogy with the admissible sets in the Brouwer degree in the sense that computations which are made on the boundary of the block (admissible set) may reveal coarse information about the maximal invariant set in the interior of the block (where in the Brouwer degree case, the boundary of the admissible set may carry information about the existence of zeros within the admissible set). The analogy to the Brouwer degree goes further in that the Conley index is stable with respect to perturbations of the maximal invariant set inside, and for any particular isolated invariant set there exist many compact sets  $\mathcal{B}$  which satisfy the conditions of being an isolating block. These last two features open the door for rigorous computational approaches to resolving isolating blocks.

The major conceptual contribution of Chapter 3 is the characterization of isolating blocks through the level and superlevel sets of smooth functions  $u, v : \partial\mathcal{B} \rightarrow \mathbb{R}$ . The first step of our strategy is a step away from the existing literature – in which we parameterize the boundary of a compact set  $\partial\mathcal{B}$  using a smooth (perhaps piecewise) function  $r : \Omega \subset$

$\mathbb{R}^{n-1} \rightarrow \partial\mathcal{B} \subset \mathbb{R}^n$  (for example, using  $r : [0, 2\pi] \times (0, \pi) \rightarrow \partial\mathcal{B}$  defined by  $r(\varphi, \theta) = (\cos \varphi \sin \theta, \sin \varphi \sin \theta, \cos \theta)$ , to parameterize the boundary of a ball in  $\mathbb{R}^3$ ). The functions  $u$  and  $v$  capture geometric information about how the flow generated by a vector field  $f : \mathbb{R}^n \rightarrow \mathbb{R}^n$  behaves on  $\partial\mathcal{B}$ . The geometric picture is this: The zero-set of  $u$  identifies points  $p \in \partial\mathcal{B}$  where  $f(p)$  is tangent to  $\partial\mathcal{B}$  ( $u$  is simply the scalar product of the vector field with an outward normal vector of  $\mathcal{B}$ ). The function  $v$  is a local comparison between a section of the orbit through  $p$  and a curve  $\gamma \subset \partial\mathcal{B}$  through  $p$ , where  $\gamma'(p) = f(p)$  (the function  $v$  involves the evaluation of the second fundamental form on  $T_p\mathcal{B}$  along the direction determined by  $f(p)$ , so the curve  $\gamma$  is more of an interpretation of the information provided by the second fundamental form rather than an explicit feature at this step). We construct the function  $v$  as a smooth, real valued indicator on all of  $\partial\mathcal{B}$ , taking positive values where orbits curve away from the manifold in both directions, and negative values where orbits curve into the manifold in both directions. Figure 1.2 is an illustration of the geometric setup provided by  $u$  and  $v$ . The characterization of isolating blocks, Theorem 3.5.4 in §3.5, can now be stated as follows: For a vector field  $f : \mathbb{R}^n \rightarrow \mathbb{R}^n$  which generates a global flow  $\varphi : \mathbb{R} \times \mathbb{R}^n \rightarrow \mathbb{R}^n$ , and a compact set  $\mathcal{B} \subset \mathbb{R}^n$  whose boundary is a smooth codimension one manifold parameterized by  $r : \Omega \subset \mathbb{R}^{n-1} \rightarrow \partial\mathcal{B}$ , we have that  $\mathcal{B}$  is an isolating block for  $\varphi$  provided that zero is a regular value for  $u$ , and the zero-set of  $u$  is a subset of the strictly positive superlevel set of  $v$ .

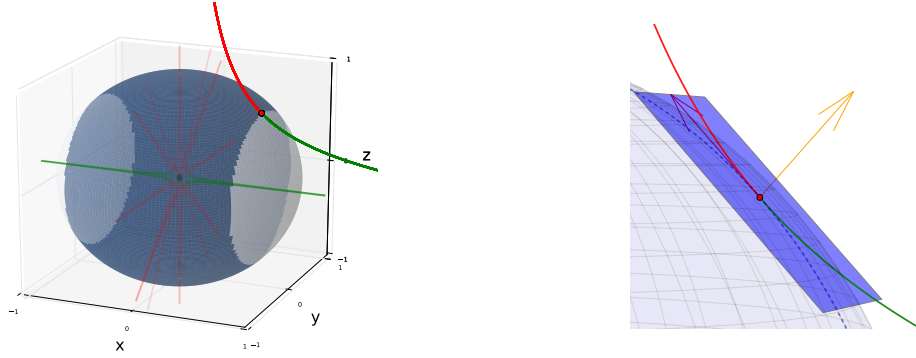


Figure 1.2: The left panel shows the evaluation of the exit set function  $u : \partial\mathcal{B} \rightarrow \mathbb{R}$ . Dark blue indicates positive values of  $u$ , revealing where the vector field points outward from  $\mathcal{B}$ , and light gray indicates the regions of  $\partial\mathcal{B}$  where the vector field points inward. The red point indicates a point  $p \in \partial\mathcal{B}$  where  $f(p)$  is tangent to  $\partial\mathcal{B}$  (so  $u(p) = 0$ ), and the space curve shows a section of the orbit through  $p$ . The right panel shows the comparison of the orbit section with the shape of the manifold along a curve  $\gamma \subset \partial\mathcal{B}$  through  $p$ , indicated by the dashed curve, where  $\gamma'(p) = f(p)$ . In this case we have  $v(p) > 0$  for the tangency test function  $v : \partial\mathcal{B} \rightarrow \mathbb{R}$ .

The major technical contribution of Chapter 3 is the bootstrapping of Algorithm (V) from Chapter 2 to rigorously establish user-defined compact sets as valid isolating blocks. We develop this new procedure as Algorithm (IB) in §3.6, and note that successful completion of (IB) guarantees that zero is a regular value for  $u$ , and guarantees that the set  $\mathcal{B}^-$  is, indeed, closed.

We propose several candidate isolating blocks for flows generated by ordinary differential equations in  $\mathbb{R}^3$  in §3.7, and provide the full output of the isolating block validation algorithm (IB), including in a case where the algorithm fails to validate a candidate block. A major benefit of having smooth indicator functions  $u$  and  $v$  defined on all of  $\partial\mathcal{B}$  is that even in cases where the algorithm fails, we are able to recover useful information about how it failed. The example in §3.7.2 shows how we can use the information obtained from  $u$  and  $v$  on an invalid block to construct a new candidate block which does pass the validation algorithm.

## Chapter 2: Homotopy Equivalent Approximation of Superlevel Sets

Let  $X$  be a topological space and  $u : X \rightarrow \mathbb{R}$  a real-valued function. For a subset  $\Omega \subset X$ , and  $\alpha \in \mathbb{R}$ , consider the partition of  $\Omega$  determined by the sets on which  $u$  is greater than  $\alpha$ , less than  $\alpha$ , and equal to  $\alpha$ . We make the following

**Definition 2.0.1.** *For the function  $u : \Omega \subset X \rightarrow \mathbb{R}$ , denote*

*the  $\alpha$ -superlevel set of  $u$  by  $N^{\geq \alpha}(\Omega, u) := \{x \in \Omega : u(x) \geq \alpha\}$ ,*

*the  $\alpha$ -sublevel set of  $u$  by  $N^{\leq \alpha}(\Omega, u) := \{x \in \Omega : u(x) \leq \alpha\}$ , and*

*the  $\alpha$ -level set of  $u$  by  $N^{\alpha}(\Omega, u) := \{x \in \Omega : u(x) = \alpha\}$ .*

### 2.1 Sublevel and Superlevel Sets in Context

Sublevel and superlevel sets are a convenient tool for encoding information. For example, consider the card game Hearts. This is a game of strategy where you, as a player, must manage your acquisition of so-called penalty cards as the game unfolds. At the start of the game you have two basic winning strategies to choose from: (1) trying to *avoid collecting* penalty cards, because each one hurts your score; or (2) trying to *collect all* of the penalty cards, called shooting the moon, which is considered a feat and is rewarded by passing the penalties onto your opponents. If you are forced to collect a penalty card (or two) during the first few hands, then you will find yourself in the position of being able to waver between the avoidance strategy and shooting the moon. Of course, whatever strategy you choose, at

some point during the game it becomes a mathematical impossibility to switch strategies and still expect to win – but, as a player, it is not clear at precisely which point in the game this tipping point occurs.

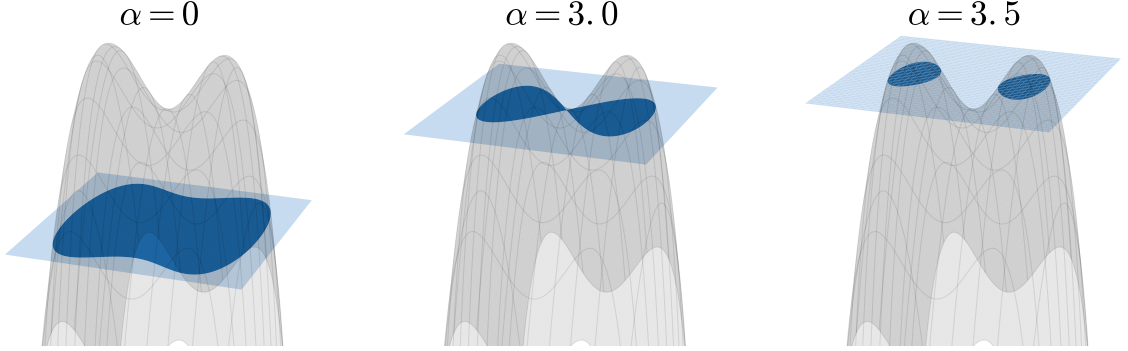


Figure 2.1: Approximations to superlevel sets of the function  $u(x) = -(x_1^2 - 1)^2 - x_2^2 + 4$  on  $\Omega \subset \mathbb{R}^2$ . The darkened regions depict  $N^{\geq \alpha}(\Omega, u)$ , and correspond to the winning strategy space in the Hearts example. Notice that  $\alpha = 3.0$  is a critical value for  $u$  in the sense of Definition 2.1.1. Figure 2.3 shows approximations to  $N^{\geq 0}(\Omega, u)$  and  $N^{\geq 3.5}(\Omega, u)$  which are homotopy equivalent to  $N^{\geq 0}(\Omega, u)$  and  $N^{\geq 3.5}(\Omega, u)$ , respectively.

Consider the space  $\Omega \subset \mathbb{R}^2$  of all strategies, or possible ways to play a game of Hearts, including ways to lose. Next, consider a model  $u$  that assigns a value to these strategies given by the continuous and differentiable function  $u : \Omega \rightarrow \mathbb{R}$ , given by  $u(x) = -(x_1^2 - 1)^2 - x_2^2 + 4$ . Let  $\alpha \in [0, 4]$  track the stage of the game such that  $\alpha = 0$  corresponds to the start of the game and  $\alpha = 4$  marks the end of the game. Finally, let  $\{x \in \Omega : u(x) \geq \alpha\}$  denote the set of winning strategies, and  $\{x \in \Omega : u(x) < \alpha\}$  the set of losing strategies at the point in the game corresponding to  $\alpha$ .

Denote the best avoidance game play by the point  $(-1, 0) \in \Omega$ , and correctly shooting the moon by  $(1, 0) \in \Omega$  (see Figure 2.1). Then at the beginning of the game  $N^{\geq 0}(\Omega, u)$  is a connected set - you, as a player, could conceivably start with a plan to shoot the moon, and then change your mind for a small increase in  $\alpha$ , the whole time maintaining a winning

strategy. As game play unfolds, switching strategies must be done with increasing care, and eventually  $N^{\geq \alpha}(\Omega, u)$  splits into two regions, locking you into your current position (perhaps one of your opponents has collected a penalty card, making it impossible for you to shoot the moon).

Many tools are available to give a qualitative and approximate *geometric* picture of sublevel and superlevel sets. In the Hearts example one could imagine plotting contours of  $u$  for more values of the parameter  $\alpha$  than are shown in Figure 2.1, which would begin to yield a dynamic picture of how the family of superlevel sets  $N^{\geq \alpha}(\Omega, u)$ , i.e. the sequence of winning strategy spaces, becomes narrowed, and then disjoint as  $\alpha$  ranges through  $[0, 4] \subset \mathbb{R}$ . This is useful, and it opens many lines of investigation into the game of Hearts, but at some point, you, as the player, are going to want a definitive answer to the question, “Is it possible to switch strategies right now and still have a shot to win?”

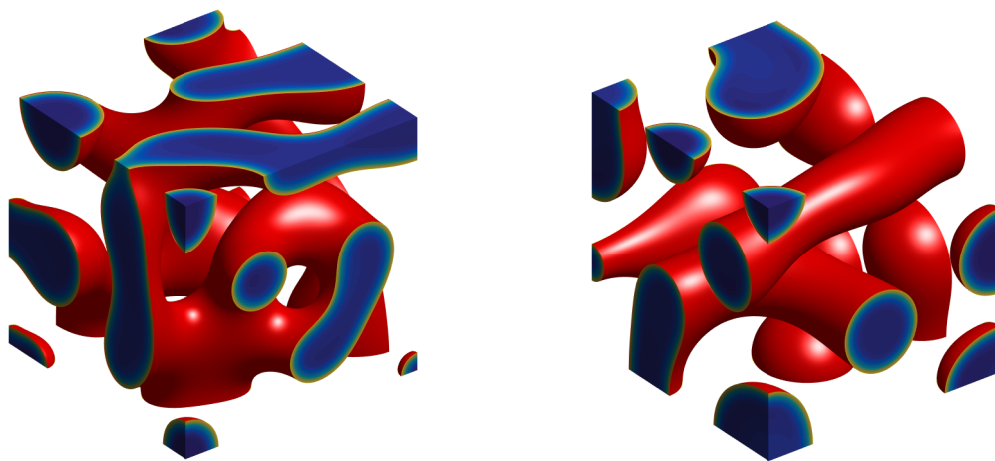


Figure 2.2: Two snapshots of the phase-field variable  $u$  on the cube  $[0, 1]^3$ , where  $u(t, x)$  describes the distribution of one of the two monomers in a diblock copolymer. Letting monomer A be represented by blue, and monomer B be represented by red, we see that the regions of monomer A can form complicated patterns, and likewise for monomer B (monomer B, partially shown using red in these figures, fills the voids formed by the complement of the blue ‘tubes’ in this image). The difference between the left and right panels is in the relative concentrations of A and B in the copolymer itself.



This is a question about the topology of  $N^{\geq \alpha}(\Omega, u)$ . In this case we are talking about the *path-connectedness* of  $N^{\geq \alpha}(\Omega, u)$ . This model of Hearts is not a very realistic example, consider the patterns that are formed during microstructure evolution as described in [38], and illustrated in Figure 2.2. In this case, a smooth function  $u : [0, 1]^3 \subset \mathbb{R}^3 \rightarrow \mathbb{R}$  is used as a phase-field variable to represent the distribution of two joined monomers, A and B, which together form a diblock copolymer in the cube  $[0, 1]^3 \subset \mathbb{R}^3$ . A free energy functional is described, and subsequently minimized, in order to drive  $u(t, x)$  toward the values  $-1$  and  $+1$  so that the pointwise evaluation of  $u(t, x)$  can be interpreted as measuring the concentration of one of the monomers, say monomer A, at  $x \in [0, 1]^3$ . Then  $u(t, x) \simeq +1$  indicates that a neighborhood of  $x \in [0, 1]^n$  is currently occupied by only the monomer A, and  $u(t, x) \simeq -1$  indicates pure monomer B at this  $x \in [0, 1]^n$ . With this description of the distribution of monomers in physical space, we can measure features such as cavities, inclusions, connected components formed by one of the monomers by considering the sets  $N^{\geq \alpha}([0, 1]^3, u)$  for  $\alpha \in [-1, 1]$ . The Betti numbers of  $N^{\geq \alpha}([0, 1]^3, u)$  are the computable topological invariants of interest in this case. We point out that the phase-field variable  $u$  is the solution to a nonlinear partial differential equation, so sets of the form  $N^{\geq \alpha}([0, 1]^3, u)$  can only be approximated from discrete solution data. See [38], and the references therein, for a thorough explanation of how computational algebraic topology is being used in modern materials science.

Typical tools that generate these geometric features (contour lines or isosurfaces) are not designed to deliver easily quantifiable topological information, and are not adequate to answer these questions rigorously for several reasons. First, these tools are generally designed to optimize convenience of use over numerical rigor, and they do an exceptionally good job to quickly deliver qualitative information. Additionally, the data structure to compute topological invariants is generally not available (where topological invariants refer to homotopy invariants, see §2.1.1). And finally, they are not generally useful above three dimensions due to obvious visualization challenges.

In this chapter we develop a new tool to rigorously obtain homotopy invariants of sets  $N^{\geq \alpha}(\Omega, u)$ . Our method accurately represents the set  $N^{\geq \alpha}(\Omega, u)$  using a data structure on which homotopy invariants are computable, and is implemented for general finite dimensional domains  $\Omega \subset \mathbb{R}^n$ . Over the next several sections we will detail the construction of a rectangular cell complex `cmplx` which approximates  $N^{\geq \alpha}(\Omega, u)$ , where  $\Omega \subset \mathbb{R}^n$  is a rectangular domain and  $u : \Omega \rightarrow \mathbb{R}$  is a  $C^1$  function having  $\alpha$  as a regular value. Theorem 2.4.4 guarantees that the positive cells in `cmplx` form an approximation to the  $\alpha$ -superlevel set  $N^{\geq \alpha}(\Omega, u)$  which is homotopy equivalent to  $N^{\geq \alpha}(\Omega, u)$ . Figure 2.3 shows an example of the cell complex `cmplx` computed for the Hearts domains with  $\alpha = 0$  and  $\alpha = 3.5$  (cf. Figure 2.1). More examples can be found in §2.5.

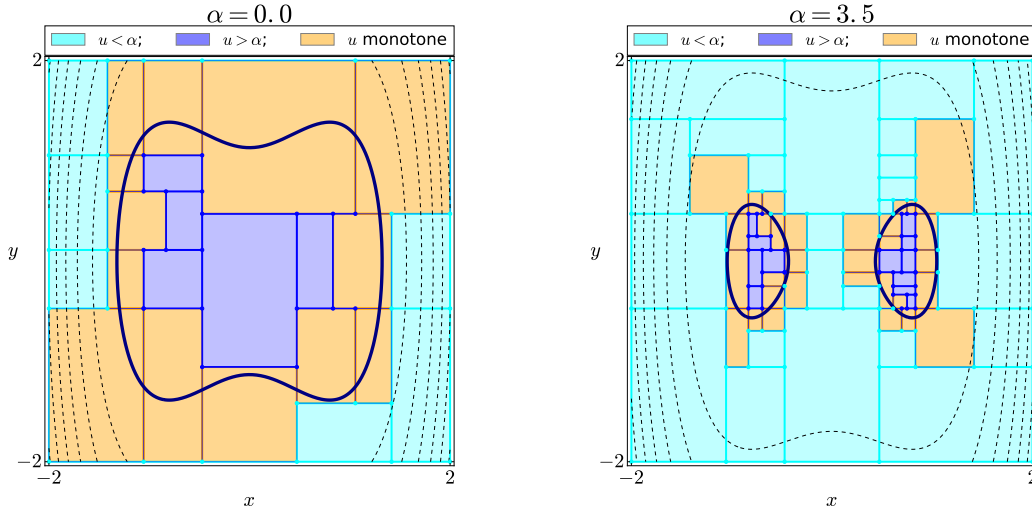


Figure 2.3: Approximations to  $N^{\geq 0}(\Omega, u)$  and  $N^{\geq 3.5}(\Omega, u)$  for  $u(x_1, x_2) = -(x_1^2 - 1)^2 - x_2^2 + 4$  which are homotopy equivalent to  $N^{\geq 0}(\Omega, u)$  and  $N^{\geq 3.5}(\Omega, u)$ , respectively. In each image the approximate contours of  $u$  have been overlayed onto the rectangular cell complex approximation, the heavy line is the  $\alpha$ -level set of  $u$ .

### 2.1.1 Regular Values and the Topology of Superlevel Sets (briefly)

Prior to developing a strategy to compute superlevel sets for  $C^1$  functions  $u : \mathbb{R}^n \rightarrow \mathbb{R}$ , it is essential to gain some understanding of these objects. Consider again the function  $u(x_1, x_2) = -(x_1^2 - 1)^2 - x_2^2 + 4$  that appeared in the above paragraphs to model strategies in the game Hearts. Figure 2.1 suggests that the path connectedness of  $N^{\geq \alpha}(\Omega, u)$  changes as  $\alpha$  moves from  $\alpha < 3$  to  $\alpha > 3$ , and that the point  $(0, 0) \in \Omega$  is somehow involved in this topological change. These facts are encoded in the derivative information of  $u$ . In particular, we find that the partial derivatives  $\frac{\partial u}{\partial x_1}(x) = -2x_1(x_1^2 - 1)$ , and  $\frac{\partial u}{\partial x_2}(x) = -2x_2$  of  $u$  are zero at  $x = (0, 0) \in \Omega$  (and also at  $x = (-1, 0)$  and  $x = (1, 0)$ ). This motivates the following

**Definition 2.1.1 (Critical points, their indices, and critical values, [28]).** *For a differentiable function  $u : \mathbb{R}^n \rightarrow \mathbb{R}$ , a point  $p \in \mathbb{R}^n$  is a critical point for  $u$  if  $\frac{\partial u}{\partial x_i}(x) = 0$  for  $i = 1, \dots, n$ . The real number  $u(p)$  is a critical value for  $u$ .*

*The index of a critical point  $p$  for the  $C^2$  function  $u$  is the number of negative eigenvalues of the Hessian matrix of  $u$ , evaluated at  $p$ .*

We intend for Figure 2.1 to also suggest that the path connectedness of  $N^{\geq \alpha}(\Omega, u)$  remains constant as  $\alpha$  ranges through the values in, say,  $[0, 2]$ . Path connectedness of the superlevel sets is preserved under the deformation that carries  $N^{\geq 0}(\Omega, u)$  to  $N^{\geq 2}(\Omega, u)$  as  $\alpha$  ranges between 0 and 2. Noticing that no critical points of  $u$  are contained in the  $\alpha$ -level sets  $N^\alpha(\Omega, u)$  for  $\alpha \in [0, 2]$ , we make the following

**Definition 2.1.2 (Regular points and regular values, [26]).** *For a differentiable function  $u : \mathbb{R}^n \rightarrow \mathbb{R}$ , a point  $p \in \mathbb{R}^n$  is a regular point for  $u$  if  $p$  is not a critical point. A real number  $c$  is a regular value of  $u$  if every point of the level set  $u^{-1}(c)$  is a regular point of  $u$ . If  $u^{-1}(c) = \emptyset$ , then  $c$  is a regular value of  $u$ .*

A useful result that accompanies this definition is

**Theorem 2.1.3 (Sard's theorem, [34]).** *For a  $k$ -times continuously differentiable function  $u : \mathbb{R}^n \rightarrow \mathbb{R}$ , the set of critical values of  $u$  have zero measure in  $\mathbb{R}$ , provided that  $k \geq n$ . In particular, the set of regular values of  $u$  is dense in  $\mathbb{R}$ .*

This language can now be used to discuss the feasibility of approximating superlevel sets in an *accurate* and *meaningful* way. We use the terms accurate and numerically rigorous somewhat interchangeably to refer to our numerical approximations to sets of the form  $N^{\geq \alpha}(\Omega, u)$  for  $C^1$  functions  $u : \mathbb{R}^n \rightarrow \mathbb{R}$ . That is to say, our method guarantees that the approximation has the same path connectedness properties and has isomorphic homology and cohomology groups as the actual superlevel set. Intuitively we can think of our approximations as being equivalent to the actual superlevel set up to a large class of smooth deformations, the homotopies.

**Definition 2.1.4 (Homotopy and deformation retract, [20], [9]).** *Let  $X$  and  $Y$  be topological spaces. A homotopy is a family of continuous maps  $h_t : X \rightarrow Y$ ,  $t \in [0, 1]$ , such that the associated map  $h : [0, 1] \times X \rightarrow Y$  given by  $h(t, x) = h_t(x)$  is continuous.*

*A subspace  $A \subset X$  is called a deformation retract of  $X$  if there is a homotopy  $r : [0, 1] \times X \rightarrow X$  such that  $r(0, x) = x$ ,  $r(1, x) \in A$ , and if  $r(1, a) = a$  for all  $a \in A$ . The homotopy  $r$  is called a deformation retraction. If  $r(t, a) = a$  for all  $t \in [0, 1]$  and  $a \in A$ , then  $r$  is a strong deformation retraction, and  $A$  is called a strong deformation retract of  $X$ .*

In Section 2.4 we explicitly construct a vector field on  $\mathbb{R}^n$  which will generate a strong deformation retraction from  $N^{\geq \alpha}(\Omega, u)$  onto a lower dimensional subset of  $\Omega$ . The usefulness of this map is that it preserves homotopy type.

**Definition 2.1.5 (Homotopy equivalence, [9]).** *Two maps  $f, g : X \rightarrow Y$  are homotopic if there exists a homotopy  $h : [0, 1] \times X \rightarrow Y$  such that  $h(0, x) = f(x)$  and  $h(1, x) = g(x)$  for all  $x \in X$ . If  $f$  is homotopic to  $g$ , we write  $f \sim g$ .*

*A map  $f : X \rightarrow Y$  is said to be a homotopy equivalence if there exists a map  $g : Y \rightarrow X$  such that  $g \circ f \sim \text{id}_X$  and  $f \circ g \sim \text{id}_Y$ . In this case the spaces  $X$  and  $Y$  are said to be*

homotopy equivalent *or to have the same* homotopy type, *which is denoted by*  $X \sim Y$ .

That covers the accuracy part, now we consider when homotopy equivalent approximations are meaningful. We hope to make it clear that seeking topological information about the  $\alpha$ -superlevel set when  $\alpha$  is a critical value is not meaningful in a practical sense. We saw that  $u(x_1, x_2) = -(x_1^2 - 1)^2 - x_2^2 + 4$  has  $\alpha = 3$  as a critical value (with critical point  $p = (0, 0)$  having index 1 in the sense of Definition 2.1.1), and that for arbitrary  $\varepsilon > 0$ , the topology of  $N^{\geq 3-\varepsilon}(\Omega, u)$  and the topology of  $N^{\geq 3+\varepsilon}(\Omega, u)$  are different. Thus we should expect that any numerical inaccuracy has the potential to alter the topology of the set  $N^{\geq 3}(\Omega, u)$ , regardless of the approximation technique. When  $u$  is a model of some physical phenomenon, or derived from a model of some phenomenon, or is in any way connected with reality, then we would like to have that our results are correct even for inaccuracies in  $u$  or in the level  $\alpha$ . We offer Figure 2.4 as an example of our method applied to  $N^{\geq \alpha}(\Omega, u)$  when  $\alpha$  is very near a critical value.

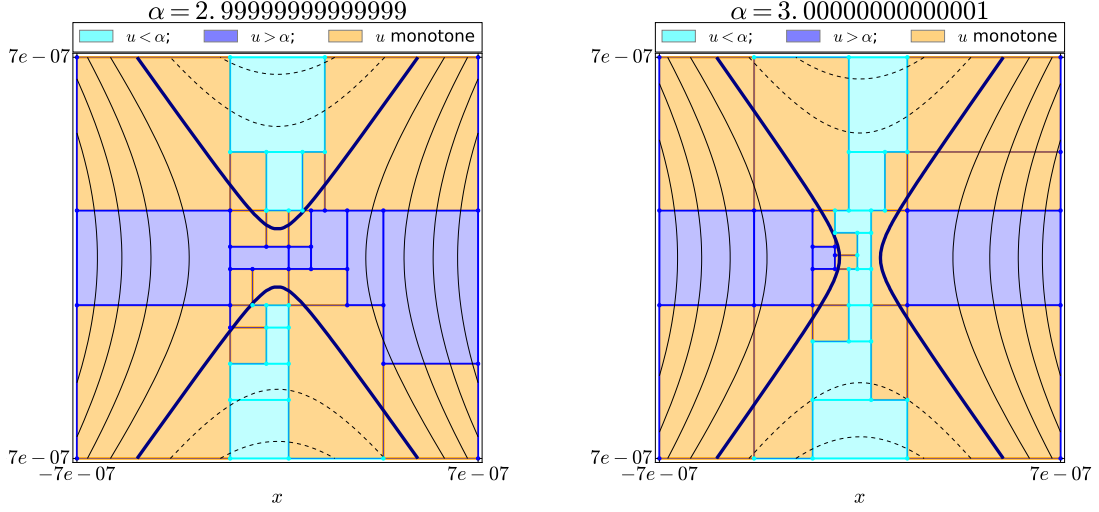


Figure 2.4: The number  $\alpha = 3.0$  is a critical value for the function  $u(x_1, x_2) = -(x_1^2 - 1)^2 - x_2^2 + 4$ , and corresponds to the index-one critical point  $p = (0, 0)$ . This figure shows a zoomed-in view of  $N^{\geq \alpha}(\Omega, u)$  near the origin for  $\alpha$  on two sides of 3.0. As expected, the topology of  $N^{\geq \alpha}(\Omega, u)$  changes as  $\alpha$  moves through the value 3.0, and our algorithm correctly captures that change (cf. Figure 2.1). Observe that the homotopy type of  $N^{\geq 3+\varepsilon}(\Omega, u)$  is a disconnected, two-point space, and that the homotopy type of  $N^{\geq 3-\varepsilon}(\Omega, u)$  is that of a one-point space. This is consistent with the Attachments theorem, Theorem 2.1.8.

We next state the Regular Level Set theorem which establishes the geometric intuition that when  $u : \mathbb{R}^n \rightarrow \mathbb{R}$  is a  $C^1$  function and  $\alpha$  is a regular value for  $u$ , then the  $\alpha$ -level sets of  $C^1$  functions  $u : \mathbb{R}^n \rightarrow \mathbb{R}$  are  $C^1$  submanifolds of dimension  $n - 1$ . This result is a consequence of the Implicit Function theorem, and guarantees that the  $\alpha$ -level sets are the boundaries of  $\alpha$ -superlevel sets, have measure zero as subsets of  $\mathbb{R}^n$ , and that these surfaces do not have self intersections, corners, cusps, or other ‘unstable’ configurations.

**Theorem 2.1.6 (Regular Level Sets, [26]).** *Every regular level set of a smooth map between smooth manifolds is a properly embedded submanifold whose codimension is equal to the dimension of the codomain.*

In the Hearts example we can see that, away from  $\alpha = 3$  (and away from  $\alpha = 4$ ), small changes in  $\alpha$  do not change the homotopy type of  $N^{\geq \alpha}(\Omega, u)$ . In fact, the Regular

Interval theorem, Theorem 2.1.7, guarantees this to be the case when  $\alpha$  is chosen from an interval that contains no critical values of  $u \in C^1$ . Furthermore, from Sard's theorem we see that critical values are easy to miss – this  $u$  has only two. A meaningful numerical approximation to a superlevel set  $N^{\geq \alpha}(\Omega, u) = \{x \in \Omega : u(x) \geq \alpha\}$  will require: (1) some flexibility in resolving<sup>1</sup> the membership condition  $u(x) \geq \alpha$  on  $x \in \Omega$ ; and (2) a reasonable expectation of finding enough regular values for  $u$ . Theorems 2.1.3 and 2.1.7 combine to justify our efforts.

**Theorem 2.1.7 (Regular Interval theorem, [28]).** *Let  $u : \Omega \rightarrow \mathbb{R}$  be a smooth real-valued function on a manifold  $\Omega$ . Let  $\alpha < \beta$  and suppose that the set  $u^{-1}[\alpha, \beta]$ , consisting of all  $p \in \Omega$  with  $\alpha \leq u(p) \leq \beta$ , is compact, and contains no critical points of  $u$ . Then  $N^{\geq \alpha}(\Omega, u)$  is diffeomorphic to  $N^{\geq \beta}(\Omega, u)$ . Furthermore,  $N^{\geq \alpha}(\Omega, u)$  is a deformation retract of  $N^{\geq \beta}(\Omega, u)$ , so that the inclusion map  $N^{\geq \alpha}(\Omega, u) \hookrightarrow N^{\geq \beta}(\Omega, u)$  is a homotopy equivalence.*

We close this section with a result from Morse theory that we will not use, but would be remiss to leave out of this discussion. Together with Theorem 2.1.7, it completely characterizes the relationship, up to homotopy equivalence, between the sets  $N^{\geq \alpha}(\Omega, u)$  and  $N^{\geq \beta}(\Omega, u)$  when we know about the gradient of  $u$  on the interval  $[a, b] \ni \alpha, \beta$ .

**Theorem 2.1.8 (Attachments, [28]).** *Let  $u : \Omega \rightarrow \mathbb{R}$  be a smooth function, and let  $p$  be a non-degenerate critical point with index  $\lambda$ . Setting  $u(p) = \alpha$ , suppose that  $u^{-1}[\alpha - \varepsilon, \alpha + \varepsilon]$  is compact, and contains no critical point of  $u$  other than  $p$ , for some  $\varepsilon > 0$ . Then, for all sufficiently small  $\varepsilon$ , the set  $N^{\geq \alpha - \varepsilon}(\Omega, u)$  has the homotopy type of  $N^{\geq \alpha + \varepsilon}(\Omega, u)$  with a  $\lambda$ -cell attached.*

## 2.2 Current State of the Art

The algorithm is the natural extension to work that has been ongoing, in which Wanner, Kalies, Day, Cochran, and Dłotko ([33], [11]) implemented a rigorous, adaptive refinement

---

<sup>1</sup>We resolve this condition using interval range enclosures on subsets of  $\Omega$ , details are given in §2.3.1.

procedure for approximating superlevel sets based on the concept of *deformation retract* in the setting of  $\mathbb{R}^2$ . This chapter can be seen as a capstone to that work in the sense that: (1) the current algorithm approximates superlevel sets in general finite dimensions; and (2) we explicitly formulate the deformation retract needed to rigorously establish homotopy equivalence as a recurrence relation with respect to the domain's dimension, which turns out to yield equivalent results when restricted to the plane (see Lemma 2.4.8 in §2.4).

The recent article [23] of Jaquette and Kramar also presents an extension to [33] and [11]. Jaquette and Kramar have the goal of rigorously computing persistent homology for sublevel sets (essentially superlevel sets of negative  $u$ ) of [differentiable] functions  $u : \mathbb{R}^n \rightarrow \mathbb{R}$ . We establish deformation retracts in a related way as they have, through an application of Ważewski's theorem. The main differences between their method and ours are that: (1) our deformation retract handles more general level set configurations, meaning that we are able to establish a deformation retract on a coarser subdivision of the domain  $\Omega \subset \text{Domain } u$ ; and (2) our subdivisions are more general in that the resulting partition of  $\Omega$  is non-uniform. This freedom allows for the possibility for strategic avoidance of grid alignment issues which will doom any algorithm we can imagine<sup>2</sup>. While Jaquette and Kramar have successfully computed persistent homology for complicated functions, their method frequently fails due to grid alignments. In Section 2.5 we present our method applied to their main example for comparison between the two approaches.

## 2.3 Rigorously Computing Homotopy Equivalent Approximations to Superlevel Sets

Let  $u : \Omega \subset \mathbb{R}^n \rightarrow \mathbb{R}$  be continuously differentiable on  $\mathbb{R}^n$  and have  $\alpha$  as a regular value.

We present an algorithm that constructs a numerically rigorous inner approximation to

---

<sup>2</sup>Grid alignments occur when the adaptive subdivision algorithm places a vertex on the  $\alpha$ -level set of the function  $u$ . The algorithm will later attempt to determine if  $u$  is either bounded above, or bounded below zero on that vertex, which will be impossible. The only way out of this situation is to discard the subdivision and try a different subdivision, which is only possible if subdivisions are nonuniform. See §2.3.4 for relevant details of our algorithm.



$N^{\geq\alpha}(\Omega, u)$  that is guaranteed to be homotopy equivalent to  $N^{\geq\alpha}(\Omega, u)$ . The algorithm acts on a data structure called `cmplx` which represents a regular CW complex, having  $N^{\geq\alpha}(\Omega, u)$  approximated by the positive cells in `cmplx`, called `cmplx+`. Working with this data structure makes the output ideal for rapid and direct computation of topological invariants of  $N^{\geq\alpha}(\Omega, u)$  (see [14] and [24] for resources on computational topology). In several examples we provide the Betti numbers computed on our approximation `cmplx+`, using the software package PHAT [6].

In the next section we make precise our working definition of rectangular CW complex, and briefly discuss automatic differentiation and interval arithmetic. Section 2.3.4 details the simple, computable collapsibility conditions and contains the validation algorithm, and Section 2.4 builds the theoretical framework required to obtain Theorem 2.4.4 establishing the homotopy equivalence between  $N^{\geq\alpha}(\Omega, u)$  and `cmplx+`.

### 2.3.1 Interval Arithmetic

We use the term **rigorous** to refer to numerical results obtained using **interval arithmetic**. This is a well-established extension of floating-point arithmetic in which *interval range enclosures* replace function evaluations at points, and *interval arithmetic operations* augment standard floating-point operations. In this framework, the fundamental data type is the *interval*. Denoting the set of floating point numbers by  $\mathcal{FP}$ , we have that the point  $a \in \mathbb{R}$  becomes the interval  $[\underline{a}, \bar{a}] \subset \mathcal{FP}$ , where  $\underline{a} \in \mathcal{FP}$  is the largest floating-point number less than  $a \in \mathbb{R}$ , and  $\bar{a} \in \mathcal{FP}$  is the smallest floating-point number greater than  $a \in \mathbb{R}$ . Usual subsets  $[a, b] \subset \mathbb{R}$  become  $[\underline{a}, \bar{b}] \subset \mathcal{FP}$ , and by denoting interval addition, subtraction,

multiplication, and division by  $\oplus$ ,  $\ominus$ ,  $\otimes$ ,  $\oslash$ , we have that

$$[\underline{a}, \bar{b}] \oplus [\underline{c}, \bar{d}] := [\underline{a} + \underline{c}, \overline{b + d}]$$

$$[\underline{a}, \bar{b}] \ominus [\underline{c}, \bar{d}] := [\underline{a} - \underline{d}, \overline{b - c}]$$

$$[\underline{a}, \bar{b}] \otimes [\underline{c}, \bar{d}] := [\min(\underline{a} \underline{c}, \underline{a} \underline{d}, \underline{b} \underline{c}, \underline{b} \underline{d}), \max(\underline{a} \underline{c}, \underline{a} \underline{d}, \underline{b} \underline{c}, \underline{b} \underline{d})]$$

$$[\underline{a}, \bar{b}] \oslash [\underline{c}, \bar{d}] := [\underline{a}, \bar{b}] \otimes [1/\bar{d}, 1/\underline{c}] \text{ if } 0 \notin [\underline{c}, \bar{d}]$$

The evaluation of a function  $u : \mathbb{R} \rightarrow \mathbb{R}$  at a point  $a \in \mathbb{R}$  translates to the evaluation of  $u$  on the interval  $[\underline{a}, \bar{a}]$ , and yields the **interval range enclosure**, denoted by the interval  $[\underline{u}([\underline{a}, \bar{a}]), \bar{u}([\underline{a}, \bar{a}])] \subset \mathcal{FP}$ , which is guaranteed to contain the actual function value  $u(a) \in \mathbb{R}$ . Interval arithmetic keeps track of rounding error and truncation error throughout all intermediate calculations in order to arrive at an interval which is guaranteed to contain the true result. The result is said to be *rigorous* in the sense that numerical errors are accounted for. Thus, we are able to evaluate functions on entire intervals, obtaining the *interval range enclosure* of the function values. As an example, evaluation<sup>3</sup> of  $\sin x$ , where  $x$  is the interval  $[0, \bar{2\pi}] \equiv [0, \overline{2\pi}]$ , results in the interval  $[\underline{\sin}([0, \bar{2\pi}]), \overline{\sin}([0, \bar{2\pi}])] \subset \mathcal{FP}$  which obeys the set inclusion  $[-1, 1] \subset [\underline{\sin}([0, \bar{2\pi}]), \overline{\sin}([0, \bar{2\pi}])]$ . The interval range enclosure of a function  $u : \mathbb{R}^n \rightarrow \mathbb{R}$  evaluated on the interval representation of some rectangle  $R \subset \mathbb{R}^n$  will henceforth be denoted by  $[u(R)]$  rather than by  $[\underline{u}(R), \bar{u}(R)]$ . The interval range enclosure of a vector is a vector of interval range enclosures. The range enclosure of  $u$  on a  $k$ -cell  $R$  is denoted by  $[u(R)]$ , and  $[\nabla u(R)] := \left\langle \left[ \frac{\partial u}{\partial x_1}(R) \right], \dots, \left[ \frac{\partial u}{\partial x_n}(R) \right] \right\rangle$ . Interval range enclosures are subadditive in the sense that for  $[\underline{a}, \bar{b}] \subset [\underline{c}, \bar{d}]$  we have that  $[u([\underline{a}, \bar{b}])] \subset [u([\underline{c}, \bar{d}])]$ .

In what follows we will use interval arithmetic in order to assemble computer-assisted proofs from the results of our algorithms. A good reference for this is Ratschek and Rokne

---

<sup>3</sup>We hasten to note that the interval range enclosure of a function evaluation on an interval may be poorly behaved in the sense that the range enclosure may be too large. However, the range enclosure is guaranteed to trap all possible function values on that interval.

*Geometric Computations with Interval and New Robust Methods* [31]. We have found the third-party toolbox INTLAB (The MATLAB/Octave toolbox for Reliable Computing [32]), and the third-party C++ library C-XSC <http://www2.math.uni-wuppertal.de/~xsc/> along with the accompanying publication [19], to be excellent for interval arithmetic operations.

### 2.3.2 Automatic Differentiation

Automatic differentiation takes as input a callable mathematical expression  $u$ , together with a point  $x \in \text{Domain } u$ , and yields a tuple  $(u(x), u'(x), u''(x), \dots)$  of values taken by  $u$  and its derivatives at the point  $x$ . The length of the tuple of derivative values is defined by the user or the limitations of the implementation. As a black-box procedure, automatic differentiation yields derivative values computed from exact derivative information rather than any finite difference approximation. The procedure is an efficient way to obtain the tuple  $(u(x), u'(x), u''(x), \dots)$ , and for  $u : \mathbb{R}^n \rightarrow \mathbb{R}$ , the point  $x = (x_1, x_2, \dots, x_n) \in \mathbb{R}^n$  can be replaced by  $[x] = ([x_1, \overline{x_1}], \dots, [x_n, \overline{x_n}])$ , a vector of intervals enclosing  $x \in \mathbb{R}^n$ , to yield a procedure that is consistent with the framework of rigorous numerics. While there exist several strategies for accomplishing this (see [19]), we describe an implementation that is based on the framework of *dual numbers* (and implemented in the C-XSC software package, found at <http://www2.math.uni-wuppertal.de/~xsc/>).

Automatic differentiation using dual numbers can be thought of as a marriage between symbolic differentiation and a new arithmetic (the arithmetic of dual numbers). The strategy is to recognize the expression for  $u$  as being made up from basic functions, and then to replace the terms in the expression for  $u$  by a tuple (a dual number) which will be a placeholder for function and derivative values. The assumption is that the derivative information for the basic functions which make up  $u$  is exactly knowable, and between the calculus rules for taking derivatives, and the laws of the arithmetic for dual numbers, we can algorithmically compute  $u$  and its derivative(s). At this point it is plausible that automatic differentiation can be exact – the next paragraphs may make clear how it is different from

symbolic differentiation.

Let  $h : \mathbb{R} \rightarrow \mathbb{R}$  be a real valued function which has a derivative at the point  $x \in \mathbb{R}$ . Label the function evaluations at  $x$  by  $a = h(x)$  and  $a' = h'(x)$ , and create the dual number  $A := (a, a')$ , so that  $(a, a') = (h(x), h'(x))$ , and  $a, a' \in \mathbb{R}$ . Then for  $A = (a, a')$  and another dual number  $B = (b, b')$ , we record the arithmetic for the dual numbers  $A$  and  $B$ :

$$A \oplus B = (a, a') \oplus (b, b') = (a + b, a' + b')$$

$$A \ominus B = (a, a') \ominus (b, b') = (a - b, a' - b')$$

$$A \otimes B = (a, a') \otimes (b, b') = (ab, a'b + ab')$$

$$A \oslash B = (a, a') \oslash (b, b') = (a/b, (a'b - ab')/b^2) \quad b \neq 0$$

When  $h(x) = x$ , the identity function, we write  $X = (x, 1)$  rather than  $A = (a, a')$ , and when  $h(x) = c$ , the constant function, we write  $C = (c, 0)$ . Again, the first coordinate of a dual number holds the function evaluation at  $x \in \mathbb{R}$ , and the second coordinate holds the evaluation of the derivative at  $x$ .

Consider the function  $u : \mathbb{R} \rightarrow \mathbb{R}$  given by  $u(x) = 7x + 3$ , and suppose we seek  $(u(x), u'(x))$  for  $x = 2$ . Straight away, basic calculus reveals  $(u(2), u'(2)) = (17, 7)$ . Using automatic differentiation, we write  $u(x) = h(x)g(x) + j(x)$ , where  $h(x) = 7$ ,  $g(x) = x$ , and  $j(x) = 3$ . Expressing  $u$  using dual numbers we have

$$u((x, 1)) = (7, 0) \otimes (x, 1) \oplus (3, 0).$$

Evaluating this expression at  $x = 2$ , we have

$$(7, 0) \otimes (2, 1) \oplus (3, 0) = (7 \cdot 2, 0 \cdot 2 + 7 \cdot 1) + (3, 0) = (14 + 3, 7 + 0) = (17, 7).$$

Dual numbers for the elementary functions must be pre-defined by any implementation

of automatic differentiation, for example,  $\sin((u, u')) = (\sin u, u' \cdot \cos u)$  must be accessible at runtime.

Consider the function  $u(x) = x \sin x / (3 - x)$ . In this example we will compute the pair  $(u(0), u'(0))$  using the same method as above. Notice below that the expression  $u'(x) = [(x \cos x + \sin x)(3 - x) - (x \sin x)(-1)] / (3 - x)^2$  is never explicitly evaluated at  $x = 0$ , and never actually appears at all.

$$\begin{aligned}
\left( \frac{x \sin x}{3 - x}, \frac{d}{dx} \frac{x \sin x}{3 - x} \right) \Big|_{x=0} &= \frac{(x, 1) \sin(x, 1)}{(3, 0) - (x, 1)} \Big|_{x=0} \\
&= \frac{(x, 1)(\sin x, \cos x)}{(3 - x, 0 - 1)} \Big|_{x=0} \\
&= \frac{(0, 1)(\sin 0, \cos 0)}{(3 - 0, 0 - 1)} \\
&= \frac{(0, 1)(0, 1)}{(3, -1)} \\
&= \frac{(0, 0)}{(3, -1)} \\
&= (0/3, (0 \cdot 3 - 0 \cdot -1)/9) \\
&= (0, 0)
\end{aligned}$$

The efficiency of this method over symbolic differentiation is in the replacement of the symbolic terms with numerical values (or intervals, as the case may be) as early as possible. The drawback is that we do not obtain a callable symbolic expression for the derivative function  $u'$ , which may be useful even if that symbolic expression is extremely cumbersome. It may look like an odd request to simultaneously seek the function value, along with the value of its derivative(s) at the same point. Generally exercises are phrased as, “Find  $u'(x)$ ”, meaning write down an expression for the function  $u' : \mathbb{R} \rightarrow \mathbb{R}$  that is the derivative of  $u$ .

From the perspective of an algorithm which behaves according to the point-wise evaluation of a function, the function and derivative values may be far more relevant than obtaining an expression which holds for all  $x$ , and then evaluating it at a handful of points. For higher-order derivatives of functions  $u : \mathbb{R} \rightarrow \mathbb{R}$ , dual numbers become longer tuples. Additionally, this framework extends to functions  $u : \mathbb{R}^n \rightarrow \mathbb{R}$ , see Chapter 12 of [19].

Algorithm (V) uses automatic differentiation to compute the gradients required in Definition 2.3.2, where the data type is an interval in the sense of §2.3.2. This means that the user only needs to specify the mathematical expression defining  $u$ , the domain  $\Omega$ , and the regular value  $\alpha$  in order to obtain the approximation to  $N^{\geq \alpha}(\Omega, u)$ . In Chapter 3, Theorem 3.5.4 requires evaluation of rather complicated functions involving higher order derivatives of smooth functions  $f : \mathbb{R}^n \rightarrow \mathbb{R}^m$  (see §3.5.1, for example, where the second fundamental form on a manifold  $\mathcal{B} \subset \mathbb{R}^n$  given by parametric equations in ). Automatic differentiation is employed here, too, requiring no derivative expressions to be entered by the user.

### 2.3.3 Rectangular Cell Complexes: A Realization of Regular CW Complexes

Working with a hierarchy of rectangular building blocks to represent a rectangular domain  $\Omega \subset \mathbb{R}^n$  is conceptually simple and computationally practical. Motivated by the desire to easily compute topological invariants of superlevel sets, we have required that our approximating data structure capture the features of a **CW complex**, a topological formalism invented specifically for this purpose. In practice we only require a very concrete realization of a CW complex, the finite, rectangular cell complex in  $\mathbb{R}^n$ , which can be described briefly as follows:

Let  $[a, b] \subset \mathbb{R}$  be a closed interval. If  $a = b$  then this interval is *degenerate* and in this

case we put  $[a, b] := \{a\}$ , if  $a < b$  then  $[a, b]$  is said to be *non degenerate*<sup>4</sup>. A rectangular  $k$ -cell  $R^k \subset \mathbb{R}^n$ , for  $k = 0, \dots, n$ , is the  $n$ -fold product of intervals in  $\mathbb{R}$  such that the product has dimension  $k$  as a subset of  $\mathbb{R}^n$ , that is  $R^k := [a_1, b_1] \times \dots \times [a_n, b_n] \subset \mathbb{R}^n$  where  $(n - k)$ -many intervals are degenerate. Usually zero-cells are called *vertices* and one-cells are called *edges*. Denoting subspaces of  $k$ -cells by  $\mathcal{R}_k$ , an  $n$ -dimensional **rectangular cell complex**  $\mathcal{C}$  on the topological space  $\Omega$  is an ascending collection of subspaces  $\mathcal{R}_0 \subset \dots \subset \mathcal{R}_n$  such that  $\Omega = \bigcup_{k=0}^n \mathcal{R}_k$ , along with the *characteristic maps* that specify how the subspaces are attached to one another<sup>5</sup>.

Given an  $n$ -dimensional cell complex  $\mathcal{C}$ , and a  $(k > 0)$ -cell  $R^k \in \mathcal{C}$ , we define the *boundary* of  $R^k$  to be the set of  $(k - 1)$ -cells  $\partial R^k = \overline{R^k} \cap \mathcal{R}_{k-1}$ , which is the intersection of the closure of the cell  $R^k$  with set of cells  $\mathcal{R}_{k-1} \subset \mathcal{C}$ , and for  $k = 0$  we put  $\partial R^0 := \emptyset$ . The *co-boundary* of  $R^k$  is the set of  $(k + 1)$ -cells in the intersection of the closure of  $R^k$  with  $\mathcal{R}_{k+1}$ , which is the empty set for  $k = n$ . These intersections must be taken with respect to the characteristic maps that specify how the subspaces are attached to one another. The *dimension* of a cell complex is defined by the highest dimensional cell contained in the complex. A *subcomplex* is a subset of  $\mathcal{C}$  which satisfies the properties to be a cell complex. The  $k$ -*skeleton* of the  $n$ -dimensional cell complex  $\mathcal{C}$  is the union of all cells in  $\mathcal{C}$  of dimension  $k$  or lower. The  $k$ -*skeleton* of the cell  $R^n \in \mathcal{C}$  is the union of all cells in  $\mathcal{C}$  of dimension  $k$  or lower which intersect the closure of the cell  $R^n$ . In our applications, all cells are taken to be closed, so the  $k$ -skeleton of a cell complex  $\mathcal{C}$  forms a subcomplex, and the  $k$ -skeleton of a cell  $R^n$  forms a subcomplex.

---

<sup>4</sup>Our data type for the implementation represents a closed interval, so we choose to construct rectangular cell complexes from closed intervals. CW complexes are usually described using open sets. The only point of confusion within this writeup is that *degenerate* open intervals  $(a, a)$  might be thought of as empty, which can be remedied by specifying the point  $\{a\}$  when needed.

<sup>5</sup>Strictly speaking, characteristic maps act on copies of simple reference sets (the closed unit disc  $E^k$ , open unit disc  $U^k$ , and the  $(k - 1)$ -dimensional unit spheres  $\Sigma^{k-1} \equiv \partial U^k$ , for  $k = 1, \dots, n$ ), and specify their placement into the Hausdorff space  $\Omega$  that is getting the CW complex structure (see Chapter 4 of [27]). Our description skips a step by naming our reference sets by the coordinates they will have in the topological space  $\Omega$ . The only job left for our ‘characteristic maps’ to do is to specify how  $k$ -cells attach to  $(k - 1)$ -cells, for  $k = 1, \dots, n$  (which they *always* do in the simplest fashion, namely by matching up coordinates). Keeping the language of characteristic maps allows us to keep the hierarchical structure of our building blocks at the forefront, and using already-mapped reference sets hides a potentially confusing layer of abstraction.

As an example, consider putting a cell complex structure on the topological space  $[0, 1] \times [0, 2] \subset \mathbb{R}^2$ , which is just a patch in the plane. Using open cells to emphasize the characteristic maps, in the simplest case the vertex set is  $\mathcal{R}_0 = \{\{0\} \times \{0\}, \{0\} \times \{2\}, \{1\} \times \{0\}, \{2\} \times \{1\}\}$ , the set of edges  $\mathcal{R}_1 = \{(0, 1) \times \{0\}, \{1\} \times (0, 2), (0, 1) \times \{2\}, \{0\} \times (0, 2)\}$ , and the set of two-cells contains just one element,  $\mathcal{R}_2 = \{(0, 1) \times (0, 2)\}$ . Then the subspaces are attached to one another in the simplest way – four characteristic maps attach the four vertices to the points  $\{(0, 0), (1, 0), (0, 2), (1, 2)\} \subset \mathbb{R}^2$ , a single characteristic map attaches two vertices to an edge, since there are four edges this requires four maps. Finally, a single characteristic map attaches all four edges to the single two-cell.

It will quickly become evident in Section 2.3.4 that the most general adaptive refinement of a rectangular set  $\Omega$  is also the most computationally efficient. The geometric minimum number of primary faces that a  $(k > 0)$ -dimensional rectangle can have is  $2k$ . Requiring rectangular  $(k > 0)$ -cells in `cmplx` to always have  $2k$  primary faces would introduce unnecessary refinements<sup>6</sup>. At the same time, the existence of a deformation retraction on a  $k$ -cell  $R^k$  is dependent on fundamentally subadditive information (namely, interval range enclosures) that must be computed on each element of its  $(k - 1)$ -skeleton. Because more general refinements will lead to a larger  $(k - 1)$ -skeleton, it is sometimes profitable to have a simple surrogate representation for the cell  $R^k$ . To this end we take the idea from the example in the previous paragraph and introduce the following

**Definition 2.3.1 (Simple  $n$ -dimensional Rectangular Cell Complex  $\mathcal{S}$ ).** *Given a closed rectangular  $n$ -cell  $R^n = [a_1, b_1] \times \cdots \times [a_n, b_n]$ , form the simple  $n$ -dimensional rectangular cell complex  $\mathcal{S}$  by putting  $S^n = R^n$ , so that  $\mathcal{S}_n = \{S^n\}$ , and for  $k = n - 1, \dots, 0$  put  $\mathcal{S}_k = \{[a_1, b_1] \times \cdots \times \partial_i[a_j, b_j] \times \cdots \times [a_n, b_n]\}_{i=1,2}^{j=1,\dots,n}$ . This generates a cell complex where every  $k$ -cell has exactly  $2k$  boundary elements.*

---

<sup>6</sup>This is analogous to the concept of a conforming mesh. The more general, non-conforming mesh is allowed so-called ‘hanging nodes’, which have analogy here to extra vertices along the edges of a rectangular cell, along with the additional higher dimensional cells that would be attached to those new vertices. See Figure 2.8 for an example of the general refinement obtained by our method.



### 2.3.4 Rigorous Validation Algorithm

The goal of the algorithm is to construct an inner approximation to  $N^{\geq \alpha}(\Omega, u)$  which easily allows for the correct computation of homotopy invariants of  $N^{\geq \alpha}(\Omega, u)$ . The strategy is to adaptively refine the data structure `cmplx` until one of the three simple, computable, mutually exclusive conditions in Definition 2.3.2 can be rigorously determined on each cell  $R^k \in \text{cmplx}$ , for  $k = 0, \dots, n$ . The three conditions correspond to positivity, negativity, or monotonicity of  $u$  on cells in `cmplx`.

The successful completion of the superlevel set validation algorithm (V) yields the refined cell complex `cmplx` where each cell  $R^k$  has been flagged as having been validated (in the sense of Definition 2.3.2) as positive, negative, or monotone along a coordinate direction  $\mathbf{e}_i$ , where  $i \in \{1, \dots, n\}$ . In Section 2.4 we show that this information is enough to establish a strong deformation retraction, for each monotone  $n$ -cell  $R^n \in \text{cmplx}$ , from  $W^n := N^{\geq \alpha}(\Omega, u) \cap R^n$  onto part of its  $(n-1)$ -dimensional boundary  $W^n \cap \partial R^n$ . This retraction can be performed at each dimension  $k = n, n-1, \dots$  until  $W^k$  is just the subcomplex of cells from `cmplx` which were flagged as having been validated as positive. We call this subcomplex of positive cells `cmplx+`, and Theorem 2.4.4 provides a computer-assisted proof that `cmplx+` is homotopy equivalent to  $N^{\geq \alpha}(\Omega, u)$ <sup>7</sup>.

The algorithm employs interval arithmetic and automatic differentiation in order to rigorously evaluate the conditions in Definition 2.3.2 on each  $n$ -cell  $R^n \in \text{cmplx}$ . Interval arithmetic and automatic differentiation are discussed briefly in Sections 2.3.1 and 2.3.2. In order to use interval arithmetic, and to ensure that the resulting CW complex is in a format suitable for existing computational topology libraries, the domains we consider must be rectangular, and we only use rectangular cells in the construction of `cmplx`. That is,  $\Omega \subset \text{Domain } u$  is rectangular, and `cmplx` is a rectangular CW complex (cf. Sections 2.3.1 and 2.3.2).

---

<sup>7</sup>Thus, in theory, following the successive collapse sequence from the  $n$ -dimensional `cmplx` yields `cmplx+`, although in practice we just extract `cmplx+` as the subcomplex of `cmplx` having (rigorously obtained) positive image under  $u$ . See Theorem 2.4.4.

A refinement step occurs when an  $n$ -cell  $R^n$  in `cmplx` cannot be validated in the sense of Definition 2.3.2, below.

**Definition 2.3.2 (Validation of  $n$ -dimensional cells).** *Let  $u : \Omega \subset \mathbb{R}^n \rightarrow \mathbb{R}$  be a differentiable function, let  $R^n$  be a closed  $n$ -cell in the rectangular cell complex representation of  $\Omega$ , and let  $\mathcal{S}_n$  be the simple  $n$ -dimensional rectangular cell complex representation of  $R^n$ . We say that  $R^n$  is*

- **validated as positive** if  $\inf [u(R^k)] > 0$  for each  $k$ -cell in the  $n$ -skeleton of  $R^n$ ,
- **validated as negative** if  $\sup [u(R^k)] < 0$  for each  $k$ -cell in the  $n$ -skeleton of  $R^n$ ,
- **validated as monotone along the coordinate direction  $\mathbf{e}_i$**  if  $R^n$  cannot be validated as positive or negative, and either  $\inf [\nabla u(R^n) \cdot \mathbf{e}_i] > 0$  or  $\sup [\nabla u(R^n) \cdot \mathbf{e}_i] < 0$  for at least one coordinate direction  $\mathbf{e}_i$ , and every lower dimensional cell in the  $(n-1)$ -skeleton of  $\mathcal{S}_n$  can be validated as either positive, negative, or monotone along at least one coordinate direction (where  $\mathcal{S}_n$  is the simple  $n$ -dimensional rectangular cell complex representation of  $R^n$ , as in Definition 2.3.1).

If none of the three conditions above can be established for a particular  $R^n \in \text{cmplx}$ , then  $R^n$  does not validate. In this case  $R^n$  is removed from `cmplx`, divided into  $R_1^n$  and  $R_2^n$ , and `cmplx` is reconstructed to include the new, unvalidated cells  $R_1^n$  and  $R_2^n$  along with the needed lower dimensional cells.

Dividing an  $n$ -cell  $R^n$  is done along the longest edge of  $R^n$  in order to preserve a bounded aspect ratio. Additionally, for each division, the division is made at a random fraction of the length of the longest edge, where that fraction is chosen at runtime from a user-specified set. For all validations in this paper we have chosen fractions from the set  $\left\{ \frac{1+\sqrt{5}}{2} - 1, 2 - \frac{1+\sqrt{5}}{2} \right\}$ , which causes the two resulting  $n$ -cells to have the golden ratio as the ratio of their new lengths.

Observe that evaluations such as  $\inf [u(R^n)] > 0$  only seek information from one side of the interval range enclosure of  $u$  (or of the vector of interval range enclosures of  $\nabla u$ , as

the case may be). Obtaining tight interval range enclosures is a significant computational challenge. In our case we only need a strategy to determine positivity of a function on an  $k$ -dimensional rectangle, not a tight interval range enclosure. Still, the infimum of a range enclosure on a full rectangle  $R^k \in \mathbf{cmplx}$  may lie below  $0 \in \mathbb{R}$ , even though the function is strictly positive on  $R^n$ , and will directly lead to an unnecessary refinement of  $\mathbf{cmplx}$ . In order to limit unnecessary refinements, if  $\inf [u(R^k)]$  does not return a strictly positive value, we take time to evaluate  $\inf [u(R^k)]$  on partitions of  $R^k$  (here viewing  $R^n$  as a set rather than a member of  $\mathbf{cmplx}$ ). Due to the subadditivity of interval range enclosures (§2.3.1), and the fact that smaller domains tend to yield tighter interval range enclosures, it is frequently possible to establish positivity on  $R^n$  even when  $\inf [u(R^n)]$  does not return a strictly positive value. The complete details of this strategy were developed in §3 of [11] as an extension of work by Skelboe (see references in [11]). In order to take advantage of the strategy, all evaluations of interval range enclosures over rectangles  $R^k$  are recast as tests for positivity over  $R^k$ , so that a check of  $\sup [u(R^k)] < 0$  becomes a check of  $\inf [-u(R^k)] > 0$ , and a check of  $\sup [\nabla u(R^n) \cdot \mathbf{e}_i] < 0$  becomes a check of  $\inf [-\nabla u(R^n) \cdot \mathbf{e}_i] > 0$ .

The validation procedure continues until all  $n$ -dimensional cells have been validated (which implies all lower dimensions cells have been validated), or a maximum number of subdivisions have occurred. We point out that successful completion of the algorithm implies that  $\alpha$  is, indeed, a regular value of  $u$ , a requirement discussed in §2.1.1. This is established in the following

**Theorem 2.3.3** ( $\alpha$  guaranteed to be regular for  $u$ ). *Let  $\Omega \subset \mathbb{R}^n$  denote a closed rectangular domain, and let  $u : \Omega \rightarrow \mathbb{R}$  be a continuously differentiable function. Furthermore, assume that Algorithm (V) successfully validates the  $\alpha$ -superlevel set  $N^{\geq \alpha}(\Omega, u)$ . Then  $\alpha$  is a regular value of  $u$ .*

*Proof.* Assume to the contrary that the algorithm yields the cell complex  $\mathbf{cmplx}$  in which every cell  $R^n$  has been validated in the sense of Definition 2.3.2, but  $\alpha$  is not a regular value of  $u$ . Then there exists a point  $x \in \Omega$  such that both  $u(x) = 0$  and  $\nabla u(x) = 0$ . Consider

the cell  $R^n \in \mathbf{cmplx}$  which contains the point  $x$ . On this cell  $R^n$ , the function  $u$  is neither entirely positive, nor is it entirely negative, so  $R^n$  must have validated as monotone. Recall that validation of monotonicity on  $R^n$  implies that  $\nabla u$  is bounded away from zero on the entire closed cell  $R^n$ , which contradicts the assumption that  $\nabla u(x) = 0$ .  $\square$

**The superlevel set validation algorithm (V) proceeds as follows:**    **Input:** A function  $u : \mathbb{R}^n \rightarrow \mathbb{R}$ , and a rectangular region  $\Omega \subset \mathbb{R}^n$  of interest.

**Output:** Failure, or the  $n$ -dimensional rectangular CW-complex  $\mathbf{cmplx}$ , with cells flagged as positive, negative, or monotone.

(V0) Initialize an unordered list  $\mathcal{L}$  to hold cells of dimension  $n$ . Create the cell complex  $\mathbf{cmplx}$  corresponding to  $\Omega$  and place the  $n$ -dimensional cells of  $\mathbf{cmplx}$  into  $\mathcal{L}$ .

**While  $\mathcal{L}$  is not empty:**

(V1) Remove an  $n$ -dimensional cell  $R^n$  from  $\mathcal{L}$ .

(V2) Construct the surrogate representation  $S^n$  for the cell  $R^n$  (according to Definition 2.3.1)

(V3) Obtain the  $n$ -skeleton of the surrogate  $S^n$ , and the  $n$ -skeleton of the original cell  $R^k$

(V4) For the skeleton in the set  $\{ n\text{-skeleton of } S^n, n\text{-skeleton of } R^n \}$ , operating first on the entire  $n$ -skeleton of  $S^k$ ,

For cell  $C$  in the current skeleton, lowest dimensional first, obtain the boundary cells of  $C$ :

- (a) If  $C$  is a zero-dimensional cell, obtain the interval range enclosure  $[u(C)]$ . If  $0 \in [u(C)]$  **the algorithm fails**. Otherwise, set the flag of  $C$  to positive (negative) based on  $\inf[u(C)] > 0$  ( $\sup[u(C)] < 0$ )
- (b) If the boundary cells of  $C$  are all positive (negative), and  $u$  can be determined to be positive<sup>†</sup> (negative) on  $C$ , then flag  $C$  as positive (negative). Else, if  $u$

cannot be determined to be positive (negative) on  $C$ , divide<sup>†</sup>  $R^n$  and place the two resulting  $n$ -dimensional cells into  $\mathcal{L}$

- (c) If some boundary cells of  $C$  are positive and some negative, and the range enclosure of a single partial derivative  $[\nabla u \cdot \mathbf{e}_i]$  is bounded away from zero on  $C$ , flag  $C$  as monotone. Else, if the range enclosure of all partial derivatives contain zero, divide<sup>†</sup> the original cell  $R^n$  and place the two resulting  $n$ -dimensional cells into  $\mathcal{L}$

<sup>†</sup> Division of an  $n$ -dimensional cell  $R^n$  occurs across its longest side in order to promote lowest aspect-ratio configurations. In particular, we follow [11] and put  $\Sigma := \left\{0.618034 \approx \frac{\sqrt{5}-1}{2}, 0.381966 \approx 1 - \frac{\sqrt{5}-1}{2}\right\}$  (built from golden ratio). Denoting the longest side of  $R$  by  $L$ , we divide  $R$  along  $L$  according to  $\sigma L$ ,  $(1 - \sigma)L$ , where  $\sigma \in \Sigma$  is chosen randomly at the time of this division. Each original  $n$ -dimensional rectangle comes with a user-defined maximum number of divisions which is inherited by its children upon division.

<sup>‡</sup> Because the computed range enclosure of a function on a rectangle  $R^n$  may be an interval that contains zero when the actual range of the function is bounded above (below) zero, we have implemented the strategy described at the end of §2.3.4

We provide pseudocode for the above algorithm below. Figure 2.5 illustrates a step-by-step demonstration of how successive refinements of `cmplx` lead to the validation of a 2-cell in the domain  $\Omega := [-1, 1] \times [-1, 1] \subset \mathbb{R}^2$ , for the function  $u(x, y) = x^2 + y^2 - 3/4$ .

---

**Algorithm (V) 1****cellComplex** validate\_superlevel\_set(**Differentiable**  $u$ , **coordinates**  $\Omega$ )**Input:** Continuously differentiable function  $u$ , description of rectangular set  $\Omega \subset$ Domain  $u \subset \mathbb{R}^n$ 

```
1: cellComplex cmplx = new cellComplex( $\Omega$ )
2: vector< cell > n_cells = cmplx.get_n_cells()
3: while n_cells is not empty, do
4:   cell n_cell = n_cells.pop()
5:   if !validates_using_surrogate( $u$ , n_cell), then
6:     if n_cell.depth < max_depth, then
7:       cell c1, c2
8:       cellComplex new_cmplx
9:       c1, c2, new_cmplx = cmplx.split(n_cell)
10:      cmplx = new_cmplx
11:      n_cells.append(c1,c2)
12:    else
13:      terminate program, max depth reached before validation
14: return cmplx
```

---

---

**Subroutine****bool** validates\_using\_surrogate( **Differentiable**  $u$ , **cell**  $n\_cell$ )

---

**Input:** Continuously differentiable function  $u$ , **cell**  $cell$ 

```
1: cellComplex surrogate = new cellComplex( $n\_cell$ .coordinates)
2: vector< vector< cell >> skeleton_of_n_cell =  $n\_cell$ .get_n_skeleton()
3: vector< vector< cell >> skeleton_of_surrogate = surrogate.get_n_skeleton()
4: for skeleton  $\in \{\text{skeleton\_of\_surrogate, skeleton\_of\_n\_cell}\}$  do
5:   for  $dim = 0, 1, \dots, n$  do
6:     vector< cell > dim_skeleton = skeleton[dim]
7:     if  $dim == 0$ , then
8:       for  $cell$  in dim_skeleton do
9:         if  $\inf[u(cell)] > 0$ , then
10:           flag cell as positive
11:         else if  $\sup[u(cell)] < 0$ , then
12:           flag cell as negative
13:         else
14:           throw:  $\alpha$ -level set crosses vertex
15:       else
16:         for  $cell$  in dim_skeleton do
17:           if dim-1 skeleton of cell is all positive &  $\inf[u(cell)] > 0$ , then
18:             flag cell as positive
19:           else if dim-1 skeleton of cell is all negative &  $\sup[u(cell)] < 0$ , then
20:             flag cell as negative
21:           else if dim-1 skeleton of cell is mixed & has_monotone_direction( $u, cell$ ), then
22:             flag cell as monotone
23:           else
24:             return false
25: return true
```

---

---

**Subroutine****bool** has\_monotone\_direction(**differentiable**  $u$ , **cell**  $cell$ )

---

**Input:** Continuously differentiable function  $u$ , **cell**  $cell$ 

```
1: for  $i = 1, \dots, cell.dim$  do
2:   if cell is thin, then
3:     continue
4:   if  $\inf[\nabla u(cell) \cdot \mathbf{e}_i] > 0$  or  $\sup[\nabla u(cell) \cdot \mathbf{e}_i] < 0$ , then
5:     return true
6: return false
```

---

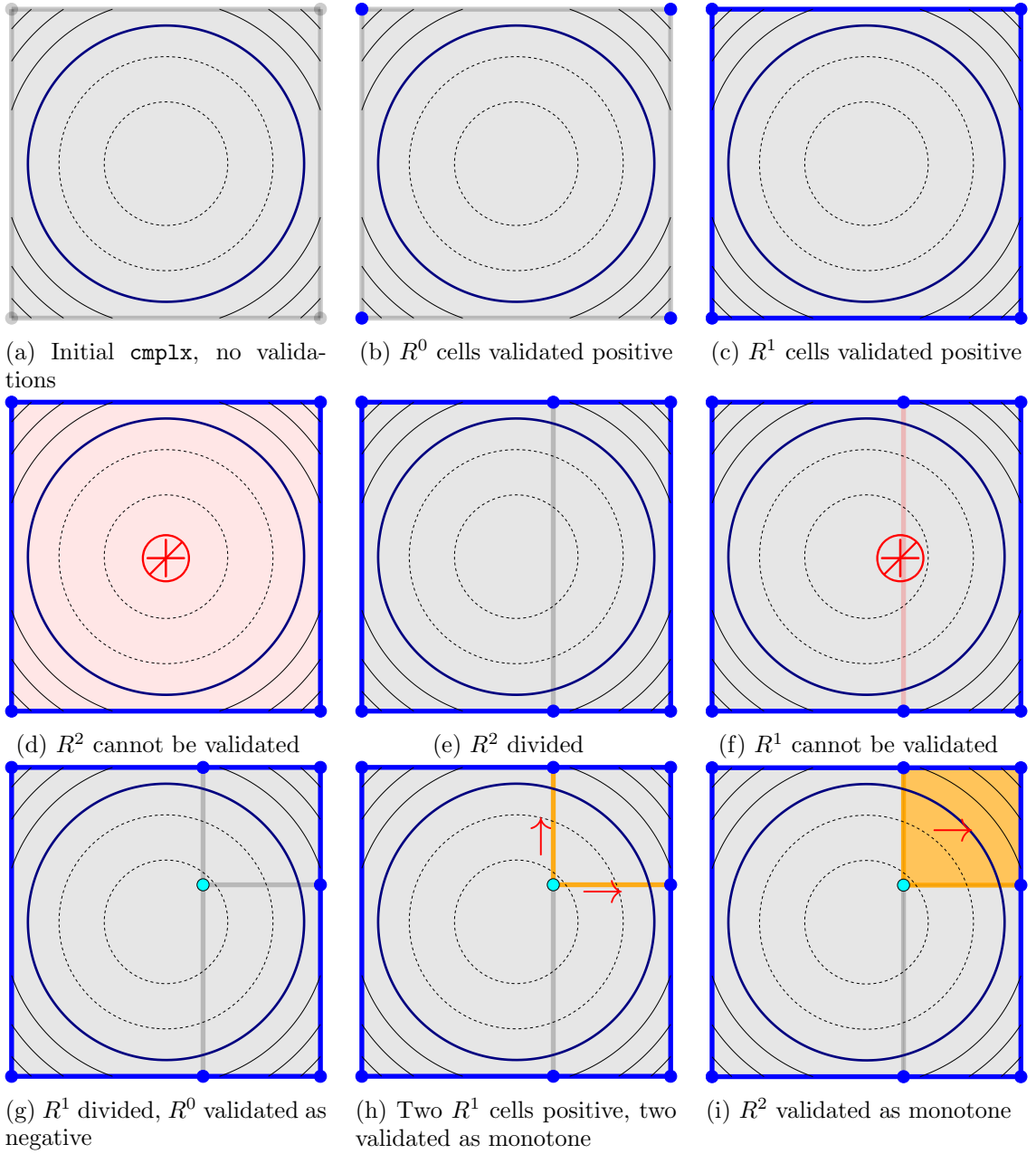


Figure 2.5: Illustration of validation steps which lead to the validation of a single 2-cell in `cmplx`. From panel (d) to (e), the single 2-cell in `cmplx` has been divided, and `cmplx` has been updated with new vertices and now contains two 2-cells. The top right 2-cell in panel (i) has been validated as monotone along the horizontal direction, and this 2-cell will not be revisited by the algorithm. Beyond panel (i), the algorithm will visit one of the two remaining 2-cells in `cmplx` and begin the validation on its 2-skeleton, starting with the lowest dimensional cells which have not yet been validated.



## 2.4 Establishing the Homotopy Equivalence Between $N^{\geq\alpha}(\Omega, u)$ and $\text{cmplx}^+$

Assume that the validation algorithm (V) has completed successfully and has returned the cell complex  $\text{cmplx}$ , where every cell  $R^k \in \text{cmplx}$ , for  $k = 0, \dots, n$ , has been validated as either positive, negative, or monotone along a coordinate direction. It is left to show that the cell complex  $\text{cmplx}^+$ , consisting of cells in  $\text{cmplx}$  which have been validated as positive, is homotopy equivalent to  $N^{\geq\alpha}(\Omega, u)$ . This is the content of Theorem 2.4.4.

The homotopy equivalence is a consequence of the existence of a strong deformation retraction performed on individual cells  $R^n \in \text{cmplx}$ . This map will be generated by a Lipschitz vector field that will be explicitly constructed as a recurrence relation with respect to the dimension of  $\text{cmplx}$ , and appears as Equation (2.1). Notice that cells in  $\text{cmplx}$  which have been validated as negative do not intersect  $N^{\geq\alpha}(\Omega, u)$ , and that cells which have been validated as positive are contained strictly within  $N^{\geq\alpha}(\Omega, u)$  (these facts follow from the continuity of  $u$ ). Thus, the deformation retraction will only be necessary on  $n$ -cells  $R^n \in \text{cmplx}$  which have been validated as monotone along a coordinate direction in the sense of Definition 2.3.2.

We present the path to establishing the theorem in three logical steps. **For an individual  $n$ -cell  $R^n \in \text{cmplx}$  which has been validated as monotone,** we: (1st) Collect information about  $u$  on the  $n$ -skeleton of  $R^n$  that was learned during the validation algorithm (V); (2nd) Rescale the cell  $R^n$  to  $[0, 1]^n$ , and reorder the basis vectors based on the direction of monotone increase for  $u$ ; and (3rd) Leverage the information learned during the validation to construct a collapsing vector field on  $R^n$ , where “collapsing” means that there exists a strong deformation retraction from the set  $W^n := N^{\geq\alpha}(\Omega, u) \cap R^n$  onto its  $(n - 1)$ -dimensional boundary,  $W^n \cap \partial\mathbb{R}^n$ .

### 2.4.1 The $\delta$ -collar on which Monotonicity is Guaranteed

Consider a  $(k > 0)$ -cell  $R^k$  in the  $n$ -dimensional cell complex `cmplx` which has been validated as monotone along the direction  $\mathbf{e}_i$  in the sense of Definition 2.3.2. The continuity of  $u$  allows for  $[\nabla u(R^k) \cdot \mathbf{e}_i]$  to be bounded away from zero on an entire  $n$ -dimensional open set containing  $R^k$ . In particular, writing  $R^k = [a_1, b_1] \times \cdots \times [a_i, b_i] \times \cdots \times [a_n, b_n]$ , there exists a  $\tilde{\delta} > 0$  such that  $[\nabla u(R^k) \cdot \mathbf{e}_i]$  is bounded away from zero on the closed  $\tilde{\delta}$ -collar of  $R^k$ , given by  $[a_1 - \tilde{\delta}, b_1 + \tilde{\delta}] \times \cdots \times [a_i, b_i] \times \cdots \times [a_n - \tilde{\delta}, b_n + \tilde{\delta}]$ . We put  $\tilde{\delta}_{\min} := \min \tilde{\delta}$ , where the minimum is taken over all (finitely many) validations that were performed by the algorithm.

Considering again a  $k > 0$ -cell  $R^k$  in the  $n$ -dimensional cell complex `cmplx` which has been validated as monotone along the direction  $\mathbf{e}_i$ , observe that some cells in the  $(k - 1)$ -skeleton of  $R^k$  may have been validated as negative. Similar to the situation above, for a cell  $R^j$  in the  $k$ -skeleton which has been validated as negative, i.e. that  $\sup [u(R^j)] < 0$ , the continuity of  $u$  allows for  $\sup [u(R^j)]$  to be bounded below zero on an entire  $n$ -dimensional open set containing  $R^j$ . In particular, writing  $R^j = [a_1, b_1] \times \cdots \times [a_n, b_n]$ , there exists a  $\hat{\delta} > 0$  such that  $\sup [u(R^j)] < 0$  on the closed  $\hat{\delta}$ -ball containing  $R^j$ , given by  $[a_1 - \hat{\delta}, b_1 + \hat{\delta}] \times \cdots \times [a_j, b_j] \times \cdots \times [a_n - \hat{\delta}, b_n + \hat{\delta}]$ . We put  $\hat{\delta}_{\min} := \min \hat{\delta}$ , where the minimum is taken over all (finitely many) validations that were performed by the algorithm.

We define  $\delta := \min \left\{ \tilde{\delta}_{\min}, \hat{\delta}_{\min} \right\}$ . The fact that we can extend the monotonicity a positive distance away from  $R^k$  is the essential fact that permits us to seek only a single direction of monotonicity on any given cell (cf. Definition 2.3.2). The fact that we can extend the negativity of  $u$  to an entire neighborhood of a face  $R^j$  allows us to collapse  $W^n := N^{\geq \alpha}(\Omega, u) \cap R^n$  onto part of its boundary  $W^n \cap \partial R^n$  using a vector field that is guaranteed to satisfy  $\nabla u \cdot \xi > 0$  on  $W^n$ . See the figures accompanying Equations (2.2), (2.3), and (2.4) for a visual representation of how we use  $\delta$  in the construction of the collapsing vector field  $\xi$ .

### 2.4.2 Rescaling Rectangular Cells $R^n$ to $[0, 1]^n$ , and Reordering the Standard Basis

In order to simplify the presentation from this point forward, we rescale cells  $R^n \in \mathbf{cmplx}$  to the unit cube  $[0, 1]^n$ . Additionally, suppose the cell  $R^n \in \mathbf{cmplx}$  has been validated as being monotone along the direction  $\mathbf{e}_i$ . To simplify the notation going forward, we reorder the standard basis  $\{\mathbf{e}_1, \dots, \mathbf{e}_n\}$  so that  $\mathbf{e}_n$  points in the direction along which  $u(R^n)$  is monotonically increasing, so if the relevant validation step yields  $\inf[\nabla u(R^n) \cdot \mathbf{e}_i] > 0$ , we put  $\mathbf{e}_n := \mathbf{e}_i$ .

Going down one dimension, if the face  $R^{n-1}$  which is perpendicular to  $\mathbf{e}_n$  is not validated as negative, then it must have been validated as monotone (it is not possible to have been both validated as positive on a face  $R^{n-1}$ , and validated as monotone increasing in the direction perpendicular to this same face). We reorder the remaining basis vectors so that  $\mathbf{e}_{n-1}$  points in the direction along which  $u(R^{n-1})$  is monotonically increasing. If, for some  $k > 0$ , the face  $R^{k-1}$  is negative, then its boundary will be negative, and the ordering of the remaining basis elements is irrelevant for our purposes (they just need to preserve the orientation of the rectangle  $R^n$ ). To summarize, the direction of increasing monotonicity for the top-dimensional cell  $R^n$  determines the direction  $\mathbf{e}_n$  points along, and we follow  $\mathbf{e}_n$  backward, to the face  $R^{n-1}$  to find the direction along which  $\mathbf{e}_{n-1}$  points. This should be made more clear by Figure 2.6. Until now we have distinguished the dimension of a cell from the direction of monotonicity established on that cell – henceforth we can simply use the same integer.

### 2.4.3 The Collapsing Vector Field $\xi : \mathbb{R}^n \rightarrow \mathbb{R}^n$

In this section we construct the vector field  $\xi$  which will be used to collapse the  $\alpha$ -superlevel set  $W^n = N^{\geq \alpha}(R^n, u)$  onto  $W^n \cap \partial R^n = N^{\geq \alpha}(\partial R^n, u)$ , for an arbitrary monotone  $n$ -cell  $R^n$  in  $\mathbf{cmplx}$ . At this stage we are only concerned about making this collapse locally, for an individual cell  $R^n \in \mathbf{cmplx}$ , so  $\xi : \mathbb{R}^n \rightarrow \mathbb{R}^n$  is constructed using local information obtained

during the validation<sup>8</sup> of  $R^n$ . With this in mind, the vector field  $\xi$  should be thought of as acting on the cube  $[0, 1]^n$ , and simply having continuous extension to zero outside of  $[0, 1]^n$ .

The verb collapse is being used here to refer to a strong deformation retraction from  $W^n$  onto  $W^n \cap \partial R^n$ , and this retraction which will be built from the global flow  $\varphi : \mathbb{R} \times \mathbb{R}^n \rightarrow \mathbb{R}^n$  generated by  $\xi$ . We use the Ważewski theorem<sup>9</sup>, stated as Theorem 2.4.3, as a convenient way to obtain a strong deformation retraction from the vector field  $\xi$ .

**Definition 2.4.1 (Exit set, [12]).** *Let  $\varphi : \mathbb{R} \times \mathbb{R}^n \rightarrow \mathbb{R}^n$  be a flow. Given  $W \subset \mathbb{R}^n$ , let  $W^\circ$  be the set of points  $x \in W$  such that, for some positive  $t$ ,  $\varphi(t, x) \notin W$ . Let  $W^-$  be the set of points  $x \in W$  such that, for any positive  $t$ ,  $\varphi([0, t], x) \not\subset W$ . The set  $W^-$  is contained in  $W^\circ$  and is called the exit set of  $W$ .*

**Definition 2.4.2 (Ważewski set, [12]).** *The set  $W$  (above) is called a Ważewski set if the following conditions are satisfied:*

- (a) *If  $x \in W$  and  $\varphi([0, t], x) \subset \text{cl}(W)$  then  $\varphi([0, t], x) \subset W$ ,*
- (b)  *$W^-$  is closed relative to  $W^\circ$ .*

**Theorem 2.4.3 (Ważewski, [12]).** *If  $W$  is a Ważewski set then  $W^-$  is a strong deformation retract of  $W^\circ$  and  $W^\circ$  is open relative to  $W$ .*

For an arbitrary monotone  $n$ -dimensional cell  $R^n \in \mathbf{cmplx}$ , we rescale  $R^n$  to  $[0, 1]^n$  according to §2.4.2, and define a point  $\mathbf{x} \in \mathbb{R}^n$  by  $\mathbf{x} := (x_1, \dots, x_n)$ . The vector field  $\xi(\mathbf{x}) := \xi_n(\mathbf{x}) + \varepsilon\eta(\mathbf{x})s(\mathbf{x})$  is constructed in three parts. The first part,  $\xi_n$ , is defined recursively, pointing always in some convex combination of directions  $\mathbf{e}_i$  along which  $u$  has been rigorously established to be monotone increasing. The second part is a perturbation of  $\xi_n$  which points out of the cube  $[0, 1]^n$ . This perturbation  $\varepsilon\eta(\mathbf{x})s(\mathbf{x})$  is designed specifically

---

<sup>8</sup>More specifically,  $\xi$  is constructed using information computed on  $\mathcal{S}_n$ , the simple  $n$ -dimensional complex representation of  $R^n$ .

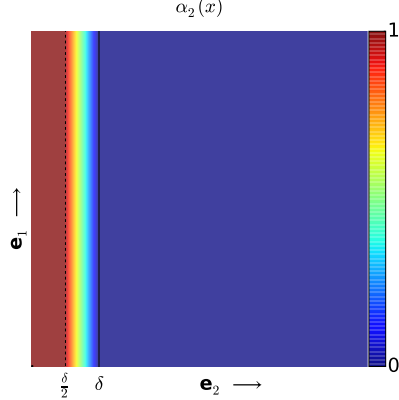
<sup>9</sup>The Ważewski theorem plays a major role in Chapter 3, and all of §3.3.2 is devoted to discussing the strong deformation retraction that we are using here.

to collapse the  $\alpha$ -superlevel set  $W^n$  onto its  $(n-1)$ -dimensional boundary,  $N^{\geq \alpha}(\Omega, u) \cap \partial R^n$ , while simultaneously allowing  $W^n$  to be a Ważewski set for  $\varphi$ , satisfying  $W^o = W^n$ , and having exit set  $W^- = W^n \cap \partial R^n$ . Lemma 2.4.8 establishes these facts. Finally, the vector field  $\xi$  is extended continuously from the cube  $[0, 1]^n$  to all of  $\mathbb{R}^n$  in such a way that  $\xi \equiv 0$  some distance away from  $[0, 1]^n$  (the particular details of the extension are unimportant, but  $\xi$  must generate a global flow in order to take advantage of the Ważewski theorem).

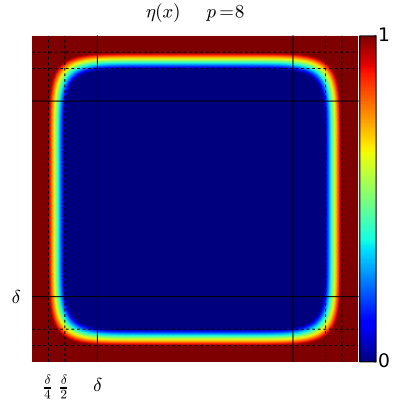
The first part of the vector field,  $\xi_n : \mathbb{R}^n \rightarrow \mathbb{R}^n$ , is defined as follows :

$$\begin{aligned}\xi_1(\mathbf{x}) &= \mathbf{e}_1 \\ \xi_k(\mathbf{x}) &= \alpha_k(\mathbf{x})\xi_{k-1}(\mathbf{x}) + (1 - \alpha_k(\mathbf{x}))\mathbf{e}_k\end{aligned}\tag{2.1}$$

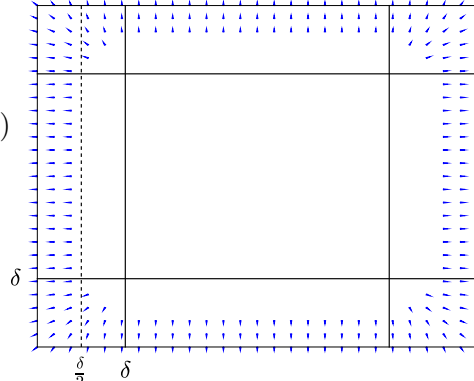
where  $k = 2, \dots, n$ , and the scalar-valued functions  $\alpha_k : [0, 1]^n \rightarrow [0, 1]$  are defined by

$$\alpha_k(\mathbf{x}) = \begin{cases} 1 & \text{for } 0 \leq x_k \leq \frac{\delta}{2} \\ -\frac{2}{\delta}x_k + 2 & \text{for } \frac{\delta}{2} < x_k < \delta \\ 0 & \text{for } \delta \leq x_k \leq 1 \end{cases} \tag{2.2}$$


The perturbation of  $\xi_n$  which pushes points near the boundary of  $[0, 1]^n$  onto the boundary  $\partial[0, 1]^n$  is expressed as  $\varepsilon\eta(\mathbf{x})s(\mathbf{x})$ , with  $\varepsilon > 0$ . We obtain the scalar-valued function  $\eta : [0, 1]^n \rightarrow [0, 1]$  from the expression

$$\eta(\mathbf{x}) = \begin{cases} 0 & \text{for } \|\mathbf{x} - \mathbf{c}\|_p < r_1 \\ \frac{\|\mathbf{x} - \mathbf{c}\|_p - r_1}{r_2 - r_1} & \text{for } r_1 \leq \|\mathbf{x} - \mathbf{c}\|_p \leq r_2 \\ 1 & \text{for } \|\mathbf{x} - \mathbf{c}\|_p > r_2, \end{cases} \quad (2.3)$$


where  $\mathbf{c} := (\frac{1}{2}, \dots, \frac{1}{2}) \in [0, 1]^n$ ,  $r_1 = \frac{1}{2} - \frac{\delta}{2}$ ,  $r_2 = \frac{1}{2} - \frac{\delta}{4}$ , and  $p = 2k$  for  $k$  large enough to keep the support of  $\eta$  within a  $\delta$  band near the boundary of  $[0, 1]^n$  (see figure). The vector field  $s : [0, 1]^n \rightarrow \mathbb{R}^n$  is given by

$$s(\mathbf{x}) = \nabla \sum_{k=1}^n \left( x_k - \frac{1}{2} \right)^p \quad (2.4)$$


#### 2.4.4 Computer-assisted Proof that $N^{\geq \alpha}(\Omega, u)$ is Homotopy Equivalent to $\mathbf{cmplx}^+$

**Theorem 2.4.4.** *The cell complex  $\mathbf{cmplx}^+$  is a strong deformation retract of  $N^{\geq \alpha}(\Omega, u)$ , and consequently  $\mathbf{cmplx}^+$  is homotopy equivalent to  $N^{\geq \alpha}(\Omega, u)$ .*

**Proposition 2.4.5 (Coordinatewise representation of  $\xi_n$ ).** *The recurrence relation  $\xi_1(\mathbf{x}) = \mathbf{e}_1$ ,  $\xi_k(\mathbf{x}) = \alpha_k(\mathbf{x})\xi_{k-1}(\mathbf{x}) + (1 - \alpha_k(\mathbf{x}))\mathbf{e}_k$  for  $k = 2, \dots, n$ , can be written coordinatewise as*

$$\xi_n(\mathbf{x}) = \prod_{\ell=2}^n \alpha_\ell(\mathbf{x}) \mathbf{e}_1 + \sum_{k=2}^{n-1} \left[ \prod_{\ell=k+1}^n \alpha_\ell(\mathbf{x}) (1 - \alpha_k(\mathbf{x})) \mathbf{e}_k \right] + (1 - \alpha_n(\mathbf{x})) \mathbf{e}_n. \quad (2.5)$$

*Proof.* This can be seen with three simple induction arguments. In what follows we will simply write  $\beta_k(\mathbf{x})$ , with  $k \in \{1, \dots, n\}$ , to refer to the sums and products of  $\alpha_i(\mathbf{x})$  which comprise the individual coefficient functions. Notice that each  $\beta_k$  satisfies  $\beta_k(\mathbf{x}) \geq 0$  for  $\mathbf{x} \in [0, 1]$  by definition.

First we look at the coefficient in front of  $\mathbf{e}_1$ . Establish the base case,  $n = 2$ :

$$\begin{aligned} \xi_2 &= \alpha_2 \xi_1 + (1 - \alpha_2) \mathbf{e}_2 \\ &= \alpha_2 \mathbf{e}_1 + (1 - \alpha_2) \mathbf{e}_2, \quad \text{so that} \end{aligned}$$

$$\alpha_2 = \prod_{\ell=2}^2 \alpha_\ell.$$

Suppose that this holds for  $n = k$ , i.e. that the  $\mathbf{e}_1$  coefficient of  $\xi_k$  is given by  $\prod_{\ell=2}^k \alpha_\ell$ . We

use this assumption to show that the  $\mathbf{e}_1$  coefficient of  $\xi_n$  is given by  $\prod_{\ell=2}^n \alpha_\ell$  for all  $n$ . Indeed,

put  $n = k + 1$ . Then we can write

$$\begin{aligned}\xi_{k+1} &= \alpha_{k+1}\xi_k + (1 - \alpha_{k+1})\mathbf{e}_{k+1} \\ &= \alpha_{k+1} \left( \prod_{\ell=2}^k \alpha_\ell \mathbf{e}_1 + \beta_2 \mathbf{e}_2 + \cdots + \beta_k \mathbf{e}_k \right) + (1 - \alpha_{k+1}) \mathbf{e}_{k+1}, \quad \text{so that}\end{aligned}$$

$$\alpha_{k+1} \prod_{\ell=2}^k \alpha_\ell = \prod_{\ell=2}^{k+1} \alpha_\ell.$$

This establishes that the  $\mathbf{e}_1$  coefficient of  $\xi_n$  is given by  $\prod_{\ell=2}^n \alpha_\ell$  for all  $n$ .

Next we consider the coefficients in front of  $\mathbf{e}_k$  for  $1 < k < n$ . We establish the base case,  $n = 3$ :

$$\begin{aligned}\xi_3 &= \alpha_3 \xi_2 + (1 - \alpha_3) \mathbf{e}_3 \\ &= \alpha_3 (\alpha_2 \mathbf{e}_1 + (1 - \alpha_2) \mathbf{e}_2) + (1 - \alpha_3) \mathbf{e}_3, \quad \text{so that} \\ \alpha_3 (1 - \alpha_2) &= \prod_{\ell=2+1}^3 \alpha_\ell (1 - \alpha_2).\end{aligned}$$

Suppose that this holds for  $n = m$ , i.e. that the  $\mathbf{e}_k$  coefficients of  $\xi_m$  are given by

$\prod_{\ell=k+1}^m \alpha_\ell (1 - \alpha_k)$ . We use this assumption to show that the  $\mathbf{e}_k$  coefficients of  $\xi_n$  are given



by  $\prod_{\ell=k+1}^n \alpha_\ell (1 - \alpha_k)$  for  $1 < k < m$ . Indeed, put  $n = m + 1$ . Then

$$\begin{aligned}\xi_{m+1} &= \alpha_{m+1} \xi_m + (1 - \alpha_{m+1}) \mathbf{e}_{m+1} \\ &= \alpha_{m+1} \left( \prod_{\ell=2}^m \alpha_\ell \mathbf{e}_1 + \prod_{\ell=2+1}^m \alpha_\ell (1 - \alpha_2) \mathbf{e}_2 + \cdots \right. \\ &\quad \left. + \prod_{\ell=m+1}^m \alpha_\ell (1 - \alpha_m) \mathbf{e}_m \right) + (1 - \alpha_{m+1}) \mathbf{e}_{m+1},\end{aligned}$$

so that

$$\alpha_{m+1} \prod_{\ell=k+1}^m \alpha_\ell (1 - \alpha_k) = \prod_{\ell=k+1}^{m+1} \alpha_\ell (1 - \alpha_k).$$

This establishes that the  $\mathbf{e}_k$  coefficients of  $\xi_n$  are given by  $\prod_{\ell=k+1}^n \alpha_\ell (1 - \alpha_k)$  for  $1 < k < n$ .

Finally, writing  $\xi_n = \beta_1 \mathbf{e}_1 + \cdots + \beta_{n-1} \mathbf{e}_{n-1} + (1 - \alpha_n) \mathbf{e}_n$ , we can see that the linear independence of the basis vectors  $\{\mathbf{e}_k\}_{k=1}^n$  imply that  $(1 - \alpha_n)$  is the coefficient for  $\mathbf{e}_n$ , for any  $n$ .  $\square$

**Lemma 2.4.6.**  $\nabla u(\mathbf{x}) \cdot (\xi_n(\mathbf{x}) + \varepsilon \eta(\mathbf{x}) s(\mathbf{x})) > 0$  for  $\mathbf{x} \in W^n$

*Proof.* To see this we first establish  $\rho > 0$  such that  $u(\mathbf{x}) \cdot \xi_n(\mathbf{x}) \geq \rho$  for all  $\mathbf{x} \in W^n$ . Next we note that  $0 \leq \eta(\mathbf{x}) \leq 1$ , and that  $\nabla f(\mathbf{x}) \cdot s(\mathbf{x})$  may be less than zero. We then establish  $\varepsilon > 0$  ensure that  $\nabla u(\mathbf{x}) \cdot \xi_n(\mathbf{x}) + \nabla u(\mathbf{x}) \cdot \varepsilon \eta(\mathbf{x}) s(\mathbf{x}) \geq \rho + \nabla u(\mathbf{x}) \cdot \varepsilon \eta(\mathbf{x}) s(\mathbf{x})$  remains bounded above zero for  $\mathbf{x} \in W^n$ .

To establish  $\rho$ :

Put  $\xi_n(\mathbf{x}) = \beta_1(\mathbf{x}) \mathbf{e}_1 + \cdots + \beta_n(\mathbf{x}) \mathbf{e}_n$  are other names for the coefficients in the coordinatewise representation of  $\xi_n(\mathbf{x})$  given in Proposition 2.4.5. We will show

that  $\bigcup_{i=1,\dots,n} \text{supp } \beta_i = [0, 1]^n$  in order to establish that  $\mathbf{x} \in W^n$  is in  $\text{supp } \beta_k$  for some  $k$ . Finally we show that if  $\mathbf{x} \in \text{supp } \beta_k$ , then  $\nabla u(\mathbf{x}) \cdot \mathbf{e}_k > 0$ . Compactness of  $W^n = N^{\geq \alpha}(\Omega, u) \cap [0, 1]^n$  will yield a  $\rho > 0$  such that  $\nabla u(\mathbf{x}) \cdot \xi_n(\mathbf{x}) \geq \rho > 0$  for  $\mathbf{x} \in W^n$ .

By Proposition 2.4.5 we can write the inner product  $\nabla u(\mathbf{x}) \cdot \xi_n(\mathbf{x})$  as

$$\begin{aligned} \nabla u(\mathbf{x}) \cdot \xi_n(\mathbf{x}) &= \prod_{\ell=2}^n \alpha_\ell(\mathbf{x}) \nabla u(\mathbf{x}) \cdot \mathbf{e}_1 + \sum_{k=2}^{n-1} \left[ \prod_{\ell=k+1}^n \alpha_\ell(\mathbf{x}) (1 - \alpha_k(\mathbf{x})) \nabla u(\mathbf{x}) \cdot \mathbf{e}_k \right] \\ &\quad + (1 - \alpha_n(\mathbf{x})) \nabla u(\mathbf{x}) \cdot \mathbf{e}_n \end{aligned}$$

We collect the following facts for  $k = 2, \dots, n$ :

- (i)  $\text{supp } \alpha_k(\mathbf{x})$  is the set  $[0, 1] \times \dots \times [0, 1] \times [0, \delta] \times [0, 1] \times \dots \times [0, 1]$ . This

is the definition of  $\alpha_k(\mathbf{x})$  in Equation (2.2).

- (ii)  $\text{supp } (1 - \alpha_k(\mathbf{x}))$  is the set  $[0, 1] \times \dots \times [0, 1] \times [\frac{\delta}{2}, 1] \times [0, 1] \times \dots \times [0, 1]$ .

Since  $\alpha_k(\mathbf{x}) = 1$  on  $[0, 1] \times \dots \times [0, 1] \times [0, \frac{\delta}{2}] \times [0, 1] \times \dots \times [0, 1]$ , then

$(1 - \alpha_k(\mathbf{x}))$  is supported on the complement of that set (taken with respect to the ambient set  $[0, 1]^n$ ).

- (iii)  $\text{supp } \prod_{\ell=2}^n \alpha_\ell(\mathbf{x})$  is the set  $[0, 1] \times [0, \delta] \times \dots \times [0, \delta]$ . The support of this prod-

uct is the intersection of the supports, so  $\text{supp } \prod_{\ell=2}^n \alpha_\ell(\mathbf{x}) = \bigcap_{i=2}^n \text{supp } \alpha_i(\mathbf{x})$ .

- (iv)  $\text{supp } \prod_{\ell=k+1}^n \alpha_\ell(\mathbf{x})$  is the set  $[0, 1] \times \dots \times [0, 1] \times [0, \delta] \times [0, \delta] \times \dots \times [0, \delta]$ .

This follows from (iii) by taking  $i$  from  $k + 1$ .

(v)  $\text{supp} \prod_{\ell=k+1}^n \alpha_\ell(\mathbf{x})(1 - \alpha_k(\mathbf{x}))$  is the set  $[0, 1] \times \cdots \times [0, 1] \times [\frac{\delta}{2}, 1] \times \underset{(k+1)st}{[0, \delta]} \times$

$[0, \delta] \times \cdots \times [0, \delta]$ . This is perhaps most easily seen by writing  $\prod_{\ell=k+1}^n \alpha_\ell(\mathbf{x})(1 -$

$\alpha_k(\mathbf{x}))$  as  $(1 - \alpha_k(\mathbf{x})) \prod_{\ell=k+1}^n \alpha_\ell(\mathbf{x})$ , and then evaluating the product of the

supports in (ii) and (iv) as the intersection of those supports.

Now,  $\bigcup_{i=1, \dots, n} \text{supp } \beta_i = [0, 1]^n$ , and in fact  $\bigcup_{i=n-1, n} \text{supp } \beta_i = [0, 1]^n$ , which can be seen from evaluating (ii) with  $k = n$ , and evaluating (v) with  $k = n - 1$ . Thus, for  $\mathbf{x} \in W^n$ , we have that  $\mathbf{x} \in \text{supp } \beta_k$  for some  $k = 1, \dots, n$ .

If  $\mathbf{x} \in \text{supp } \beta_k$  for some  $k \in \{1, \dots, n\}$  and also  $\mathbf{x} \in W^n$ , then  $\mathbf{x}$  is in the  $\delta$ -collar of the (rescaled)  $k$ -cell given by  $[0, 1] \times \cdots \underset{kth}{[0, 1]} \times [0, \delta] \times \cdots \times [0, \delta]$ . By

the construction of  $\delta$  in §2.4.1, the  $k$ -cell must have been validated as either monotone or positive. By the reordering described in §2.4.2, that  $k$ -cell must have been validated as monotone increasing along  $\mathbf{e}_k$ . Thus,  $\nabla u(\mathbf{x}) \cdot \mathbf{e}_k > 0$  for this  $k$ . Compactness of  $W^n = N^{\geq \alpha}(\Omega, u) \cap [0, 1]^n$ , and the nonnegativity of  $\beta_k(\mathbf{x})$ , guarantees that there exists a  $\rho > 0$  such that  $\nabla u(\mathbf{x}) \cdot \xi_n(\mathbf{x}) \geq \rho > 0$  for  $\mathbf{x} \in W^n$ .

To establish  $\varepsilon$ :

The continuity of  $u$ , along with the compactness of  $W^n$ , provide for a finite

$M > 0$  such that  $0 \leq |\nabla u(\mathbf{x}) \cdot s(\mathbf{x})| < M$  for  $\mathbf{x} \in W^n$ . Put  $\varepsilon = \frac{\rho}{2M}$ .

Then  $\nabla u(\mathbf{x}) \cdot \xi_n(\mathbf{x}) + \nabla u(\mathbf{x}) \cdot \varepsilon \eta(\mathbf{x}) s(\mathbf{x}) \geq \rho - \varepsilon M > 0$  for  $\mathbf{x} \in W^n$ . □

**Notation 2.4.7 (The flow  $\varphi$  generated by the vector field  $\xi$ ).** *For the Lipschitz vector field  $\xi : \mathbb{R}^n \rightarrow \mathbb{R}^n$ , and the evolution parameter  $t \in \mathbb{R}$ , let  $\varphi : \mathbb{R} \times \mathbb{R}^n \rightarrow \mathbb{R}^n$  be the flow generated by  $\xi$ .*

**Lemma 2.4.8.** *The vector field  $\xi : \mathbb{R}^n \rightarrow \mathbb{R}^n$ , given by  $\xi(\mathbf{x}) := \xi_n(\mathbf{x}) + \varepsilon\eta(\mathbf{x})s(\mathbf{x})$ , is collapsing on  $W^n$ , meaning that the set  $W^n := N^{\geq\alpha}(\Omega, u) \cap [0, 1]^n$  is a Ważewski set for the flow  $\varphi$ , and that  $W^o = W$ . Additionally, the exit set  $W^-$  is the  $(n-1)$ -dimensional set given by  $W^- = W^n \cap \partial[0, 1]^n$ .*

*Proof.* The set  $W^n$  is closed, so the first condition of Definition 2.4.2 is satisfied. We will establish the second condition of Definition 2.4.2 by noticing  $W^-$  is closed when we resolve  $W^-$  below. The main content of this theorem is to see that  $W^o = W^n$  and that  $W^-$  is the  $(n-1)$ -dimensional set given by  $W^- = W^n \cap \partial[0, 1]^n$  – or more plainly, that every point of  $W^n$  gets carried out of  $W^n$  in finite time, and only through the portions of the  $(n-1)$ -dimensional faces of  $[0, 1]^n$  where  $u$  is nonnegative.

To obtain  $W^o = W^n$ , notice first that  $W^o \subset W^n$  by construction. The fact that  $W^n \subset W^o$ , i.e. that every  $\mathbf{x} \in W^n$  is pushed out of  $W^n$  in finite time, we recall the LaSalle invariance principle (see [1]). The function  $-u$  is a (strict) Lyapunov function for  $\varphi$  on the closed set  $W^n$ , since  $\nabla(-u(\mathbf{x})) \cdot \xi(\mathbf{x}) < 0$  for  $\mathbf{x} \in W^n$ . Suppose there exists an  $\mathbf{x} \in W$  that is not pushed out of  $W$  in finite time, i.e. that  $\omega(\mathbf{x}) \subset W^n$ . Then LaSalle invariance requires that  $\omega(\mathbf{x}) \subset \Gamma := \{\mathbf{y} \in W^n : \nabla(-u(\mathbf{y})) \cdot \xi(\mathbf{y}) = 0\}$ , but  $\Gamma$  is empty because  $\nabla(-u(\mathbf{y})) \cdot \xi(\mathbf{y}) < 0$  for all  $\mathbf{y} \in W^n$ . This shows that all  $\mathbf{x}$  leave  $W^n$  in finite time.

To obtain  $W^- = W^n \cap \partial[0, 1]^n$ , we have  $(W^n \cap \partial[0, 1]^n) \subset W^-$  since points from the  $(n-1)$ -dimensional faces of  $[0, 1]^n$  leave  $W$  immediately under  $\varphi$ . To see  $W^- \subset (W^n \cap \partial[0, 1]^n)$ , note that  $\mathbf{x} \in W^-$  will not be pushed across any level set line by  $\varphi$  (by virtue of  $\nabla u(\mathbf{x}) \cdot \xi(\mathbf{x}) > 0$ ), so can only exit through the boundary of the box where  $u$  is nonnegative, i.e.  $W^n \cap \partial[0, 1]^n$ .

Finally we see that  $W^- = W^n \cap \partial[0, 1]^n$  is closed, being the intersection of two closed sets, so  $W^n$  satisfies the second condition of Definition 2.4.2, hence  $W^n$  is a Ważewski set. □

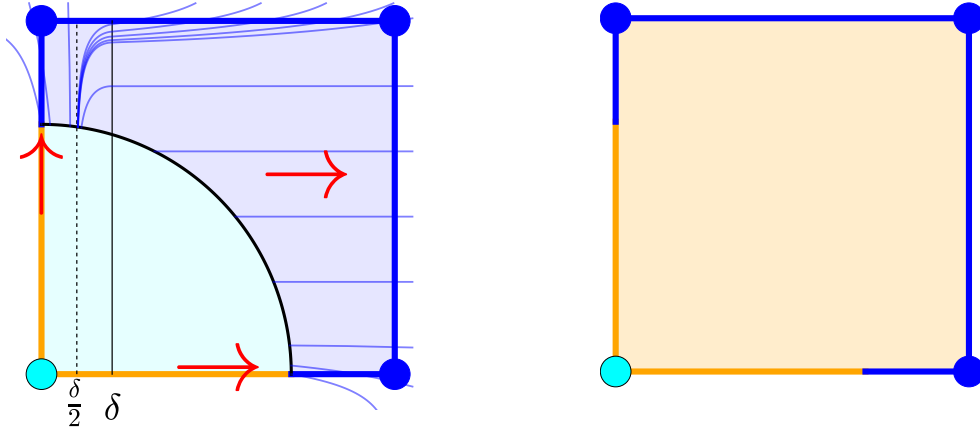


Figure 2.6: The vector field  $\xi$ , from Lemma 2.4.8, applied to the set  $W^2 = N^{\geq \alpha}(\Omega, u) \cap \mathbb{R}^2$ . Cyan indicates the domain on which  $u$  is negative, and blue indicates the domain on which  $u$  is positive. Red arrows indicate the direction of monotonicity established by the algorithm (V). Some trajectories of the flow generated by  $\xi$  are drawn as blue lines moving out of the rectangle. The right panel is an illustration of Lemma 2.4.8, which establishes the fact that the two-dimensional blue set  $W^2$  collapses onto the one-dimensional set  $W^2 \cap \partial \mathbb{R}^2$ .

We are now ready to prove Theorem 2.4.4.

*Proof.* For an arbitrary  $n$ -cell  $R^n \in \mathbf{cmplx}$  which has been validated as monotone along a coordinate direction, Lemma 2.4.8 establishes that the  $(n-1)$ -dimensional set  $W^- = W^n \cap \partial[0, 1]^n$  is a strong deformation retraction of  $W^n = N^{\geq \alpha}(\Omega, u) \cap [0, 1]^n$ . This implies that the  $(n-1)$ -dimensional set  $W^-$  is the set of fixed points for the strong deformation retraction (and is therefore closed), hence all of the information from the original validation procedure remains true on  $W^-$ . Furthermore, because the vector field  $\xi$  is always increasing with respect to  $u$ , the monotone  $n$ -cell  $R^n$  has been collapsed onto a subset of the  $(n-1)$ -dimensional cells in  $\mathbf{cmplx}$  which have either been validated as monotone, or have been validated as positive. At this point, all of the results established in this section are valid for arbitrary  $(n-1)$ -dimensional cells  $R^{n-1}$  which have been validated as monotone, and the relevant set to collapse is the  $(n-1)$  dimensional set  $W^- = \partial W^n$ . For some dimension  $k > 0$  there will be no more cells  $R^k$  from  $\mathbf{cmplx}$  which have been validated as monotone, and we are left with  $\mathbf{cmplx}^+$ . As these collapses have all carried the homotopy type of the

$k$ -dimensional set  $W^k$  onto the  $(k-1)$ -dimensional set  $W^-$ , the homotopy type of  $N^{\geq \alpha}(\Omega, u)$  is the same as that of  $\mathbf{cmplx}^+$ .  $\square$

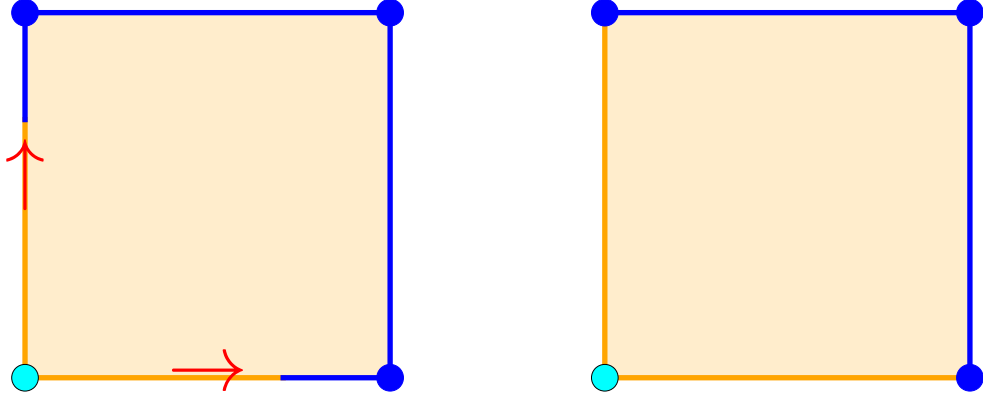


Figure 2.7: The left panel shows a cell  $R^2$  from  $\mathbf{cmplx}$  after a collapse from  $W^2$  onto  $W^2 \cap \partial R^2$ , cf. Figure 2.6. Each cell in  $\mathbf{cmplx}$  still holds information obtained during the validation algorithm – in this case two one-cells are seen to be monotone along the directions indicated by the red arrows (the remaining one-cells have been validated as positive). The panel on the right illustrates an application of Theorem 2.4.4, with  $W^1 := W^2 \cap \partial R^2$ , to establish the fact that  $N^{\geq \alpha}(\Omega, u) \cap \partial R^2$  is homotopy equivalent to the subcomplex of  $\mathbf{cmplx}^+$  indicated by the two dark blue edges and three dark blue vertices.

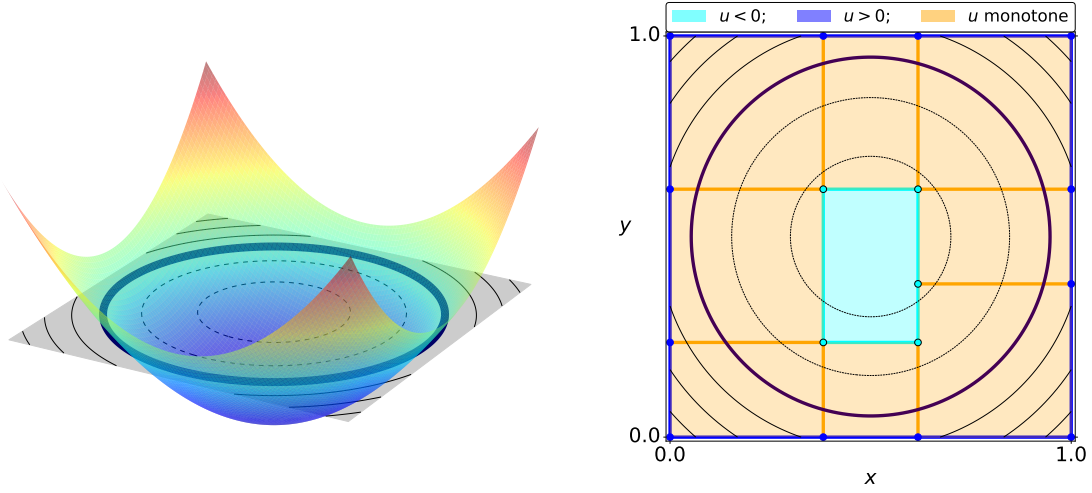


Figure 2.8: The left panel shows the paraboloid used in this example, with minimum below the  $(x, y)$ -plane. The right panel shows the output of the validation algorithm run on this paraboloid over a patch  $\Omega \subset \mathbb{R}^2$ . Cells from the rectangular cell complex `cmplx` have been flagged as positive (blue), negative (cyan), and validated as monotone (orange). Theorem 2.4.4 establishes that the 0-superlevel set of the paraboloid on this patch is homotopy equivalent to the subcomplex `cmplx+` of `cmplx`, indicated in dark blue.

## 2.5 Examples

### 2.5.1 A Random Trigonometric Polynomial

The algorithm developed in the recent paper [23] is intended to compute persistent homology of sublevel sets of real-valued functions  $u : \mathbb{R}^n \rightarrow \mathbb{R}$ . In §2.2 we described the similarity between their approach and ours, perhaps most notably the appeal to the Ważewski theorem 2.4.3 to establish the correctness of the approximating complex. While the goal of [23] is different than ours, we still think it is useful to compare the resulting cellular approximations obtained by their method with ours. In §8.2 of [23], the random trigonometric polynomial

$$\begin{aligned}
 u(x, y) = & \sum_{i=1}^5 \sum_{j=1}^5 a_{i,j,1} \sin(2\pi i x) \sin(2\pi j y) + a_{i,j,2} \sin(2\pi i x) \cos(2\pi j y) \\
 & + a_{i,j,3} \cos(2\pi i x) \sin(2\pi j y) + a_{i,j,4} \cos(2\pi i x) \cos(2\pi j y),
 \end{aligned} \tag{2.6}$$

where the coefficients  $a_{i,j,k}$  are taken from a normal distribution of mean zero and standard deviation one, is introduced, and the persistence homology of  $\alpha$ -sublevel sets (or  $\alpha$ -superlevel sets of  $-u$ ) is computed. We have applied our algorithm to the function in (2.6) and obtained the rectangular cell complex shown in the right panel of Figure 2.9. Two fundamental differences between their work and ours are that: (1) Our subdivisions result in a non-uniform refinement of the approximating CW complex `cmplx`, where the side lengths are chosen randomly at runtime from the set of fractions defined by the golden ratio, as discussed in §2.3.4. This differs from the algorithm in [23] in that it permits smaller complexes (fewer overall cells), and is capable of recovering from grid alignment issues because we are free to discard a particular subdivision and choose a new subdivision point from a user-defined set; and (2) Our vector field  $\xi$  which establishes the collapse is defined for more general configurations of  $W^k := N^{\geq \alpha}(\Omega, u) \cap R^k$ , for cells  $R^k \in \text{cmplx}$  (cf. our §2.4 and §6 of [23]). This means that we are able to establish a collapse of  $W^k$  onto  $\partial W^k$  more easily, resulting in fewer subdivisions, ultimately resulting in a smaller approximating complex `cmplx`. We provide Figure 2.9 for direct comparison with the method in 2.3.4. We report the number of cells in the approximating complex in the caption of the figure, and note that, for  $\alpha = 0$ , the validation algorithm (V) completes within twenty minutes, on average, for this example.



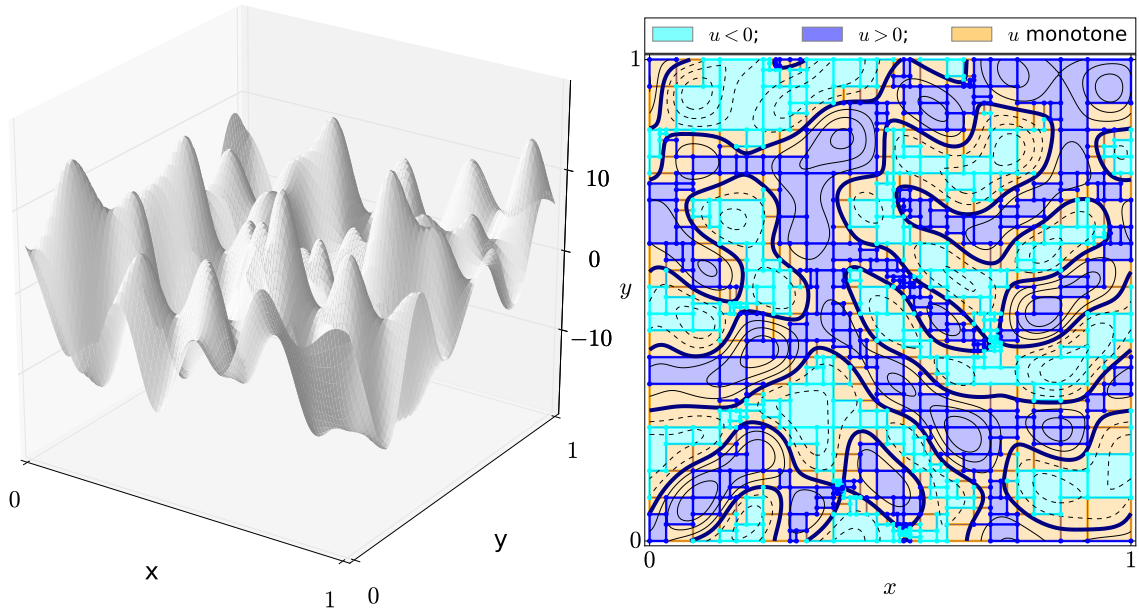


Figure 2.9: The CW complex has 642 cells of dimension two, 1,778 of dimension one, and 1,137 cells of dimension zero. The panel on the left is an approximation of the surface for the function  $u$  given by Equation (2.6). The right panel shows positive cells in dark blue, monotone cells in orange, and negative cells in cyan.

### 2.5.2 An Atoll-like Superlevel Set

The solution set of the following equation describes a downward-opening paraboloid with a sagging apex. The example comes from [31], Example 6.12, where it is introduced as an ‘ill-posed’ problem in the sense that its zero-level sets can be made arbitrarily close to one another, making them difficult to resolve numerically. We use it here because as the distance between the concentric rings becomes smaller, the height of the positive part of the function also becomes smaller, and thus more susceptible to numerical errors. The superlevel set is also curved, which we presume to pose a challenge to rectangular approximation. Let

$$f(x, y) = (x^2 + y^2 - 1) (x^2 + y^2 - 1.01). \quad (2.7)$$

This function has two zero-level sets in the form of concentric circles centered at the origin with radius 1 and  $\sqrt{1.01}$ , where the positive zero-superlevel set is the narrow band

between the circles. The input to the algorithm is the function  $u$  and the rectangular region  $[-1.5, 1.5] \times [-1.5, 1.5] \subset \mathbb{R}^2$ . The output is the CW-complex approximation `cmplx`, holding the inner approximation of the superlevel set  $\mathcal{N}^{\geq 0}(u)$  as `cmplx+`. We compute the Betti numbers from the homology groups of `cmplx+` and arrive at  $\beta_0 = 1, \beta_1 = 1, \beta_2 = 0$ , corresponding to the topological characterization of a ring. See Figure 2.10 for a plot of the individual cells in the CW-approximation to  $N^{\geq 0}(\Omega, u)$ .

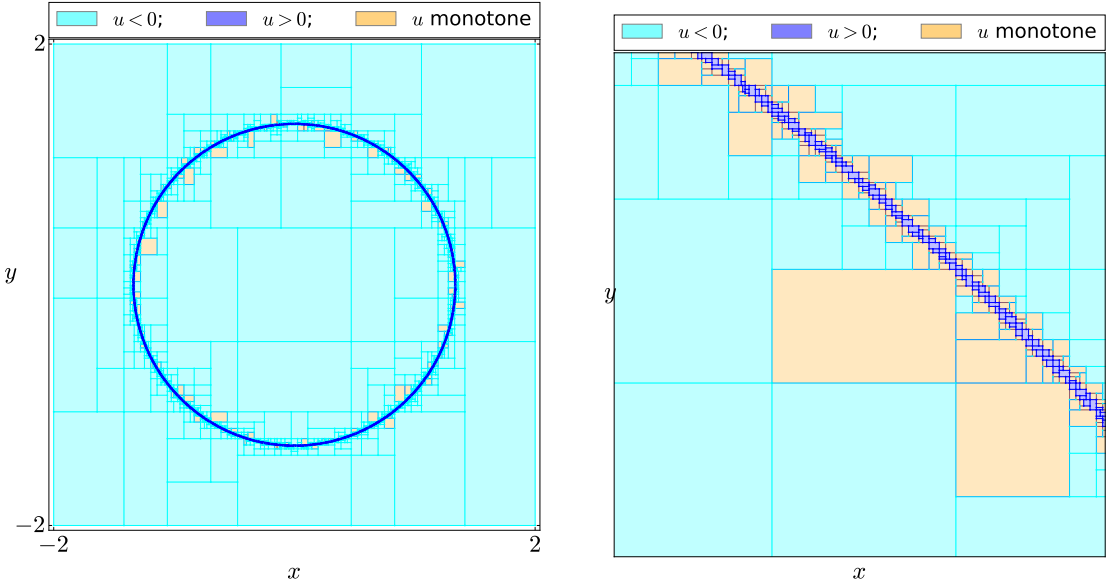


Figure 2.10: The CW complex has 17,632 cells of dimension two, 27,308 of dimension one, and 9,677 cells of dimension zero. The left panel shows positive cells in dark blue for the function  $u$  given by Equation (2.7). On the right is a zoomed-in image giving a detailed view of the subdivisions made by the algorithm. Passing the rectangular cell complex to PHAT [6] yields Betti numbers  $\beta_0 = 1$  and  $\beta_1 = 1$  for the superlevel set  $N^{\geq 0}(\Omega, u)$ , as expected.

### 2.5.3 The Double-torus, a Three-dimensional Example

Consider the function  $f : \mathbb{R}^3 \rightarrow \mathbb{R}$  given by

$$f(x, y, z) = -[(x^2 + y^2)^2 - x^2 + y^2]^2 - z^2 + \frac{1}{100}. \quad (2.8)$$

The level set  $\{(x, y, z) \in \mathbb{R}^3 : f(x, y, z) = 0\}$  forms the surface of a double torus in such a way that  $\mathcal{N}^{\geq 0}(\Omega, u)$  forms the interior of the torus and  $\mathcal{N}^{\leq 0}(\Omega, u)$  forms the exterior of the torus. As input to the algorithm we supply  $u$  and the rectangular region  $\Omega := [-1, 1] \times [-1, 1] \times [-0.35, 0.35] \subset \mathbb{R}^3$ . The output is the CW-complex approximation `cmplx`, holding the inner approximation of the superlevel set  $\mathcal{N}^{\geq 0}(u)$  as `cmplx+`. We compute the Betti numbers from the homology groups of `cmplx+` and arrive at  $\beta_0 = 1, \beta_1 = 2, \beta_2 = 0$ , and  $\beta_3 = 0$ , corresponding to the topological characterization of the solid double torus (the positive cells live inside the torus). See Figure 2.11 for a plot of the individual cells in the CW-approximation to  $N^{\geq 0}(\Omega, u)$ . Cells of select dimension have been plotted in Figure 2.11.

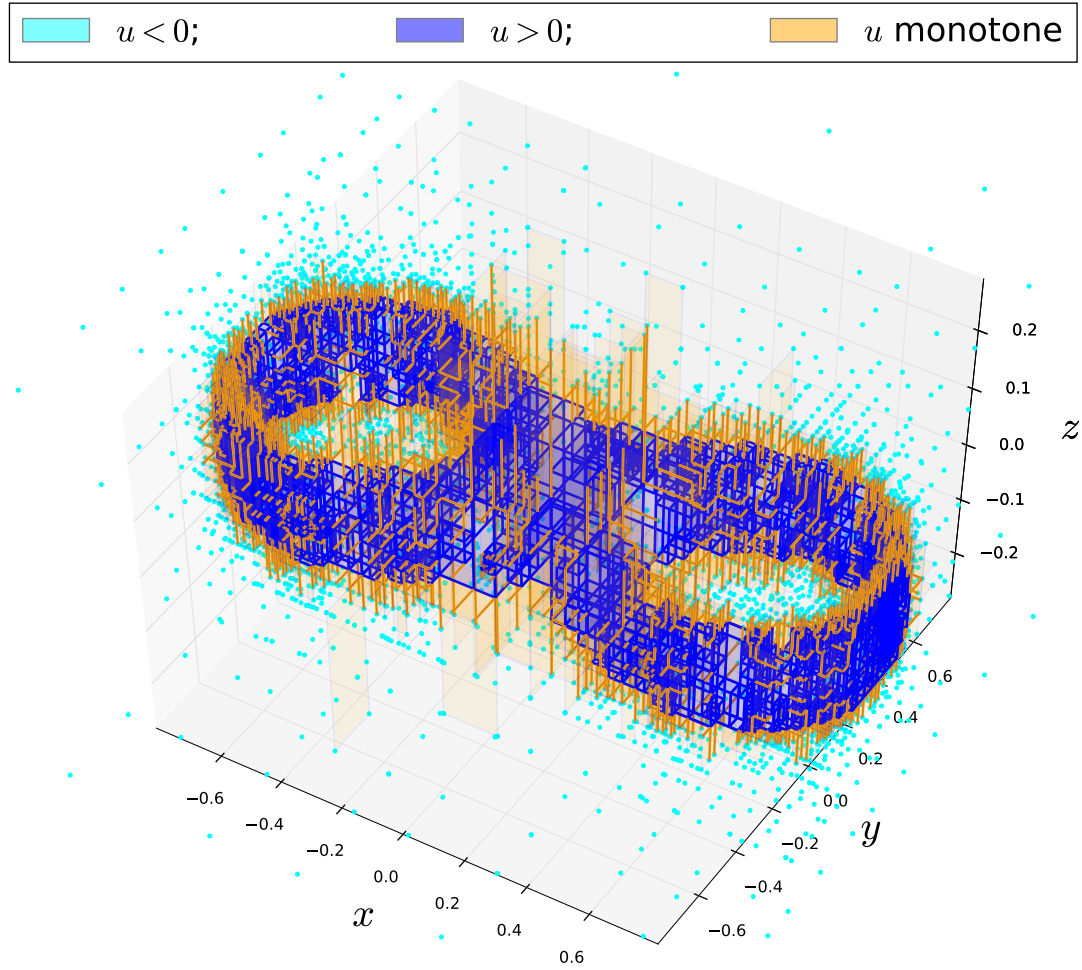


Figure 2.11: The CW complex has 2,797 cells of dimension three, 15,294 of dimension two, 23,905 of dimension one, and 11,409 cells of dimension zero. The figure shows the one and two dimensional cells in `cmplx+` in dark blue, and just vertices in `cmplx` which were validated as negative. Monotone cells of dimension one and two are shown in orange. The Betti numbers  $\beta_0 = 1$ ,  $\beta_1 = 2$ ,  $\beta_2 = 0$ , and  $\beta_3 = 0$ , were computed directly from `cmplx+`, and correspond to the topological characterization the solid double torus.

## Chapter 3: Rigorous Isolating Blocks for Flows and their Conley Indices

The goal of this chapter is to develop a rigorous computational framework to accompany the Conley index for continuous flows in  $\mathbb{R}^n$ . We begin with general background introducing the Conley index in our context in §§3.1, 3.2, and 3.3, and §3.4 outlines the current state of the art. There are two main contributions in this chapter that are new, namely: (1) A new perspective on an abstract construction in Conley index theory, the isolating block. This new perspective allows for a computable characterization of Conley's abstract object, and is found in §3.5; and (2) A new, rigorous algorithm based on the work in Chapter 2, which provides the concrete realization of isolating blocks, and is described in §3.6. This work has been published in [36], however this chapter contains perspective and details not found in the paper.

### 3.1 Flows and Bounded Invariant Sets

The following section establishes the setting we will work in for the entirety of this chapter, and fixes our notation for some standard concepts in dynamical systems.

#### 3.1.1 Qualitative Perspective

Let  $f : \mathbb{R}^n \rightarrow \mathbb{R}^n$  be a Lipschitz vector field and consider a model that evolves according to

$$\dot{x}(t) := \frac{dx}{dt} = f(x(t)). \tag{3.1}$$

For example, consider

$$\dot{x} = f(x) = \begin{pmatrix} x_1(1 - x_1) \\ -x_2 \end{pmatrix}, \quad (3.2)$$

which may describe the flow of water over a landscape whose topography corresponds locally to the height function  $F(x_1, x_2) = -\frac{x_1^2}{2} + \frac{x_1^3}{3} + \frac{x_2^2}{2}$ , shown in Figure 3.1. In this scenario  $f$  is defined by the steepest descent along the landscape  $F$ , so that  $f(x) := -\nabla F(x)$ .

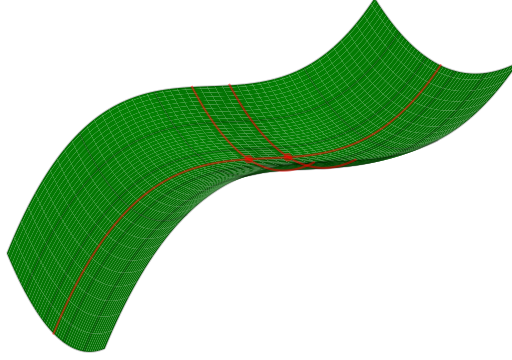


Figure 3.1: Plot of the ‘landscape’  $F(x_1, x_2) = -\frac{x_1^2}{2} + \frac{x_1^3}{3} + \frac{x_2^2}{2}$ , corresponding to (3.2). The saddle point  $(0, 0, F(0, 0)) \in \mathbb{R}^3$  and the sink  $(1, 0, F(1, 0)) \in \mathbb{R}^3$  are plotted on the landscape, along with red lines corresponding to the images of the  $x$  and  $y$  axes.

Given such a model one can describe the path that a floating bead would follow if it were placed onto this landscape. To accomplish this one specifies the *initial value*  $x(0) = \xi \in \mathbb{R}^2$ , which is the starting position of the float on the landscape. The path that the float will take is specified by the *solution to the initial value problem*  $x(t) = \xi + \int_0^t f(x(s)) ds$  (Picard-Lindelöf guarantees, in this setting, that the solution exists and is unique on some time interval around  $t_0 = 0$ ,  $[t_0 - \varepsilon, t_0 + \varepsilon] \subset \mathbb{R}$ ,  $\varepsilon > 0$ , meaning that it is also possible to resolve the path that an object would have taken in order to get where it is now, see [1])<sup>1</sup>.

---

<sup>1</sup>We are not interested integrating the vector field  $f$  in this thesis, but we would like to point out that, aside

The above paragraph recalls the standard solutions-based perspective of ordinary differential equations. Individual solutions  $x(t)$  parameterize curves in the *phase space* of (3.2), which is just the domain of the vector field  $f : \mathbb{R}^2 \rightarrow \mathbb{R}^2$ . Plotting several solutions at once, as in Figure 3.2, begins to reveal how the vector field twists the phase space into organized structures. For example, several solutions of (3.2) reveal that the topography of the landscape may have a saddle point with a shallow basin nearby. Resolving features such as basins of attraction, saddle points, and paths connecting them are topics in the dynamics-based perspective of differential equations, and this is the perspective that we will take in this chapter.

In order to move from initial value problems to the more global perspective, we introduce the map  $\varphi : \mathbb{R} \times \mathbb{R}^n \rightarrow \mathbb{R}^n$  defined uniquely by the property that for every  $\xi \in \mathbb{R}^n$ ,  $\varphi$  is the unique solution of the initial value problem  $\dot{x} = f(x)$ ;  $x(0) = \xi$ . The map  $\varphi$  is referred to as the *flow map generated by  $f$* , or just simply the **flow** for (3.1). The following two useful properties<sup>2</sup> of flows hold for all  $x \in \mathbb{R}^n$ , and for all  $t_1, t_2 \in \mathbb{R}$ :

- (i)  $\varphi(0, x) = x$
- (ii)  $\varphi(t_1 + t_2, x) = \varphi(t_2, \varphi(t_1, x))$

Notice that (3.2) specifies a system of two separable differential equations, so we can explicitly write down a mapping  $\tilde{\varphi}$  as

$$\tilde{\varphi} : (t, x) \mapsto \begin{pmatrix} \frac{x_1}{x_1 + (1 - x_1)e^{-t}} \\ x_2 e^{-t} \end{pmatrix} \quad (3.3)$$

The map  $\tilde{\varphi}$  is not a global flow in the sense we require. In particular, points  $x = (x_1, x_2) \in \mathbb{R}^2$  having  $x_1 < 0$  have orbits under  $\tilde{\varphi}$  which are not defined for all  $t \in \mathbb{R}$ . Noticing that this

---

from standard numerical integration techniques such as Runge-Kutta, there exist many rigorous numerical integrators, such as VNODE [30]

<sup>2</sup>The map  $\varphi : \mathbb{R} \times \mathbb{R}^n \rightarrow \mathbb{R}^n$  is a *continuous group action*, where the topological group  $\mathbb{R}$  is acting on the topological space  $\mathbb{R}^n$ . Much of the terminology for flows comes from algebra and topology. The map  $\varphi$  is sometimes called a *dynamical system* generated by the vector field  $f$ .

is a feature of the vector field  $f$  in (3.2), we can always recover a global flow through a reparameterization of the map  $\tilde{\varphi}$  by considering the associated equation

$$\dot{x} = \frac{f(x)}{1 + \|f(x)\|^2}. \quad (3.4)$$

Equation (3.4) is guaranteed to generate a global flow, and the orbits of (3.4) coincide with the orbits of (3.2). With this rescaling in mind, we will henceforth refer to the flow associated with (3.1) by the mapping  $\varphi : \mathbb{R} \times \mathbb{R}^n \rightarrow \mathbb{R}^n$ , which may have been generated by the normalization (3.4).

The benefit of working with  $\varphi : \mathbb{R} \times \mathbb{R}^2 \rightarrow \mathbb{R}^2$  comes from the fact that entire subsets of the phase space can be evolved according to (3.2), providing a formal meaning to the intuitive notion of the ‘flow’ of water over the landscape in our example. We can now interpret Figure 3.2 as a view of the map  $\varphi$  acting on the entire landscape at once, and is called a *phase portrait*, and is the most convenient guide in the study of a dynamical system.



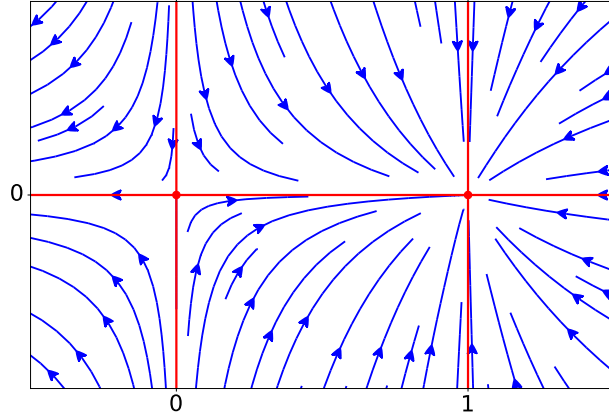


Figure 3.2: Phase portrait for (3.2). Arrows indicate the path a floating bead would take if it were placed on the landscape shown in Figure 3.1. These integral curves can be viewed either as a collection of particular solutions to initial value problems derived from (3.2), or one can interpret this as an indication of how the flow defined in (3.3) acts on the phase space  $\mathbb{R}^2$ .

For the differential equation (3.1) and its associated flow  $\varphi$ , we call  $\varphi(\mathbb{R}, \xi) \subset \mathbb{R}^n$  the *orbit of  $\xi$* , or the *solution of (3.1) through  $\xi$* . This corresponds to the initial value problem specified by (3.1), with the initial value  $x(0) = \xi$ , in the sense that, from the solutions-based perspective, the solution would be  $x(t) = \xi + \int_0^t f(x(s)) ds$ , whereas in the present notation we have  $\varphi(t, \xi) = x(t)$ , so that  $\varphi(0, \xi) = x(0) = \xi$ . Harnessing the full utility of  $\varphi$ , we say that a subset  $S \subset \mathbb{R}^n$  is *invariant under the action of  $\varphi$*  if  $\varphi(\mathbb{R}, S) = S$ . Of immediate interest are the **bounded invariant sets**, sets  $S \subset \mathbb{R}^n$  such that  $\varphi(\mathbb{R}, S) = S$  and the diameter of the set  $S$  is finite. Examples of bounded invariant subsets of the flow of a differential equation are fixed points, periodic orbits, heteroclinic, and homoclinic orbits. Letting  $\mathbb{R}^+$  denote the nonnegative reals and  $\mathbb{R}^-$  the nonpositive reals, we will use the term *forward orbit* of a point  $\xi \in \mathbb{R}^n$  to mean  $\varphi(\mathbb{R}^+, \xi)$ , and *backward orbit* to mean  $\varphi(\mathbb{R}^-, \xi)$ . A set  $S \subset \mathbb{R}^n$  being *positively invariant* will mean that  $\varphi(\mathbb{R}^+, S) \subset S$ , and *negatively invariant* will mean that  $\varphi(\mathbb{R}^-, S) \subset S$ .

We illustrate the above structures in the phase portrait for Equation (3.2), shown in

Figure 3.2. Recall that the flow  $\varphi : \mathbb{R} \times \mathbb{R}^2 \rightarrow \mathbb{R}^2$  is given by (3.3). One can check that if  $S = (0, 1) \times \{0\} \subset \mathbb{R}^2$ , then the orbit of any point  $\xi \in S$  remains in  $S$ . In fact,  $S$  is a bounded invariant set for  $\varphi$ . The set  $\{0\} \times (0, \infty) \subset \mathbb{R}^2$  is an invariant set under the action of  $\varphi$ , but it is not bounded. Unions of invariant sets are invariant, for example the entire vertical axis  $(\{0\} \times (0, \infty)) \cup (\{0\} \times \{0\}) \cup (\{0\} \times (0, -\infty)) \subset \mathbb{R}^2$  is made up from three invariant sets, and is itself invariant. Finally, we point out that the fixed points  $(0, 0)$  and  $(1, 0)$  are bounded invariant sets for  $\varphi$ .

### 3.1.2 Remarks about the Quantitative Perspective

Bounded invariant sets of a flow are comprised of unions of orbits, and computing a single orbit directly from a flow can be surprisingly difficult. A property of continuous flows is that orbits do not intersect, that is, for distinct initial values  $\varphi(0, \xi_1) \neq \varphi(0, \xi_2)$ , we obtain  $\varphi(\mathbb{R}, \xi_1) \cap \varphi(\mathbb{R}, \xi_2) = \emptyset$ . Thus, between numerical approximation error and floating point truncation error, a direct iterative computation along a trajectory from one time step to the next, i.e. from  $\varphi(t_0, \xi_1)$  to  $\varphi(t_1, \xi_1)$ , will almost surely land on  $\varphi(t_1, \xi_2)$  for some  $\xi_2 \neq \xi_1$ . Many flows have orbits that are unstable with respect to the elements they act upon, meaning that while  $\varphi(t_0, \xi_1)$  and  $\varphi(t_0, \xi_2)$  may be nearby, the points  $\varphi(t_1, \xi_1)$  and  $\varphi(t_1, \xi_2)$  may be very far apart. This suggests that direct numerical approximation may lead to vastly different long-term behavior stemming from nearly identical initial states.

In addition to numerical errors along a trajectory, a structural instability of the flow itself may contribute to incorrect results from direct computation. For example, consider the equation  $\dot{x} = x^2 + \lambda$ . For  $\lambda < 0$  the flow generated by this equation has three bounded orbits consisting of one stable and one unstable equilibrium at  $x = -\sqrt{|\lambda|}$  and  $x = \sqrt{|\lambda|}$ , respectively, along with the orbit connecting  $x = \sqrt{|\lambda|}$  to  $x = -\sqrt{|\lambda|}$ . For  $\lambda = 0$  this equation has a single bounded orbit, the degenerate equilibrium  $x = 0$ , and for  $\lambda > 0$  this equation has no bounded orbits whatsoever. These are significant qualitative dynamical differences, and each can easily be obtained for perturbations of  $\lambda$  near zero.

On the other hand,  $\varphi$  is a very nice map in the abstract. We will see that, in the spirit of the Brouwer degree, one can seek admissible subsets of the phase space, make computations far away from sensitive behavior, and obtain results that hold for perturbations of the flow at hand. The framework we consider is Conley index theory, and it offers a means of extracting information about these sensitive structures indirectly. The results are formulated in the abstract, using properties of flow maps and the relative compactness of the phase space  $\mathbb{R}^n$ . One half of our work in this chapter can be seen as a way to cast the abstract objects of Conley's theory in terms of eminently computable information. The other half of our work is doing the actual computations!

## 3.2 Isolated Invariant Sets, Isolating Blocks, and the Conley Index

An **isolated invariant set**  $\mathcal{S}$  is the maximal invariant set contained in the interior of a compact neighborhood of itself. Call such a compact neighborhood an **isolating neighborhood**  $\mathcal{N}_{\mathcal{S}}$ . The term maximal indicates that an isolated invariant set is made up from a union of invariant sets,  $S_i$ . The verbiage ‘interior of a compact neighborhood of itself’ is used to indicate that  $\mathcal{S}$  (and therefore each  $S_i$ ) do not touch the boundary of the isolating neighborhood,  $\partial\mathcal{N}_{\mathcal{S}}$ .

The condition that  $\mathcal{S} = \bigcup S_i$  is contained in  $\text{int}\mathcal{N}_{\mathcal{S}}$  should be thought of as a condition on the union rather than on the compact neighborhood  $\mathcal{N}_{\mathcal{S}}$ . To gain some intuition, consider the flow depicted in Figure 3.2. Take  $S_1 = \{(0,0)\}$ ,  $S_2 = \{(1,0)\}$ , and  $S_{12} = \{(x,0) : 0 < x < 1\}$ . Each of these sets are bounded invariant sets for the flow given by (3.3), and  $\mathcal{S} = S_1 \cup S_2 \cup S_{12}$  is actually an isolated invariant set. If we choose the compact set  $\mathcal{N} = \{(x,y) : \sqrt{(x-1/2)^2 + y^2} \leq 1/2\}$ , the disc centered at  $(1/2,0)$ , then  $\mathcal{N}$  is not an isolating neighborhood for  $\mathcal{S}$  because the equilibria  $S_1$  and  $S_2$  touch  $\partial\mathcal{N}$ . This is not a deficiency of  $\mathcal{S}$ , rather a deficiency in our choice of  $\mathcal{N}$  (to remedy this, simply increase the radius of the disc  $\mathcal{N}$  by any positive amount). On the other hand, consider the equation

$\dot{x} = (x_2, -x_1)$ , whose phase portrait is shown in Figure 3.3. For any compact  $\mathcal{N} \subset \mathbb{R}^2$  which contains the origin, the maximal invariant set contained in  $\mathcal{N}$  will touch the boundary  $\partial\mathcal{N}$ . This is a deficiency in the structure of the bounded invariant sets for this equation.

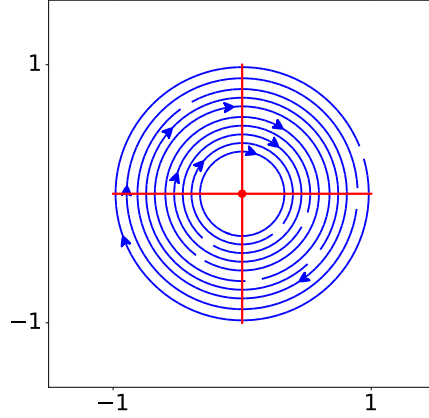


Figure 3.3: Phase portrait for  $\dot{x} = (x_2, -x_1)$ . Arrows indicate the direction of the flow. The origin is called a center, and cannot be isolated.

Provided that  $\mathcal{S}$  is not empty, the closedness of both  $\mathcal{S}$  and  $\mathcal{N}_{\mathcal{S}}$  permit  $\mathcal{N}_{\mathcal{S}}$  to remain an isolating neighborhood for any flow generated by a vector field  $\tilde{f}$  in a sufficiently small neighborhood of  $f$  (where the ‘neighborhood’ is taken in the  $C^0$  topology on Lipschitz vector fields, see [12], and Theorem 1.7 in [13]). With this we have the first step in the analogy with the Brouwer degree – the isolating neighborhoods play the role of admissible sets. A class of isolating neighborhoods suitable for computation are **isolating blocks**, defined below.

**Definition 3.2.1.** *An isolating block  $\mathcal{B} \subset \mathbb{R}^n$  is an isolating neighborhood with the additional properties*

- (i)  $\mathcal{B}^- := \{x \in \mathcal{B} : \varphi([0, T], x) \not\subset \mathcal{B} \text{ for all } T > 0\}$  is closed, and
- (ii)  $\text{Inv}_T(\mathcal{B}, \varphi) := \{x \in \mathcal{B} : \varphi([-T, T], x) \subset \mathcal{B}\} \subset \text{int}\mathcal{B}$  for all  $T > 0$ .

We look first at Property (ii). This should be thought of as a condition barring any ‘internal tangencies’, these would be orbits that travel in  $\text{int } \mathcal{B}$ , come to the boundary of  $\mathcal{B}$ , and then back into  $\text{int } \mathcal{B}$ . Property (i) concerns the **exit set**  $\mathcal{B}^-$ , this is the set of points which immediately leave  $\mathcal{B}$  in forward time under the flow. We also put  $\mathcal{B}^+ := \{x \in \mathcal{B} : \varphi([-T, 0], x) \not\subset \mathcal{B} \text{ for all } T > 0\}$ , denoting the set of points that are immediately pushed into  $\mathcal{B}$  in forward time. Note that the closedness of the exit set  $\mathcal{B}^-$  is part of the definition of an isolating block, and does not follow automatically<sup>3</sup> from Property (ii).

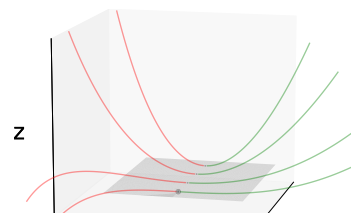
Isolating blocks are examples of the more general concept of an index pair introduced by Conley in [12], but the work in this thesis does not make direct use of them. For reference, given an isolating block  $\mathcal{B}$  and its exit set  $\mathcal{B}^- \subset \mathcal{B}$ , the ‘pair’ is formed by  $(\mathcal{B}, \mathcal{B}^-)$ .

The **homological**<sup>4</sup> **Conley index** of an isolated invariant set  $\mathcal{S}$  is defined by

$$CH_*(\mathcal{S}) := H_*(\mathcal{B}, \mathcal{B}^-), \quad (3.5)$$

where  $H_*(\mathcal{B}, \mathcal{B}^-)$  is relative homology. In all of our applications, the relative homology operation can be thought of as collapsing  $\mathcal{B}^- \subset \mathcal{B}$  to a point, and then computing the reduced homology groups of the resulting space. In all computations we will report the

<sup>3</sup> More should be said here. First of all, we will need closedness so that  $\mathcal{B}^-$  may coincide with the set of fixed points of a strong deformation retraction (cf. §3.3.2). Additionally, Property (ii) does not automatically imply that  $\mathcal{B}^-$  is closed. Indeed, let  $\varphi$  be generated by  $(\dot{x}, \dot{y}, \dot{z}) = (0, -y-1, -15x^2y-y^2)$ , and let  $\mathcal{B}$  coincide with the plane  $z = 0$  in a neighborhood of the origin  $(0, 0, 0) \in \mathbb{R}^3$ . Selected trajectories of this system are shown to the right. For  $p \rightarrow (0, 0, 0)$  along the line  $\{(x, 0, 0) : x \geq 0\}$ , we see that  $p \in \mathcal{B}^-$ , except at the origin, so  $\mathcal{B}^-$  is not closed, while at the same time  $\varphi([- \varepsilon, \varepsilon], p) \not\subset \mathcal{B}$ , so these points do not destroy Property (ii). In the language of Lemmas 3.5.2 and 3.5.3, we have that  $u(p) > 0$  on the open line segment, and that  $u(p) = v(p) = 0$  at the origin. This is a pathological scenario, and zero is not a regular value of  $u$ , so  $\mathcal{B}$  can be perturbed locally to avoid this configuration.



<sup>4</sup>If one considers an isolating block  $\mathcal{B}$  and its exit set  $\mathcal{B}^- \subset \mathcal{B}$  as forming an index pair, then the Conley index of the maximal invariant set  $\mathcal{S}$  in  $\text{int } \mathcal{B}$  is defined as the homotopy type of the pointed topological space  $(\mathcal{B}/\mathcal{B}^-, [\mathcal{B}^-])$ , where  $\mathcal{B}/\mathcal{B}^-$  is the quotient of  $\mathcal{B}$  by  $\mathcal{B}^-$ , and  $[\mathcal{B}^-]$  is the equivalence class:  $x \sim y$  if and only if  $x, y \in \mathcal{B}^-$ , which essentially collapses  $\mathcal{B}^-$  to a point. For results on pointed topological spaces we refer the reader to [27], [29], [25], and [12]. We use the weaker homological formulation of the Conley index because homology is a computable homotopy invariant of a topological space, and often homology groups are sufficient to distinguish between two spaces having different homotopy type (refer to §2.1.1 for definitions related to homotopies and homotopy equivalence).

homological Conley index as the sequence of abelian groups  $\{CH_k(\mathcal{S})\}_{k=0}^\infty$ , written as

$$CH_*(\mathcal{S}) = \{CH_0(\mathcal{S}), CH_1(\mathcal{S}), CH_2(\mathcal{S}), \dots\}. \quad (3.6)$$

**Example: the Conley index of a hyperbolic fixed point.** Consider the ordinary differential equation  $\dot{x} = f(x) = (x_1, -x_2)$ . The flow generated by  $f$  can be written explicitly as  $\varphi : (t, x) \mapsto (x_1 e^t, x_2 e^{-t})$ . If  $\mathcal{B}$  is the unit disc, we can see that  $\mathcal{B}$  is a compact set, and the union of all bounded invariant sets for  $\varphi$  contained  $\mathcal{B}$  is also contained in  $\text{int } \mathcal{B}$  ( $\mathcal{S}$  is just the origin), hence it is an isolating neighborhood for the flow  $\varphi$ . Figure 3.4 shows  $\mathcal{B}$  in light blue, and the exit set  $\mathcal{B}^- \subset \partial\mathcal{B}$  as two disjoint dark blue segments. Red arrows indicate the direction of the flow on  $\mathcal{B}$ , and we can see that  $\mathcal{B}$  satisfies Properties (i) and (ii) of Definition 3.2.1, and is therefore an isolating block for  $\varphi$ . It therefore makes sense to compute  $H_*(\mathcal{B}, \mathcal{B}^-)$  using this block. Taking the quotient  $\mathcal{B}/\mathcal{B}^-$  in two steps, first identify the disjoint segments of  $\mathcal{B}^-$  to form a sort of empty taco with the flaps touching each other, and second imagine collapsing the rest of the shell to a thin ring, as in the right image of Figure 3.4. The Conley index of the (Morse) index-one hyperbolic equilibrium point which comprises  $\mathcal{S}$  is  $CH_*(\mathcal{S}) = (0, \mathbb{Z}, 0, \dots)$ . A fact which will not be proved here is that the Conley index of a hyperbolic equilibrium of (Morse) index  $k$  has the same homotopy type as the  $k$ -sphere  $\Sigma^k$ , see [12]. For reference, the  $k$ -sphere has reduced homology  $H_*(\Sigma^k) = (0, \dots, \mathbb{Z}_{kth}, 0, \dots)$ .

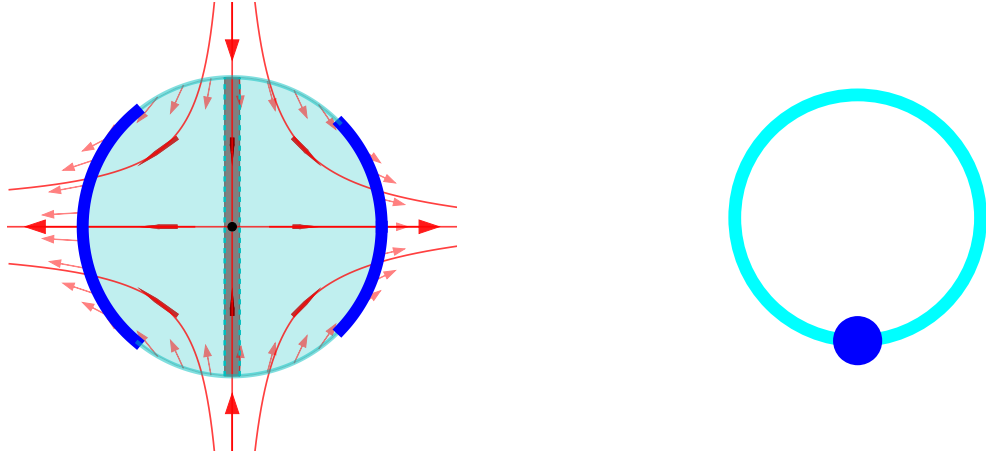


Figure 3.4: The left image shows an isolating block around a hyperbolic equilibrium point. The light blue disc is the block  $\mathcal{B} \subset \mathbb{R}^2$ , and the two disjoint dark blue segments form the exit set  $\mathcal{B}^- \subset \partial\mathcal{B}$ . The gray region indicates the portion of the flow which enters  $\mathcal{B}$  and never leaves (as it converges onto the origin). Red arrows indicate the direction of the flow on  $\mathcal{B}$ . The image on the right shows a topological space that is homotopy equivalent to the collapse of  $\mathcal{B}^-$  in Figure 3.4. The Conley index of  $\mathcal{S}$ , which is just the (Morse) index-one hyperbolic equilibrium at the origin, is expressed as the reduced homology groups of this space, so  $CH_*(\mathcal{S}) = (0, \mathbb{Z}, 0, \dots)$ .

In the next section we collect properties of the Conley index that we use in our work, as well as present some perspective on how information on the boundary of an isolating block can hold information about the maximal invariant set  $\mathcal{S}$  inside the block. We also give an indication of what can be learned from the index when  $\mathcal{S}$  is not known, which we expect would be the case in applications of our work.

### 3.3 Properties of, and Perspectives on, the Conley Index

Observe that the Conley index is a description of an isolated invariant set  $\mathcal{S}$ , but one only needs information about an isolating block for  $\mathcal{S}$  in order to compute it. Consequently, one can propose a block  $\mathcal{B}$ , verify that properties (i) and (ii) hold, and if  $H_*(\mathcal{B}, \mathcal{B}^-)$  is not trivial, one can ‘discover’  $\mathcal{S}$  (see §3.3.3). How this works, and what one can expect to discover about  $\mathcal{S}$ , is the subject of the next several subsections.

### 3.3.1 (Property) Isolating Blocks Exist

Let  $\varphi : \mathbb{R} \times \mathbb{R}^n \rightarrow \mathbb{R}^n$  be a global flow, and let the compact set  $\mathcal{N}_{\mathcal{S}} \subset \mathbb{R}^n$  be an isolating neighborhood for the isolated invariant set  $\mathcal{S}$ . From a practical perspective, the two most important considerations at this point are whether or not there exists an isolating block for  $\mathcal{S}$ , and whether or not the Conley index of  $\mathcal{S}$  depends on the choice of block.

A fundamental result in the theory is that given any isolated invariant set  $\mathcal{S}$ , there exists an isolating block for it. The existence proof is constructive, albeit not computable, and is given in [13]. A second fundamental feature of the theory is that the Conley index  $CH_*(\mathcal{S})$  does not depend on the choice of isolating block  $\mathcal{B}$  (or, for that matter, the choice of index pair). This result appears as the first theorem in Chapter III, §5.1, of [12].

### 3.3.2 (Perspective) Isolating Blocks as Ważewski Sets

This section addresses how information about an isolated invariant set  $\mathcal{S}$  can be transmitted to the boundary of an isolating block  $\mathcal{B}$  having  $\mathcal{S}$  as the maximal invariant set in its interior.

Consider the set of points  $\xi \in \mathcal{B}$  which are carried out of  $\mathcal{B}$  by the flow in positive finite time, that is  $\mathcal{B}^\circ := \{\xi \in \mathcal{B} : \exists t > 0 \text{ with } \varphi(t, \xi) \notin \mathcal{B}\}$ . If the forward orbit of  $\xi \in \mathcal{B}$  does not leave  $\mathcal{B}$  through  $\mathcal{B}^-$ , then it must converge onto  $\mathcal{S}$ . In other words  $\mathcal{S} = \omega(\mathcal{B} \setminus \mathcal{B}^\circ)$ , where the  $\omega$ -limit set  $\omega(\mathcal{B} \setminus \mathcal{B}^\circ)$  is defined as  $\bigcap_{s \in \mathbb{R}} \overline{\{\varphi(t, \xi) : \xi \in \mathcal{B} \setminus \mathcal{B}^\circ, t > s\}}$ . With this notation we see that the definition of an isolating block  $\mathcal{B}$  coincides with that of a **Ważewski set** (cf. Definition 2.4.2 in §2.4.3), where  $\mathcal{B}^-$  is closed relative to  $\mathcal{B}^\circ$ . We restate Theorem 2.4.3 from §2.4.3 with the current notation.

**Theorem 3.3.1 (Ważewski, from [12] with adapted notation).** *If  $\mathcal{B}$  is a Ważewski set then  $\mathcal{B}^-$  is a strong deformation retract of  $\mathcal{B}^\circ$ , and  $\mathcal{B}^\circ$  is open relative to  $\mathcal{B}$ .*

The strong deformation retraction of the theorem is built using from the flow map  $\varphi$ . In particular, putting  $\tau(\xi) := \sup \{t \geq 0 : \varphi(t, \xi) \in \mathcal{B}\}$ , then for  $\xi \in \mathcal{B}^\circ$ , and  $\sigma \in [0, 1]$ , we



define  $h : [0, 1] \times \mathcal{B}^\circ \rightarrow \mathcal{B}^\circ$  by

$$h : (\sigma, \xi) \mapsto \varphi(\sigma\tau(\xi), \xi). \quad (3.7)$$

The claim is that  $h$  is a strong deformation retraction (refer back to Definition 2.1.4 in §2.1.1). That is,  $h$  is continuous in both  $t$  and  $\xi$ , and for all  $\xi \in \mathcal{B}^\circ$  we have

$$h(0, \xi) = \varphi(0, \xi) = \xi,$$

$$h(1, \xi) = \varphi(\tau\xi, \xi) \in \mathcal{B}^-, \text{ and} \quad (3.8)$$

$$h(\sigma, \xi \in \mathcal{B}^-) = \varphi(0, \xi), \text{ so } h(\sigma, \mathcal{B}^-) = \text{id}_{\mathcal{B}^-}.$$

The equations in 3.8 hold by construction. The claim that  $h$  is, indeed, a strong deformation retraction, requires verification that  $h$  is continuous, and in particular, that  $\tau$  is. It is here where we find that  $\mathcal{B}^-$  must be closed (see [12] for more detail, and cf. Footnote 3 in §3.2).

Having defined the isolating block  $\mathcal{B}$  to have its isolated invariant set strictly within its interior, Conley built the room necessary to use this feature of flows to shuttle the dynamics of  $\mathcal{B}^\circ$  away from  $\mathcal{S}$ . To quote Conley directly<sup>5</sup>, “...the index is a measure of the impossibility of deforming  $\mathcal{B}$  to  $\mathcal{B}^-$ ; in particular if the index is nontrivial,  $\mathcal{B} \setminus \mathcal{B}^\circ$ , and consequently  $\mathcal{S} = \omega(\mathcal{B} \setminus \mathcal{B}^\circ)$ , is nonempty.”

### 3.3.3 (Property) Ważwesi: If the Index of $\mathcal{S}$ is Nontrivial, then so is $\mathcal{S}$

The Ważwesi property was stated above in passing, but it is important enough to stand on its own.

**Theorem 3.3.2 (Ważewski Property, [12]).** *If  $CH(\mathcal{S})$  is non-trivial, then  $\mathcal{S} \neq \emptyset$ .*

We will use this property of the Conley index several times in our proposed computer-assisted proofs of the existence of heteroclinic orbits in §3.7. (In accordance with our analogy

---

<sup>5</sup>The quote appears in the first paragraph of Chapter III, on page 43 of [12].

to the Brouwer degree, if an isolated invariant set  $\mathcal{S}$  has trivial Conley index, then  $\mathcal{S}$  is not necessarily empty.)

### 3.3.4 (Property) Summation Formula

A useful property of the Conley index is known as the **summation formula**, “The index of the disjoint union of two isolated invariant sets is the sum of their indices<sup>6</sup>.” Suppose we have isolated invariant sets  $\mathcal{S}_1 = \{p_1\}$  and  $\mathcal{S}_2 = \{p_2\}$ , isolated by blocks  $\mathcal{B}_1$  and  $\mathcal{B}_2$ , where  $p_1$  and  $p_2$  are just equilibrium points. Suppose further that one can find an isolating block  $\mathcal{B}_{12}$  such that the disjoint union  $\mathcal{S}_{12} := \mathcal{S}_1 \cup \mathcal{S}_2$  is the maximal invariant set contained by  $\mathcal{B}_{12}$  (hence  $\mathcal{S}_{12}$  is an isolated invariant set). Then

$$CH(\mathcal{S}_{12}) \simeq CH(\mathcal{S}_1) \oplus CH(\mathcal{S}_2).$$

This is useful because in certain situations we can *propose* a maximal invariant set, say  $\mathcal{S}^*$ , comprised only of simpler, *known* isolated invariant sets  $\mathcal{S}_i$ , and test if the summation formula holds. If it does not hold, then  $\mathcal{S}^*$  is comprised of more than just the known  $\mathcal{S}_i$ . With some assumptions on the flow of interest we can describe the additional bounded invariant sets that must be in  $\mathcal{S}^*$ . We make repeated use of this in §3.7.

### 3.3.5 (Perspective) Usefulness of the Conley Index

The usefulness of the Conley index is that it provides a coarse description of the structure of the dynamics on an isolated invariant set  $\mathcal{S}$ , and this information is robust with respect to small perturbations of the differential equation. The canonical example of the type of information measured by the index can be seen in the following

**Example: Bifurcation in a simple one parameter family.** Consider the one-parameter family of differential equations defined as

$$\dot{x} = f(x) = x(1 - x^2) - \lambda, \tag{3.9}$$

---

<sup>6</sup>This is a direct quote from [12], page 54,

and consider its bifurcation diagram in Figure 3.5.

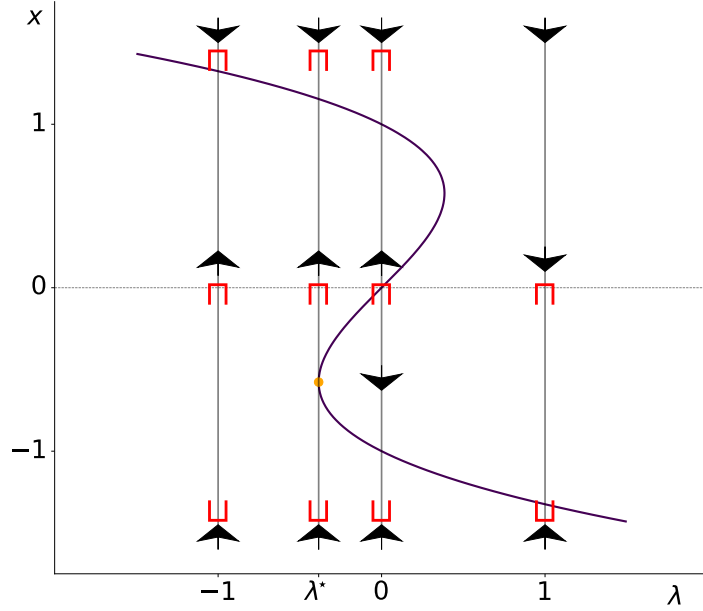


Figure 3.5: Bifurcation diagram for (3.9), with phase portraits for various values of  $\lambda \in \mathbb{R}$ . Interval markers define the isolating blocks  $\mathcal{A} := [-1.5, 1.5]$  and  $\mathcal{B} := [-1.5, 0]$  along the abscissa. An orange dot appears at  $(\lambda^*, x) = (1\sqrt{3}(1\sqrt{3} - 1), -1\sqrt{3})$ , where there is a degenerate equilibrium point for (3.9).

The interval  $\mathcal{A} := [-1.5, 1.5]$  forms an isolating block for the flow generated by  $f$  in (3.9) when  $\lambda \in (-1, 1)$ . The exit set for  $\mathcal{A}$  is empty for all values of  $\lambda \in (-1, 1)$ , meaning that the flow generated by (3.9) is attracting on the interval  $[-1.5, 1.5]$  for all values of  $\lambda \in (-1, 1)$ . The Conley index computed from the block  $\mathcal{A}$  with empty exit set is defined as the two-pointed space, and therefore has the homotopy type of the zero-sphere.

The interval  $\mathcal{B} := [-1.5, 0]$  forms an isolating block for the flow generated by  $f$  in (3.9) when  $\lambda \in (-1, 0)$ , and again when  $\lambda \in (0, 1)$ . For  $\lambda = 0$ , the interval  $[-1.5, 0]$  fails to be an isolating block because the maximal invariant set  $\mathcal{S}$  contained in  $\mathcal{B}$  is not isolated, in particular the equilibrium  $x = 0$  intersects the boundary of  $\mathcal{B}$  when  $\lambda = 0$ . In contrast to

$\mathcal{A}$ , the flow is not attracting on  $\mathcal{B}$ . In fact, for  $\lambda \in (-1, 0)$ , the Conley index of the compact set  $\mathcal{B}$  is trivial (to see this note that  $\mathcal{B}$  is contractible, and  $\mathcal{B}^-$  is a single point).

This example appears in most discussions of the Conley index (see [12],[25],[35]) as an illustration of just how coarse the information provided by the Conley index is. The Conley index computed from the block  $\mathcal{A}$  remains constant for  $\lambda \in (-1, 1)$ , while  $\mathcal{A}$  variously isolates the invariant sets  $\mathcal{S}_1$ , the single hyperbolic equilibrium (for  $\lambda \in (-1, \lambda^*)$ ), the invariant set  $\mathcal{S}_2$ , being the union of the single hyperbolic equilibrium, a degenerate equilibrium, and the heteroclinic between them (for  $\lambda = \lambda^*$ ), and  $\mathcal{S}_3$ , the union of three hyperbolic equilibria and the heteroclinics between them. Thus,  $CH_*(\mathcal{S}_1) \simeq CH_*(\mathcal{S}_2) \simeq CH_*(\mathcal{S}_3)$ . The isolated invariant sets  $\mathcal{S}_1$ ,  $\mathcal{S}_2$ , and  $\mathcal{S}_3$  are said to be *related by continuation*.

Notice that  $\mathcal{A}$  cannot isolate a pair of hyperbolic equilibria on the line. Additionally, notice that  $\mathcal{B}$  variously isolates the empty set  $\mathcal{S}_0$  as an isolated invariant set (for  $\lambda \in (-1, \lambda^*)$ ), the set  $\mathcal{S}_{01}$  consisting of the single degenerate equilibrium (for  $\lambda = \lambda^*$ ), and the set  $\mathcal{S}_{02}$  consisting of the union of two hyperbolic points and the heteroclinic connecting them (for  $\lambda \in (-\lambda^*, 0)$ ). Evidently, the isolated invariant sets  $\mathcal{S}_0$ ,  $\mathcal{S}_{01}$ , and  $\mathcal{S}_{02}$  are related by continuation.

A useful property of the Conley index is that it can be used to rule out certain behavior on entire regions of phase space. Furthermore, as this example illustrates, the Conley index is stable under perturbation of the vector field. Combined, these two features say that if a perturbation does not destroy the isolating block  $\mathcal{B}$ , then the isolated invariant set within  $\mathcal{B}$  may change its structure, but can only do so ‘up to continuation.’ See [12] and [25] for a more complete discussion.

The purported analogy with the Brouwer degree is finally evident; where the Brouwer degree yields existence results for zeros of a function in the interior of an admissible compact set, and those existence statements are robust under perturbation, the Conley index yields existence results (and slightly more) for an isolated invariant set  $\mathcal{S}$  in the interior of a compact isolating block, and while the structure of  $\mathcal{S}$  may change under perturbation, its Conley index will not.

### 3.4 Current State of the Art

An early effort in this field is due to Boczko [7] and Boczko, Kalies, and Mischaikow in [8]. In this work the authors directly build isolating blocks and obtain index pairs. Their effort can be briefly described as first explicitly moving to a discrete dynamical system that is guaranteed to be an outer approximation to the flow defined by an ordinary differential equation and computing a triangulation of the (discrete) phase space that: (1) Is flow-transverse, meaning that it does not permit tangencies of the flow with the boundary of the triangulation; and (2) Forms an index pair from collections of triangles, ultimately capturing ‘recurrent’ dynamics. We point out here that one of the highlights of the current chapter is the relaxation of the flow-transverse requirement (see Theorem 3.5.4). Theirs is a monumental effort, intellectually and computationally, and culminates in an interesting aside – that the invariant sets can be resolved ‘arbitrarily closely’ by tuning the triangulation parameters (i.e. forcing more triangles). The reason this is interesting in our context is that it appears that they are able to not only prove existence, but also deliver a quantitative and graphical description of what those dynamics look like. Their method explicitly constructed index pairs from an approximating discrete dynamical system – the work is highly technical and appears to suffer from enormous computational overhead. However, it is important because these authors faced the challenge of constructing sets satisfying the requirement to be an isolating block. Furthermore, in their conclusion section they suggest the use of robust methods (interval arithmetic) in order to obtain computer-assisted proofs of these results.

We point out that our work is rather more in line with an effort that appears in the doctoral thesis of Eberlein [17], and shortly after in Eberlein, Scheurle [18]. The similarity is found in the goal of surrounding some suspected isolated invariant set with an approximation to a topological manifold in a data structure that permits homology computations. Their technique is (roughly) to construct a polytope outer approximation to some isolating neighborhood and then refine this polytope in order to resolve the exit set and ensure

there are no internal tangencies. We point out several difficulties in this approach and how they proceeded through them. First, establishing transversality of the flow on a face of a polytope is simply a matter of checking whether the vector field has a nonzero component in the normal direction to the face. The geometry of the situation is simple, but the numerics are not - the Eberlein/Scheurle work does not address the numerical accuracy of this computation. Second, resolving the 'internal tangency' criterion for isolating blocks is essential. Their approach integrates the flow for some time and see where it ends up (inside or outside of the polytope). This directly addresses the question of whether or not the flow exits the polytope, but does not amount to a numerically rigorous result. Their work is an important first step and has identified several challenges that we have been able to resolve, and remains an inspiration for more automated procedures for proposing candidate isolating blocks. However, in each of the challenges listed above, we are able to provide a more simple and completely rigorous approach.

### 3.5 Characterization of Isolating Blocks via Superlevel Sets

The definition of an isolating block  $\mathcal{B} \subset \mathbb{R}^n$ , its isolated invariant set  $\mathcal{S}$ , and the Conley index of  $CH_*(\mathcal{S}) := H_*(\mathcal{B}, \mathcal{B}^-)$  naturally provide for the following eminently practical workflow for dynamical systems. For a wide class of ordinary differential equations  $\dot{x} = f(x)$  which permit a global flow  $\varphi : \mathbb{R} \times \mathbb{R}^n \rightarrow \mathbb{R}^n$ , one can: (1) *Propose* a compact set  $\mathcal{B} \subset \mathbb{R}^n$  as a candidate isolating block; (2) Validate properties (i) and (ii) in Definition 3.2.1 to establish that the candidate  $\mathcal{B}$  is, indeed, an isolating block for  $\varphi$ ; and (3) Compute  $H_*(\mathcal{B}, \mathcal{B}^-)$  to yield new information about the dynamics of  $\varphi$  on  $\mathcal{B}$ .

The purpose of this section is to address Step (2) above, by establishing Theorem 3.5.4, which is an *easily stated condition*, which can be validated algorithmically using rigorous computations based on interval arithmetic, and which either provides a computer-assisted proof that the given candidate  $\mathcal{B}$  is an isolating block, or provides guidance as to where  $\mathcal{B}$  has to be adjusted in order to arrive at an isolating block.

The basic idea is to observe that once a suitable candidate block  $\mathcal{B}$  has been chosen, it is only left to: (1) Approximate  $\mathcal{B}^- \subset \partial\mathcal{B}$  up to homotopy equivalence, and establish that it is closed; and (2) Establish that any points  $p \in \partial\mathcal{B}$  where the flow is tangent to  $\mathcal{B}$ , that the tangency is external in the sense of Property (ii) in Definition 3.2.1. We point out that items (1) and (2) describe geometric relationships between the vector field  $f$  and the boundary of the candidate block  $\mathcal{B}$ . Our strategy is to construct smooth, real-valued functions on  $\partial\mathcal{B}$  which characterize the exit set  $\mathcal{B}^-$ , and identify any tangencies as internal or external, in terms of their zero level sets and positive superlevel sets, respectively (this is the content of Lemmas 3.5.2 and 3.5.3). The algorithmic validation of these conditions is explained in §3.6, where we build on the  $\alpha$ -superlevel set validation algorithm (V) in Chapter 2.

For the remainder of this dissertation we concern ourselves with  $\alpha$ -superlevel sets,  $\alpha$ -sublevel sets, and  $\alpha$ -level sets of smooth functions where  $\alpha = 0$ . In order to set unambiguous notation, make the following

**Definition 3.5.1.** *For the function  $u : \Omega \subset X \rightarrow \mathbb{R}$ , denote*

the **positive superlevel set** of  $u$  by  $N^+(\Omega, u) := \{x \in \Omega : u(x) > 0\}$ ,

the **negative sublevel set** of  $u$  by  $N^-(\Omega, u) := \{x \in \Omega : u(x) < 0\}$ , and

the **zero level set** of  $u$  by  $N^0(\Omega, u) := \{x \in \Omega : u(x) = 0\}$ .

Our method begins with the specification of a candidate isolating block  $\mathcal{B} \subset \mathbb{R}^n$  which satisfies the following assumption:

(A1) The set  $\mathcal{B} \subset \mathbb{R}^n$  is connected and compact, and  $\partial\mathcal{B} \subset \mathbb{R}^{n-1}$  is a smooth, compact, orientable embedded manifold of codimension one in  $\mathbb{R}^n$ .

We write  $T_p\mathcal{B} \subset \mathbb{R}^n$  to denote the tangent space of  $\mathcal{B}$  at the point  $p \in \partial\mathcal{B}$ , and we use

$\nu_p \neq 0 \in \mathbb{R}^n$  to denote an **outward normal vector**. For  $q \in \mathbb{R}^n$ , we put

$$\pi_p^\top q := q - \frac{\langle q, \nu_p \rangle}{\langle \nu_p, \nu_p \rangle} \cdot \nu_p,$$

the **orthogonal projection** of  $q$  onto  $T_p\mathcal{B} \subset \mathbb{R}^n$ , where  $\langle \cdot, \cdot \rangle$  denotes the standard scalar product on  $\mathbb{R}^n$ .

In order to evaluate flow tangencies at points  $p \in \partial\mathcal{B}$  as internal or external, we are led to compare the vector field  $f$  with the local curvature of the manifold  $\partial\mathcal{B}$  at  $p$  in the direction of  $f(p)$ . This can be accomplished by evaluating the **second fundamental form**  $\mathbb{I} : T_p\mathcal{B} \times T_p\mathcal{B} \rightarrow \mathbb{R}$  along the single direction<sup>7</sup>  $\pi_p^\top f(p)$ , and will appear as  $\mathbb{I}(\pi_p^\top f(p), \pi_p^\top f(p))$  for points  $p \in \partial\mathcal{B}$ . A good reference for the differential geometry employed here can be found in [37]. Several steps in the proofs below require slightly deeper results, and references are given as needed. We also point the reader to §3.5.1 for detailed calculations using these quantities.

With this notation in place, we present Lemmas 3.5.2 and 3.5.3 characterizing the exit sets and external tangencies, respectively.

**Lemma 3.5.2.** *Consider the ordinary differential equation (3.1) with smooth right-hand side  $f : \mathbb{R}^n \rightarrow \mathbb{R}^n$ , and suppose that  $\mathcal{B} \subset \mathbb{R}^n$  is a compact set as in (A1). Furthermore, define the function  $u : \partial\mathcal{B} \rightarrow \mathbb{R}$  as*

$$u(p) = \langle f(p), \nu_p \rangle, \tag{3.10}$$

---

<sup>7</sup>For concreteness, a codimension-one smooth manifold  $\mathcal{M}$  embedded in  $\mathbb{R}^3$ , locally parameterized by  $r : \Omega \subset \mathbb{R}^2 \rightarrow \mathbb{R}^3$ , has second fundamental form  $\mathbb{I} : T_p\mathcal{B} \times T_p\mathcal{B} \rightarrow \mathbb{R}$ , given by

$$(\lambda, \mu) \mapsto \begin{pmatrix} \lambda^1 & \lambda^2 \end{pmatrix} \begin{pmatrix} \langle r_{\theta\theta}(p), \nu_p \rangle & \langle r_{\theta\varphi}(p), \nu_p \rangle \\ \langle r_{\varphi\theta}(p), \nu_p \rangle & \langle r_{\varphi\varphi}(p), \nu_p \rangle \end{pmatrix} \begin{pmatrix} \mu^1 \\ \mu^2 \end{pmatrix},$$

for  $\lambda, \mu \in T_p\mathcal{M}$ . One can roughly think of evaluating  $\mathbb{I}$  at the pair  $(\lambda, \lambda)$  as akin to taking a second derivative on the manifold, along the direction  $\lambda$ .



where  $p \in \mathcal{B}$ , and  $\nu_p$  denotes a normal vector at  $p$ . Then we have the inclusions

$$N^+(\partial\mathcal{B}, u) \subset \mathcal{B}^- \setminus \mathcal{B}^+ \quad \text{and} \quad N^-(\partial\mathcal{B}, u) \subset \mathcal{B}^+ \setminus \mathcal{B}^- ,$$

where  $N^\pm(\partial\mathcal{B}, u)$  were defined in Definition 3.5.1, and  $\mathcal{B}^\pm$  were defined along with  $\mathcal{B}$  in Definition 3.2.1.

*Proof.* Let  $p \in \partial\mathcal{B}$ . According to [26, Proposition 5.16], there exists a neighborhood  $U \subset \mathbb{R}^n$  of  $p$  and a smooth submersion  $\Phi : U \rightarrow \mathbb{R}$  such that  $\partial\mathcal{B} \cap U$  is the zero set of  $\Phi$ . Since  $\nabla\Phi(p)$  is orthogonal to  $T_p\mathcal{B}$ , we can assume without loss of generality that  $\nabla\Phi(p)$  is a positive multiple of  $\nu_p$ . Thus, for all  $q \in U$  we have  $q \notin \mathcal{B}$  if and only if  $\Phi(q) > 0$ , and  $q$  is contained in the interior of  $\mathcal{B}$  if and only if  $\Phi(q) < 0$ .

Now let  $x(t)$  denote the solution of (3.1) satisfying  $x(0) = p$ . Evaluating  $\Phi$  along the solution  $x(t)$  close to  $p$  and differentiating with respect to  $t$  then furnishes

$$\frac{d}{dt}\Phi(x(t)) = \langle \nabla\Phi(x(t)), \dot{x}(t) \rangle = \langle \nabla\Phi(x(t)), f(x(t)) \rangle .$$

For  $t = 0$  one therefore has

$$\left. \frac{d}{dt}\Phi(x(t)) \right|_{t=0} = \langle \nabla\Phi(p), f(p) \rangle = c \cdot u(p) ,$$

where  $c > 0$  is a positive scalar. If we now assume  $u(p) > 0$ , then there exists a  $T > 0$  such that  $\Phi(x(t)) > 0$  for all  $t \in (0, T]$ , and  $\Phi(x(t)) < 0$  for all  $t \in [-T, 0)$ . Together with the above characterization of the interior and exterior of  $\mathcal{B}$  in  $U$  given above, this immediately implies  $N^+(\partial\mathcal{B}, u) \subset \mathcal{B}^- \setminus \mathcal{B}^+$ . Since the proof of  $N^-(\partial\mathcal{B}, u) \subset \mathcal{B}^+ \setminus \mathcal{B}^-$  is completely analogous, Lemma 3.5.2 follows.  $\square$

Notice that the above lemma only uses the normal vector field  $\nu$  on the manifold  $\partial\mathcal{B}$ , and it allows us to locate the exit set  $\mathcal{B}^-$  up to points at which  $u(p) = 0$ . However, in the

setting of the lemma we cannot make any statements about the behavior of the flow near points  $p \in \partial\mathcal{B}$  with  $u(p) = 0$ . These points of course are candidates for flow tangencies with the boundary of  $\mathcal{B}$ . In order to exclude internal tangencies, understanding the local curvature of the manifold in the direction of the flow is crucial. The following lemma makes use of the second fundamental form of the manifold  $\partial\mathcal{B}$  at these points.

**Lemma 3.5.3.** *Consider the ordinary differential equation (3.1) with smooth right-hand side  $f : \mathbb{R}^n \rightarrow \mathbb{R}^n$ , and suppose that  $\mathcal{B} \subset \mathbb{R}^n$  is a compact set as in (A1). Let  $u$  denote the function from (3.10), and define the function  $v : \partial\mathcal{B} \rightarrow \mathbb{R}$  as*

$$v(p) = \langle Df(p)f(p), \nu_p \rangle - \mathbb{I} \left( \pi_p^\top f(p), \pi_p^\top f(p) \right),$$

where  $p \in \mathcal{B}$ , and  $\nu_p$  denotes the normal vector field at  $p$ , and  $\mathbb{I}$  is the second fundamental form on  $T_p\mathcal{B}$ . If the point  $p \in \partial\mathcal{B}$  satisfies  $u(p) = 0$  and  $v(p) > 0$ , then the solution of (3.1) through  $p$  forms an external tangency with  $\partial\mathcal{B}$ , i.e., there exists a time  $T > 0$  such that  $\varphi([-T, T], p) \cap \mathcal{B} = \{p\}$ , where  $\varphi$  denotes the flow associated with (3.1). On the other hand, if  $u(p) = 0$  and  $v(p) < 0$ , then the solution of (3.1) through  $p$  forms an internal tangency with  $\partial\mathcal{B}$ , i.e., there exists a time  $T > 0$  such that  $\varphi([-T, T], p) \setminus \{p\} \subset \text{int } \mathcal{B}$ .

*Proof.* Let  $p \in \partial\mathcal{B}$ . As in the proof of the previous lemma, there exists a neighborhood  $U \subset \mathbb{R}^n$  of  $p$  and a smooth submersion  $\Phi : U \rightarrow \mathbb{R}$  such that  $\partial\mathcal{B} \cap U$  is the zero set of  $\Phi$ , and that  $\nabla\Phi(p)$  is a positive multiple of  $\nu_p$ . Now let  $\alpha : U \rightarrow \mathbb{R}^+$  be a smooth function with  $\alpha(q) = \|\nu_q\|$  for all  $q \in \partial\mathcal{B} \cap U$ . Such a function can always be constructed, possibly after choosing a smaller neighborhood  $U$ . For example, using a tubular neighborhood of  $\partial\mathcal{B} \cap U$  as in [21, Theorem 5.1], one can simply define  $\alpha$  to be constant on each of the normal fibres. If we then define  $\Psi : U \rightarrow \mathbb{R}$  via  $\Psi(q) = \alpha(q)\Phi(q)/\|\nabla\Phi(q)\|$  for all  $q \in U$ , then also  $\Psi$  is a smooth submersion such that  $\partial\mathcal{B} \cap U$  is the zero set of  $\Psi$ . In addition, one can easily see that

$$\nabla\Psi(q) = \nu_q \quad \text{for all } q \in \partial\mathcal{B} \cap U. \quad (3.11)$$

Thus, we still have for all  $q \in U$  that  $q \notin \mathcal{B}$  if and only if  $\Psi(q) > 0$ , and  $q$  is contained in the interior of  $\mathcal{B}$  if and only if  $\Psi(q) < 0$ . But in addition, the smooth vector field  $\nabla \Psi$  is an extension of  $\nu$  onto  $U$ .

After these preparations, let  $p \in \partial \mathcal{B}$  be a point with  $u(p) = 0$ , and let  $x(t)$  denote the solution of (3.1) with  $x(0) = p$ . If we define the real-valued function  $\tau$  in a small neighborhood of  $0 \in \mathbb{R}$  via  $\tau(t) = \Psi(x(t))$ , then  $\tau(0) = \Psi(p) = 0$ . Furthermore, due to the above construction of  $\Psi$ , the solution  $x(t)$  forms an external tangency with  $\partial \mathcal{B}$ , if there exists a time  $T > 0$  such that  $\tau(t) > 0$  for all  $t \in [-T, T] \setminus \{0\}$ . Similarly,  $x(t)$  forms an internal tangency if we have  $\tau(t) < 0$  on  $[-T, T] \setminus \{0\}$ . As in the proof of Lemma 3.5.2, the derivative of  $\tau$  can be computed as

$$\tau'(t) = \frac{d}{dt} \Psi(x(t)) = \langle \nabla \Psi(x(t)), \dot{x}(t) \rangle = \langle \nabla \Psi(x(t)), f(x(t)) \rangle ,$$

which implies  $\tau'(0) = \langle \nabla \Psi(p), f(p) \rangle = \langle \nu_p, f(p) \rangle = u(p) = 0$  due to (3.11). The second derivative of  $\tau$  is

$$\tau''(t) = \langle \nabla \Psi(x(t)), Df(x(t))f(x(t)) \rangle + \langle \text{Hess } \Psi(x(t))f(x(t)), f(x(t)) \rangle ,$$

and evaluation at  $t = 0$  furnishes in combination with (3.11) the identity

$$\tau''(0) = \langle \nu_p, Df(p)f(p) \rangle + \langle \text{Hess } \Psi(p)f(p), f(p) \rangle .$$

According to our above discussion, the solution  $x(t)$  forms an external tangency with  $\partial \mathcal{B}$ , if  $\tau''(0) > 0$ , and an internal tangency if  $\tau''(0) < 0$ . Thus, in order to complete the proof of the lemma it suffices to show that  $\tau''(0) = v(p)$ . Since we already know that  $f(p) \in T_p \mathcal{B}$  (recall that  $u(p) = 0$ ), this in turn follows immediately from the fact that

$$\text{II}(y, z) = -\langle \text{Hess } \Psi(p)y, z \rangle \quad \text{for all } y, z \in T_p \mathcal{B} , \quad (3.12)$$

which will be established in the remainder of the proof.

In order to verify (3.12), we make use of some results from Riemannian geometry. According to [15, Chapter 6, Proposition 2.3], the second fundamental form is

$$\mathbb{I}(y, z) = -\langle \pi_p^\top \bar{\nabla}_y \nabla \Psi(p), z \rangle \quad \text{for all } y, z \in T_p \mathcal{B}. \quad (3.13)$$

In this formula,  $\pi_p^\top$  denotes the orthogonal projection from  $\mathbb{R}^n$  onto  $T_p \mathcal{B}$ , and  $\bar{\nabla}$  denotes the Riemannian connection on  $\mathbb{R}^n$ . For any vector field  $N$  on  $\mathbb{R}^n$ , the latter is the directional derivative  $\bar{\nabla}_y N = DNy$ , see [15, pp. 51–56]. This yields

$$\pi_p^\top \bar{\nabla}_y \nabla \Psi(p) = \pi_p^\top \text{Hess } \Psi(p)y = \text{Hess } \Psi(p)y - \frac{\langle \text{Hess } \Psi(p)y, \nu_p \rangle}{\langle \nu_p, \nu_p \rangle} \cdot \nu_p,$$

as well as  $\mathbb{I}(y, z) = -\langle \text{Hess } \Psi(p)y, z \rangle$ , since  $z \in T_p \mathcal{B}$  implies  $\langle \nu_p, z \rangle = 0$ . This completes the verification of (3.12), and thus also of Lemma 3.5.3.  $\square$

The following theorem characterizes isolating blocks via zero level sets and positive superlevel sets. It says that the candidate block  $\mathcal{B}$  is an isolating block if *all tangencies are external*, and that if zero is a regular value of  $u$ , then  $\mathcal{B}^-$  is closed. This theorem makes it possible to adapt the superlevel set validation algorithm (V) in order to rigorously establish candidate blocks as valid isolating blocks.

**Theorem 3.5.4 (Isolating Blocks via zero level sets and positive superlevel sets).**

*Consider the flow  $\varphi$  associated with the ordinary differential equation (3.1), and suppose that  $\mathcal{B} \subset \mathbb{R}^n$  is a compact set as in (A1).*

*Furthermore, define the smooth functions  $u, v : \partial \mathcal{B} \rightarrow \mathbb{R}$  via*

$$u(p) = \langle f(p), \nu_p \rangle, \quad (3.14)$$

$$v(p) = \langle Df(p)f(p), \nu_p \rangle - \mathbb{I} \left( \pi_p^\top f(p), \pi_p^\top f(p) \right). \quad (3.15)$$

If in addition we have

$$N^0(\partial\mathcal{B}, u) \subset N^+(\partial\mathcal{B}, v) , \quad \text{and if } \text{zero is a regular value of } u , \quad (3.16)$$

then  $\mathcal{B}$  is an isolating block for (3.1) in the sense of Definition 3.2.1. In this case, the exit set  $\mathcal{B}^-$  defined in (3.2.1) is

$$\mathcal{B}^- = N^+(\partial\mathcal{B}, u) \cup N^0(\partial\mathcal{B}, u) = \overline{N^+(\partial\mathcal{B}, u)} , \quad (3.17)$$

i.e., it is the closure of the positive superlevel set  $N^+(\partial\mathcal{B}, u)$  of  $u$ .

*Proof.* According to the definition of positive superlevel sets and the zero level set in Definition 3.5.1, the boundary of  $\mathcal{B}$  can be partitioned in the form

$$\partial\mathcal{B} = N^+(\partial\mathcal{B}, u) \cup N^0(\partial\mathcal{B}, u) \cup N^-(\partial\mathcal{B}, u) .$$

Due to Lemma 3.5.2 we have both  $N^+(\partial\mathcal{B}, u) \subset \mathcal{B}^- \setminus \mathcal{B}^+$  and  $N^-(\partial\mathcal{B}, u) \subset \mathcal{B}^+ \setminus \mathcal{B}^-$ . Now let  $p \in N^0(\partial\mathcal{B}, u)$  be arbitrary. Then (3.16) implies  $p \in N^+(\partial\mathcal{B}, v)$ , and Lemma 3.5.3 shows that the solution of (3.1) through  $p$  forms an external tangency with  $\mathcal{B}$ , i.e., there exists a  $T > 0$  such that  $\varphi([-T, T], p) \cap \mathcal{B} = \{p\}$ , where  $\varphi$  denotes the flow associated with (3.1). This readily implies  $p \in \mathcal{B}^- \cap \mathcal{B}^+$ , i.e., we have  $N^0(\partial\mathcal{B}, u) \subset \mathcal{B}^- \cap \mathcal{B}^+$ . As mentioned above, the sets  $N^+(\partial\mathcal{B}, u)$  and  $N^0(\partial\mathcal{B}, u)$  form a partition of  $\partial\mathcal{B}$ . Since in addition the sets  $\mathcal{B}^- \setminus \mathcal{B}^+$ ,  $\mathcal{B}^+ \setminus \mathcal{B}^-$ , and  $\mathcal{B}^- \cap \mathcal{B}^+$  are pairwise disjoint, we obtain both

$$\partial\mathcal{B} = (\mathcal{B}^- \setminus \mathcal{B}^+) \cup (\mathcal{B}^+ \setminus \mathcal{B}^-) \cup (\mathcal{B}^- \cap \mathcal{B}^+) ,$$

as well as

$$N^+(\partial\mathcal{B}, u) = \mathcal{B}^- \setminus \mathcal{B}^+ , \quad N^-(\partial\mathcal{B}, u) = \mathcal{B}^+ \setminus \mathcal{B}^- , \quad \text{and} \quad N^0(\partial\mathcal{B}, u) = \mathcal{B}^- \cap \mathcal{B}^+ .$$

The first statement shows that Property (ii) in Definition 3.2.1 is satisfied. Moreover, due to the second statement we have  $\mathcal{B}^- = N^+(\partial\mathcal{B}, u) \cup N^0(\partial\mathcal{B}, u)$ , and thus  $\mathcal{B}^- = \{p \in \partial\mathcal{B} : u(p) \geq 0\}$ . Due to the continuity of  $u$ , this set is closed. Together this implies that the set  $\mathcal{B}$  is an isolating block in the sense of Definition 3.2.1.

In order to complete the proof we still need to verify that  $\mathcal{B}^- = \overline{N^+(\partial\mathcal{B}, u)}$ . Due to  $N^+(\partial\mathcal{B}, u) \subset \mathcal{B}^-$  and the closedness of  $\mathcal{B}^-$  one clearly has  $\overline{N^+(\partial\mathcal{B}, u)} \subset \mathcal{B}^-$ . Since we have already established  $\mathcal{B}^- = N^+(\partial\mathcal{B}, u) \cup N^0(\partial\mathcal{B}, u)$ , we only need to show that  $N^0(\partial\mathcal{B}, u) \subset \overline{N^+(\partial\mathcal{B}, u)}$ . According to [26, Corollary 5.14](reprinted as Theorem 2.1.6 in Chapter 2), the level set  $N^0(\partial\mathcal{B}, u) \subset \partial\mathcal{B}$  is a properly embedded submanifold of codimension one, since we assumed that zero is a regular value of  $u$ . Now let  $p \in N^0(\partial\mathcal{B}, u)$  be arbitrary. Since  $u$  is a submersion at  $p$ , every neighborhood of  $p$  in  $\partial\mathcal{B}$  has to contain points which lie in  $N^+(\partial\mathcal{B}, u)$ , and points in  $N^-(\partial\mathcal{B}, u)$ . This readily shows that  $p \in \overline{N^+(\partial\mathcal{B}, u)}$ , and this completes the proof of the theorem.  $\square$

### 3.5.1 A Worked Example

In this section we will define a candidate isolating block  $\mathcal{B}$  for the flow  $\varphi$  generated by the simple ordinary differential equation 3.18, and then present a detailed evaluation of both  $u$  and  $v$  from Theorem 3.5.4 at a single point  $p \in \partial\mathcal{B}$ . We will show images from a non-rigorous numerical approximation to argue that  $N^0(u) \subset N^+(v)$  for the block  $\mathcal{B}$ , and show by hand that zero is a regular value of  $u$ , which together are the assumptions required by Theorem 3.5.4 to validate  $\mathcal{B}$  as an isolating block. Along the way we will see that the flow makes an external tangency with  $\mathcal{B}$  at the point  $p$ , and we verify that  $v(p) > 0$ . Finally, we will compute the Conley index of the maximal invariant set  $\mathcal{S}$  contained in the interior of  $\mathcal{B}$ , and use it in conjunction with standard results for gradient systems to show<sup>8</sup> that  $\mathcal{S}$  is simply the (Morse) index 2 hyperbolic equilibrium point at the origin.

---

<sup>8</sup>The result shown in this section is completely non-rigorous as presented due to the appeal to Figure 3.7 to show that  $N^0(u) \subset N^+(v)$ . In §3.6 we will introduce the rigorous numerical algorithm (IB), which has been designed specifically to produce a computer-assisted proof of the fact that  $N^0(\partial\mathcal{B}, u) \subset N^+(\partial\mathcal{B}, v)$ , and that zero is a regular value for  $u$ .

Let  $\dot{\mathbf{x}} = f(\mathbf{x})$ , where  $\mathbf{x} = (x, y, z) \in \mathbb{R}^3$ . Suppose this differential equation is given by the following system

$$\begin{aligned}\dot{x} &= -x \\ \dot{y} &= y \\ \dot{z} &= z\end{aligned}\tag{3.18}$$

Put  $\mathcal{B} := \{(x, y, z) \in \mathbb{R}^3 : \sqrt{x^2 + y^2 + z^2} \leq 1\}$ . Then  $\partial\mathcal{B} = \{(x, y, z) \in \mathbb{R}^3 : \sqrt{x^2 + y^2 + z^2} = 1\}$  is a smooth, compact, orientable manifold in accordance with Assumption (A1) in §3.5.

From Theorem 3.5.4, we have the functions  $\partial\mathcal{B} \rightarrow \mathbb{R}$  given by

$$u(p) := \langle f(p), \nu_p \rangle$$

and

$$v(p) := \langle Df(p)f(p), \nu_p \rangle - \Pi(\pi_p^\perp f(p), \pi_p^\perp f(p)).$$

Consider the point  $p = (1/\sqrt{2}, 0, 1/\sqrt{2}) \in \partial\mathcal{B}$ . Notice that Figure 3.6 suggests that the solution of the differential equation 3.18 through the point  $p$  is tangent to  $\mathcal{B}$ , implying that  $u(p) = 0$ . In order for  $\mathcal{B}$  to be a valid isolating block we need to show that this tangency is external (which appears to be), i.e. we need to show that  $v(p) > 0$ .

We first compute  $u(p) = \langle f(p), \nu_p \rangle$ . The vector  $f(p)$  is  $f(1/\sqrt{2}, 0, 1/\sqrt{2}) = (-1/\sqrt{2}, 0, 1/\sqrt{2})$ . In general, the outward normal vector  $\nu_p$  can be obtained either from a parameterization  $r : \Omega \subset \mathbb{R}^{n-1} \rightarrow \mathbb{R}^n$  of  $\partial\mathcal{B}$ , or from  $\nu_p = \nabla\Psi(p)$ , where  $\Psi$  is an explicit smooth level set expression  $\Psi : \Omega \subset \mathbb{R}^3 \rightarrow \mathbb{R}$ , having  $\partial\mathcal{B} = \{(x, y, z) \in \mathbb{R}^3 : \Psi(x, y, z) = 0\}$ . In the present

case of  $\partial\mathcal{B}$  being the unit sphere centered at the origin, we simply have  $\nu_p = p$ . Thus

$$\begin{aligned} u(p) &= \langle f(p), \nu_p \rangle \\ &= \langle (-1/\sqrt{2}, 0, 1/\sqrt{2}), (1/\sqrt{2}, 0, 1/\sqrt{2}) \rangle \\ &= 0, \end{aligned} \tag{3.19}$$

indicating that the flow is tangent to  $\mathcal{B}$  at the point  $p$ . Figure 3.6 shows the point  $p$  and a segment of the solution of 3.18 through  $p$ . A numerical approximation to the positive superlevel set  $N^+(\Omega, u)$  is shown in Figure 3.7.

Next we compute  $v(p) = \langle Df(p)f(p), \nu_p \rangle - \mathbb{I}(\pi_p^\perp f(p), \pi_p^\perp f(p))$ . The vector  $Df(p)f(p)$  is the Jacobian matrix of  $f$  applied to the vector  $f(p)$ , and appears as

$$Df(p)f(p) = \begin{pmatrix} -1 & 0 & 0 \\ 0 & 1 & 0 \\ 0 & 0 & 1 \end{pmatrix} \begin{pmatrix} -1/\sqrt{2} \\ 0 \\ 1/\sqrt{2} \end{pmatrix} = \begin{pmatrix} 1/\sqrt{2} \\ 0 \\ 1/\sqrt{2} \end{pmatrix}. \tag{3.20}$$

At this point we have expressions for the inner product  $\langle Df(p)f(p), \nu_p \rangle$  forming the first term of  $v(p)$ . We now look at the projection  $\pi_p^\perp := q - \frac{\langle q, \nu_p \rangle}{\|\nu_p\|} \nu_p$ . Thus,  $\pi_p^\perp f(p)$  projects the vector field  $f$  passing through the point  $p \in \partial\mathcal{B}$  onto the tangent plane of the manifold  $\mathcal{B}$  at  $p$ . We have chosen  $p = (1/\sqrt{2}, 0, 1/\sqrt{2})^T$  so that the vector field has no normal component to the unit sphere at this point, so  $\pi_p^\perp f(p) = f(p) = (-1/\sqrt{2}, 0, 1/\sqrt{2})$ .

Next we evaluate the second fundamental form on  $\partial\mathcal{B}$  in the direction  $\pi_p^\perp f(p) = (-1/\sqrt{2}, 0, 1/\sqrt{2}) \in T_p\mathcal{B}$ . We proceed through the standard notation. Let the two-dimensional surface  $\partial\mathcal{B}$  be locally smoothly embedded in  $\mathbb{R}^3$  as a graph over the parametric domain  $\Omega \subset \mathbb{R}^2$  given by  $r : \Omega \subset \mathbb{R}^2 \rightarrow \mathcal{B}$ . Denote the preimage of the point  $p \in \partial\mathcal{B}$  by  $\hat{p} \in \Omega$ . Let



$T_p\mathcal{B}$  denote the tangent space of  $\mathcal{B}$  at  $p \in \partial\mathcal{B}$ . Then we have

$$\mathbb{I}(\lambda, \lambda) := L(\lambda^1)^2 + 2M\lambda^1\lambda^2 + N(\lambda^2)^2, \quad (3.21)$$

where  $\lambda = (\lambda^1, \lambda^2) \in T_p\mathcal{B}$ , and

$$L := \langle r_{\theta\theta}(\hat{p}), \nu_p \rangle \quad (3.22)$$

$$= \langle (-1/\sqrt{2}, 0, 0), (1/\sqrt{2}, 0, 1/\sqrt{2}) \rangle$$

$$= -1/2$$

$$M := \langle r_{\theta\varphi}(\hat{p}), \nu_p \rangle \quad (3.23)$$

$$= \langle (0, 1/\sqrt{2}, 0), (1/\sqrt{2}, 0, 1/\sqrt{2}) \rangle$$

$$= 0$$

$$N := \langle r_{\varphi\varphi}(\hat{p}), \nu_p \rangle \quad (3.24)$$

$$= \langle (-1/\sqrt{2}, 0, -1/\sqrt{2}), (1/\sqrt{2}, 0, 1/\sqrt{2}) \rangle$$

$$= -1$$

The standard parametric equations for the unit sphere will form our chart, so we put  $(\varphi, \theta) \in \Omega := [0, 2\pi] \times [0, \pi]$ , and specify  $r : (\theta, \varphi) \mapsto (\cos \theta \sin \varphi, \sin \theta \sin \varphi, \cos \varphi)$ . Technically, for  $p = (0, 0, 1)$  or  $(0, 0, -1)$ , i.e. the poles of the sphere, we will need a different chart because  $r^{-1}(0, 0, 1)$  is the entire line  $[0, 2\pi] \times \{0\}$ , so something like  $r : (\theta, \varphi) \mapsto (\cos \theta \sin(\varphi + \varepsilon), \sin \theta \sin(\varphi + \varepsilon), \cos(\varphi + \varepsilon))$  with  $\varepsilon \in (0, \pi)$  will do. This is not a problem in practice, see

### §3.5.2.

Recall our setting:  $\mathcal{B}$  is the unit ball with boundary  $\partial\mathcal{B}$ , the unit sphere. The point  $p \in \partial\mathcal{B}$  defines the tangent plane  $T_p\mathcal{B}$ . For the point  $p$ , the second fundamental form provides access to a local quadratic approximation to  $\partial\mathcal{B}$  as a graph over  $T_p\mathcal{B}$ . In particular, the second fundamental form at  $p \in \mathcal{B}$ , in the direction  $\lambda \in T_p\mathcal{M}$ , (denoted  $\mathbb{I}(\lambda, \lambda)$ ) yields the quadratic term of the Taylor expansion of the curve  $\gamma : [-\varepsilon, \varepsilon] \rightarrow \partial\mathcal{B}$ , with  $\gamma(0) = p$ , and having  $\gamma' = \alpha\lambda$  ( $\alpha \in \mathbb{R}$ ). This implies that in order to compute the second fundamental form in the direction of  $\pi_p^\perp f(p)$ , we need this vector to be written as a linear combination of the vectors spanning the tangent plane to  $\mathcal{B}$  at  $p$  (cf. Equation 3.21). In particular, we need to solve

$$[r_\theta(\hat{p}); r_\varphi(\hat{p})]\lambda^T = \left( \begin{array}{cc} -\sin\theta \sin\varphi & \cos\theta \cos\varphi \\ \cos\theta \sin\varphi & \sin\theta \cos\varphi \\ 0 & -\sin\varphi \end{array} \right) \left( \begin{array}{c} \lambda^1 \\ \lambda^2 \end{array} \right) \bigg|_{(\theta, \varphi) = \hat{p}} = \pi_p^\perp f(p). \quad (3.25)$$

We have that  $\hat{p} = (0, \pi/4)$ , and  $\pi_p^\perp f(p) = (-1/\sqrt{2}, 0, 1/\sqrt{2})$ , so Equation (3.25) appears as

$$[r_\theta(0, \pi/4); r_\varphi(0, \pi/4)]\lambda^T = \left( \begin{array}{cc} 0 & 1/\sqrt{2} \\ 1/\sqrt{2} & 0 \\ 0 & -1/\sqrt{2} \end{array} \right) \left( \begin{array}{c} \lambda^1 \\ \lambda^2 \end{array} \right) = \left( \begin{array}{c} -1/\sqrt{2} \\ 0 \\ 1/\sqrt{2} \end{array} \right), \quad (3.26)$$

so that  $\lambda = (0, -1)$ . That is, we can express the projection of the vector  $f(p)$  onto  $T_p\mathcal{B}$  in a local basis for  $T_p\mathcal{B}$ . We now have

$$\pi_p^\perp f(p) = 0 \cdot r_\theta(\hat{p}) - 1 \cdot r_\varphi(\hat{p}). \quad (3.27)$$

Finally, we can compute  $v(p)$  from Theorem 3.5.4.

$$\begin{aligned}
v(p) &= \langle Df(p)f(p), \nu_p \rangle - \Pi(\pi_p^\perp f(p), \pi_p^\perp f(p)) \\
&= \langle (-1/\sqrt{2}, 0, 1/\sqrt{2}), (1/\sqrt{2}, 0, 1/\sqrt{2}) \rangle - \Pi((0, -1), (0, -1)) \\
&= 0 - (L(0)^2 + 2M(0)(1) + N(-1)^2) \\
&= -(-1(-1)^2) \\
&= 1
\end{aligned} \tag{3.28}$$

We have arrived at the fact that see that  $p$  is in the zero level set  $\mathcal{N}^0(\Omega, u)$ , and also in  $\mathcal{N}^+(\Omega, v)$ , where  $\Omega = [0, 2\pi] \times [0, \pi]$ . We have not resolved the sets  $\mathcal{N}^0(\Omega, u)$  and  $\mathcal{N}^+(\Omega, v)$ . In order to use Theorem 3.5.4 to validate  $\mathcal{B}$  as an isolating block for Equation (3.18), the set inclusion  $N^0(u) \subset N^+(v)$  must be shown to be valid at each point  $p \in \partial\mathcal{B}$ , or equivalently for the chart  $r$  above,  $N^0(u) \subset N^+(v)$  must be shown to be valid at each point  $\hat{p} \in \Omega = [0, 2\pi] \times (0, \pi)$ , and zero must be shown to be regular value of  $u$ .

The regularity of zero can be achieved in this example by noting that  $\nabla u(p) = (-2x, 2y, 2z)$ , which is nonzero for all  $p \in \partial\mathcal{B} = \{(x, y, z) \in \mathbb{R}^3 : \sqrt{x^2 + y^2 + z^2} = 1\}$ . This is a rigorous statement in the sense that it does not come from an approximation, numerical or otherwise.

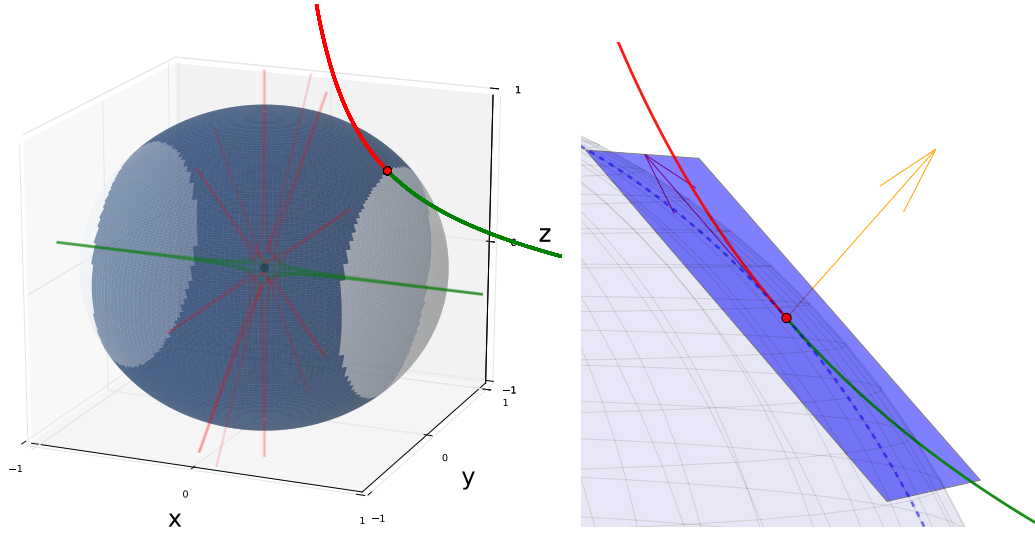


Figure 3.6: Selected trajectories of the system (3.18). The left panel shows the sphere  $\mathcal{B}$  isolating the fixed point at the origin. The point  $p = (1/\sqrt{2}, 0, 1/\sqrt{2})$  is shown by the red dot. The right panel shows the tangent plane  $T_p \mathcal{B}$  spanned by  $\{\Phi_\theta(\hat{p}), \Phi_\varphi(\hat{p})\}$ , along with a normal vector  $\nu_p$  in orange. A segment of the solution of (3.18) through  $p$  is shown by the red and green curve (for forward time, red indicates moving away from  $p$  and green indicates moving toward  $p$ ), and  $\pi^\perp f(p) = f(p) \in T_p M$  is indicated in purple. The dashed curve lies in  $\partial \mathcal{B}$ , and has tangent vector  $f(p)$  at  $p$ . The tangency test function  $v(p) = \langle Df(p)f(p), \nu_p \rangle - \mathbb{I}(\pi^\perp f(p), \pi^\perp f(p))$  can be thought of as comparing the second derivatives of these two curves at  $p$ , where the orientation of the space curves is taken relative to  $\nu_p$ .

At the moment we offer only a numerical approximation of the level sets of both  $u$  and  $v$  to argue that the set inclusion  $N^0(u) \subset N^+(v)$  holds. Figure 3.7 shows the output of calls to `contour(u)` and `contour(v)` over the domain  $\Omega = [0, 2\pi] \times [0 + \varepsilon, \pi - \varepsilon]$  from a typical numerical library (in this case we used `numpy` from the Python programming language). In the left image we have plotted  $N^+(\Omega, u)$  in dark blue and  $N^-(\Omega, u)$  in light blue. The right image shows  $N^+(\Omega, v)$  and  $N^-(\Omega, v)$ , along with the level set  $N^0(\Omega, u)$ . The fact that the level set does not appear to cross into any region where  $v$  is negative suggests that  $N^0(\Omega, u) \subset N^+(\Omega, v)$  (in fact,  $N^-(\Omega, v) = \emptyset$ ).

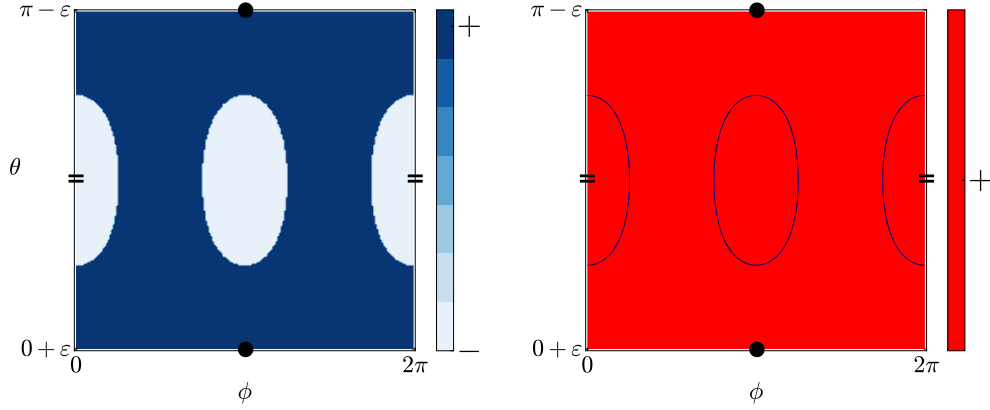


Figure 3.7: The patches  $\Omega = [0, 2\pi] \times (0, \pi)$  in both panels represent the domain of the parameterization  $r : \Omega \rightarrow \mathcal{B}$  in Figure 3.6. The left panel shows a the evaluation of  $u$  on  $\Omega$ , where the dark blue region indicates  $u > 0$  and the light blue indicates  $u < 0$ . The (image under  $r$  of the) border of these two regions corresponds to lines along  $\partial\mathcal{B}$  where  $u = 0$ , that is  $N^0(\Omega, u) \subset \partial\mathcal{B}$ . The right panel shows a filled contour plot of  $v$  on  $\Omega$  (although  $v > 0$  on all of  $\Omega$ ), with an overlay of  $N^0(\Omega, u)$ . It is essential that the contours  $N^0(\Omega, u)$  do not intersect regions on the right which are not positive, and in fact the it is the purpose of (IB) to establish this fact rigorously (cf. Theorem 3.5.4).

In §3.6 we present the numerically rigorous Algorithm (IB), which builds on Algorithm (V) from Chapter 2, and we present Theorem 3.6.1 establishing that successful completion of Algorithm (IB) guarantees  $\mathcal{B}$  is an isolating block. Section 3.7 contains several examples of the rigorous, algorithmic validation of isolating blocks in systems that are more complicated than the current example.

This final paragraph discusses the computation of the Conley index given the information that  $\mathcal{B}$  is a valid isolating block, and knowledge of  $\mathcal{B}^- \subset \partial\mathcal{B}$  up to homotopy equivalence. Observe that in Figure 3.6, the isolating block  $\mathcal{B}$  is the closed unit ball, and the exit set  $\mathcal{B}^- \subset \partial\mathcal{B}$  forms a belt around the ball. With some effort, the configuration of  $\mathcal{B}^-$  can also be seen from Figure 3.7. Computing  $H_*(\tilde{\mathcal{B}}, \tilde{\mathcal{B}}^-)$ , where  $\tilde{\mathcal{B}}$  is a cubical set that is homotopy equivalent to  $\mathcal{B}$ , and  $\tilde{\mathcal{B}}^- \subset \partial\tilde{\mathcal{B}}$  is a cubical set homotopy equivalent to  $\mathcal{B}^-$ , is automated using the computer program `homcubes`, which is a utility provided by the Computational Homology Project, CHomP [10]. Figure 3.8 shows the cube  $\tilde{\mathcal{B}} \subset \mathbb{R}^3$  as a cubical set

representing  $\mathcal{B}$ , along with the cubical set  $\tilde{\mathcal{B}}^- \subset \tilde{\mathcal{B}}$  representing  $\mathcal{B}^-$ . These cubes are used to obtain the Conley index of the maximal invariant set  $\mathcal{S}$  in the interior of  $\mathcal{B}$ ,

$$CH_*(\mathcal{S}) = H_*(\mathcal{B}, \mathcal{B}^-) = (0, 0, \mathbb{Z}, 0, \dots),$$

and corresponds to an isolated invariant set having the structure of a hyperbolic fixed point of (Morse) index 2.

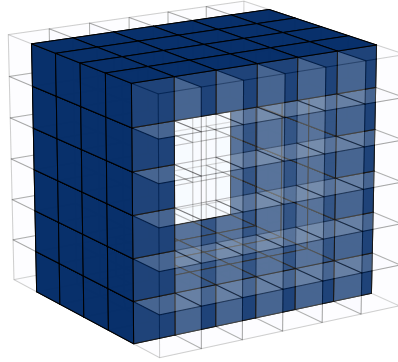


Figure 3.8: Cubical set representing the isolating block  $\mathcal{B}$  and  $\mathcal{B}^- \subset \partial\mathcal{B}$  which appears in the left panel of Figure 3.6. This cubical representation of  $\mathcal{B}$  and  $\mathcal{B}^-$  can be passed to the computer program `homcubes` to compute the relative homology groups  $H_*(\mathcal{B}, \mathcal{B}^-)$ , and therefore  $CH_*(\mathcal{S})$  for the maximal invariant set in  $\text{int } \mathcal{B}$ . The Conley index of the (Morse) index-2 hyperbolic equilibrium  $\mathcal{S}$  from (3.18) is  $CH_*(\mathcal{S}) = (0, 0, \mathbb{Z}, 0, \dots)$ , corresponding to the homology groups of the two-sphere  $\Sigma^2$ .

### 3.5.2 Local Charts and Piecewise-smooth Boundaries

We briefly indicate a possible extension of our approach. So far, we have always assumed that the boundary of the potential isolating block  $\mathcal{B}$  is given by a smooth manifold. For some applications, however, it might be useful to consider regions with piecewise smooth boundary  $\partial\mathcal{B}$ . Of course, on each of the maximal smooth subsets  $\mathcal{M}_k$  of  $\partial\mathcal{B}$ , we can still use the isolating block validation algorithm to verify the assumptions of Theorem 3.5.4. But

what can be said about the points in  $\partial\mathcal{B}$  at which the smooth submanifolds with boundary meet? For this, let  $\mathcal{M}_1 \subset \partial\mathcal{B}$  and  $\mathcal{M}_2 \subset \partial\mathcal{B}$  denote two closed smooth submanifolds of  $\partial\mathcal{B}$  with boundary, and assume that their intersection is contained in each of their boundaries. Furthermore, assume that both submanifolds satisfy the assumptions of Theorem 3.5.4, and that along their intersection, the region  $\mathcal{B}$  is convex in the following sense, which is due to [17]:

- (C) If  $p \in \mathcal{M}_1 \cap \mathcal{M}_2$ , then there exists a neighborhood  $U$  of  $p$  in  $\partial\mathcal{B}$ , such that for any point  $p_1 \in \mathcal{M}_1 \cap U$  and any point  $p_2 \in \mathcal{M}_2 \cap U$  their connecting line segment is completely contained in  $\mathcal{B}$ .

In this case, at all points  $p \in \mathcal{M}_1 \cap \mathcal{M}_2$  the flow of (3.1) either enters or exits in a non-trivial way, i.e., we have  $p \in \mathcal{B}^+ \setminus \mathcal{B}^-$  or  $p \in \mathcal{B}^- \setminus \mathcal{B}^+$ , respectively, or there exists a time  $T > 0$  such that  $\varphi([-T, T], p) \cap \mathcal{B} = \{p\}$ . In other words, it suffices to study only the smooth submanifolds up to and including their boundaries to establish an isolating block.

### 3.6 Rigorous, Algorithmic Validation of Candidate Isolating Blocks

We present a new algorithm that starts with a candidate isolating block  $\mathcal{B}$  for  $\mathcal{S}$  and either: (1) Rigorously proves that the candidate is a valid isolating block and returns a CW approximation to  $\partial\mathcal{B}$  and  $\mathcal{B}^- \subset \partial\mathcal{B}$ ; or (2) Fails to prove the candidate is a valid isolating block, yet returns a CW approximation to  $\mathcal{B}^-$ , and reveals where the candidate block needs to be altered in order to succeed; or (3) Fails to produce a CW-approximation to  $\mathcal{B}^-$  entirely<sup>9</sup>.

In §2.3.4 we established that the superlevel set validation algorithm (V) constructs CW complex approximations to  $N^+(\Omega, u)$ , where  $u : \Omega \subset \mathbb{R}^n \rightarrow \mathbb{R}$ , with the property that the positive cells in the resulting complex `cmplx` are guaranteed to be homotopically equivalent

---

<sup>9</sup>After all, the algorithm bootstraps the superlevel set algorithm (V).

to the set  $N^+(\Omega, u)$ . Recall also that the algorithm does not attempt to trace the zero level set, but uses interval arithmetic to determine if a zero level set crosses any given cell. Thus, once the top-dimensional cells `cmplx` are obtained, we can revisit those cells which were flagged as being monotone, and evaluate  $v$  on them (and only on them).

Let the boundary of a candidate isolating block be given by a coordinate chart  $r : \Omega \subset \mathbb{R}^{n-1} \rightarrow \mathbb{R}^n$ , where  $\Omega$  is a rectangular region. For example, if the candidate block is the unit sphere embedded in  $\mathbb{R}^3$  then one could have  $r : (\theta, \varphi) \mapsto (\sin \theta \cos \varphi, \sin \theta \sin \varphi, \cos \varphi)$ , where  $\Omega = [0, 2\pi] \times [0, \pi] \subset \mathbb{R}^2$ . This permits the direct application of Theorem 3.5.4 since  $u$  and  $v$  can be computed immediately from this chart (we refer to 3.5.1 for a more complete construction). Given this,

**The isolating block validation algorithm (IB) proceeds as follows:**

**Input:** The functions  $u$  and  $v$ , and the rectangular region  $\Omega$ .

**Output:** One of three possible pairs:

(Success, CW-complex)	The algorithm was able to validate the assumptions of Theorem 3.5.4 on $\Omega$ , and the rigorous CW-complex approximation to $N^+(\Omega, u)$ on $\Omega$ from the Algorithm (V).
(No Success, CW-complex)	The algorithm was not able to validate the assumptions of Theorem 3.5.4 on $\Omega$ , yet the Algorithm (V) was able to generate the rigorous CW-complex approximation to $N^+(\Omega, u)$ .
(No Success, No CW-complex)	The algorithm was not able to validate the assumptions of Theorem 3.5.4 on $\Omega$ because the Algorithm (V) failed to generate the rigorous CW-complex approximation to $N^+(\Omega, u)$ on $\Omega$ .

(IB1) Apply the superlevel set validation algorithm (V) to the function  $u$  on the region  $\Omega \subset \mathbb{R}^{n-1}$ . If this algorithm fails then the isolating block validation algorithm fails as well. If it succeeds, initialize the list  $\mathcal{Q}$  with the  $(n - 1)$ -cells of the resulting



CW-complex `cmplx`.

(IB2) For  $C \in \mathcal{Q}$ :

- (a) If the boundary cells of  $C$  were all positive or all negative (as determined in step (V4, b)<sup>†</sup>), add  $C$  to the list  $\mathcal{V}$ .
- (b) If some boundary cells of  $C$  were positive and some negative, and  $C$  was validated as monotone (as determined in step (V4, c)), obtain the range enclosure  $[v(C)]$ . If  $v$  can be determined to be positive on  $C$ , then add  $C$  to the list  $\mathcal{V}$ , otherwise add  $C$  to the list  $\mathcal{T}$ .

If the list  $\mathcal{T}$  is empty after all cells in  $\mathcal{Q}$  have been examined, then the algorithm returns True – this is a valid isolating block. Otherwise, proceed to (IB3).

(IB3) For  $C \in \mathcal{T}$ , divide  $C$  to obtain the  $(n - 1)$ -dimensional cells  $C_1$  and  $C_2$ . Apply the superlevel set validation algorithm to the function  $u$  on the cells  $C_1$  and  $C_2$ . If this algorithm fails then the isolating block validation algorithm fails as well. If it succeeds, add the  $(n - 1)$ -dimensional cells of the resulting CW-complex to the list  $\mathcal{Q}$ . Once  $\mathcal{T}$  is empty, return to step (IB2) to examine all cells in  $\mathcal{Q}^\ddagger$ .

<sup>†</sup> This requires adding another flag in the superlevel set validation algorithm at steps (V4b) and (V4c).

<sup>‡</sup> There is a user-defined number of times step (IB2) can be re-entered.

We include the following theorem for future reference:

**Theorem 3.6.1 (Isolating Block Verification).** *Let  $r : \Omega \rightarrow \partial\mathcal{B}$ , where  $\Omega \subset \mathbb{R}^{n-1}$  and  $\partial\mathcal{B} \subset \mathbb{R}^n$ , be a parameterization for the manifold  $\partial\mathcal{B}$ , and let  $u, v : \partial\mathcal{B} \rightarrow \mathbb{R}$  denote the smooth exit set and tangency test functions from the theorem, expressed in coordinates on  $\Omega$ . If the isolating block validation algorithm (IB) successfully finishes when applied to  $u, v$  on  $\Omega$ , then (3.16) is satisfied on the closed subset of  $\partial\mathcal{B}$  which is parametrized over  $\Omega$ .*

Moreover, if the above holds for a finite number of parametric domains whose images cover the manifold  $\partial\mathcal{B}$ , then the set  $\mathcal{B}$  is an isolating block for (3.1).

*Proof.* Let  $\mathcal{V}$  denote the collection of validated rectangles at the end of algorithm (IB). Since each of these rectangles has passed the validation steps from (V), Theorem 2.3.3 implies that zero is a regular value over each rectangle, hence over all of  $\Omega$ .

Now let  $p \in \partial\mathcal{B}$  be any point with  $u(p) = 0$ . Then there exists a rectangle  $R \in \mathcal{V}$  with  $r^{-1}(p) \in R$ . Since  $R$  has passed step (IB2) and contains a zero of  $u$ , it must have passed step (IB2)(b). This shows that  $v > 0$  on  $R$ , and therefore we have  $v(p) > 0$ . This completes the proof of the theorem.  $\square$

Pseudocode is provided for Algorithm (IB) below.

---

**Algorithm (IB) 4**

(**cellComplex**, **vector**< **cell** >, **bool**) isolating\_block\_validation(  
**Differentiable** exit\_set\_u, **Differentiable** tangency\_test\_v, **coordinates** U)

---

**Input:** Continuously differentiable functions exit\_set\_u and tangency\_test\_v, description of rectangular set  $U \subset \text{Domain}$   $u, v \in \mathbb{R}^n$

```
1: bool is_valid_block = False
2: cellComplex Q_original = validate_superlevel_set(exit_set_u, U)
3: vector< cell > Q = Q_original.get_n_dimensional_cells()
4: list T, V
5: while Q is not empty, do
6:   for q in Q do
7:     if has_mixed_boundary(q), then
8:       T.append(q)
9:     else
10:      V.append(q)
11:    Q.remove(q)
12:  while T is not empty, do
13:    cell t = T.pop()
14:    if tangency_test_v is positive on t, then
15:      V.append(t)
16:    else
17:      cell t1, t2
18:      t1, t2 = split(t)
19:      cellComplex A = validate_superlevel_set(exit_set, t1.coordinates)
20:      cellComplex B = validate_superlevel_set(exit_set, t2.coordinates)
21:      vector< cell > A_n_cells = A.get_n_dimensional_cells()
22:      vector< cell > B_n_cells = B.get_n_dimensional_cells()
23:      Q.append(A_n_cells)
24:      Q.append(B_n_cells)
25:  if T is empty, then
26:    is_valid_block = True
27: return (Q_original, V, is_valid_block)
```

---

---

**Subroutine bool has\_mixed\_boundary(cell cell)**

---

**Input:** Validated **cell** cell

```
1: bool has_mx_bd = False
2: bool contains_neg = False
3: bool contains_pos = False
4: vector< cell > skeleton_of_cell = cell.get_n_skeleton()
5: while skeleton_of_cell is not empty, do
6:   cell boundary_cell = skeleton_of_cell.pop()
7:   if boundary_cell is validated as negative, then
8:     contains_neg = True
9:   else if boundary_cell is validated as positive, then
10:    contains_pos = True
11:   if contains_neg & contains_pos, then
12:     has_mx_bd = True
13:   break
14: return has_mx_bd
```

---

### 3.7 Applications: Computer-assisted Proofs of Dynamical Behavior using the Conley Index

In this section we will consider ordinary differential equations  $\dot{x} = f(x)$  which permit a global flow  $\varphi : \mathbb{R} \times \mathbb{R}^n \rightarrow \mathbb{R}^n$ . The isolated invariant sets we identify may be thought of as benchmarks of sorts, because in each case<sup>10</sup> the isolated invariant sets we discover are either known, or have been found by other means. We are pleased to be able to meet these benchmarks with a single, unified method. Furthermore, the infrastructure teardown and rebuild between examples is very minor. That is, transitioning between examples requires only obtaining a parameterization or a level set description of the boundary  $\partial\mathcal{B}$  of a candidate block  $\mathcal{B}$  (cf. §3.5.2). Obtaining a computer-assisted proof about the structure of the maximal invariant set  $\mathcal{S}$  isolated by  $\mathcal{B}$  requires the successful completion of Algorithm (IB) applied to  $\mathcal{B}$ , and typically some knowledge about the vector field  $f$  (for example, that  $f$  is gradient-like on some subset of  $\mathcal{B}$ , or that  $f$  is invariant on some subset of  $\mathcal{B}$ ).

The first result, Result (1), of the first example is explained in great detail in order to firmly establish our framework. With this in place, we progress easily through the remaining examples. For all examples, the workflow will follow the general pattern:

1. *Identify a region of interest* in the phase space of the flow generated by a vector field  $f : \mathbb{R}^n \rightarrow \mathbb{R}^n$
2. *Propose compact sets*  $\mathcal{B}_i \subset \mathbb{R}^n$  as candidate isolating blocks for the flow
3. *Apply Algorithm (IB)* to the candidate blocks  $\mathcal{B}_i$ , and **if Algorithm (IB) succeeds**
4. *Compute the Conley index*  $CH(\mathcal{S}_i)$  of the isolated invariant sets  $\mathcal{S}_i \subset \mathcal{B}_i$
5. *Combine information* from the Conley index and facts about the vector field  $f$  to obtain computer-assisted proofs of the structure of the isolated invariant sets  $\mathcal{S}_i$

---

<sup>10</sup>Each case except one – to our knowledge, the heteroclinics in §3.7.1 between the equilibria  $p_0$  and  $p_2$ , and between the equilibria  $p_1$  and  $p_2$ , have not been individually identified. The statement obtained in [17] was along the lines of ‘*at least one* of the heteroclinics is guaranteed to exist.’

### 3.7.1 A Simple Gradient System

Our first example is taken from Eberlein's thesis [17] and is the system

$$\begin{aligned}\dot{x} &= 2x(z - y) , \\ \dot{y} &= 1 + z - x^2 , \\ \dot{z} &= -1 + y + x^2 .\end{aligned}\tag{3.29}$$

This system is a gradient system with associated potential

$$V(x, y, z) = x^2y - x^2z - yz - y + z ,\tag{3.30}$$

i.e., the right-hand side of (3.29) is given by  $-\nabla V(x, y, z)$ , and the flow generated by (3.29) decreases the potential  $V$ .

The system (3.29) has exactly three equilibrium solutions given by  $p_0 = (-1, 0, 0)$ ,  $p_1 = (1, 0, 0)$ , and  $p_2 = (0, 1, -1)$ . Each of these are hyperbolic with (Morse) indices 2, 2, and 1, respectively.

**In this section we will show:** Result (1) The result in [17]: establishing that there is at least one heteroclinic connection between  $p_2$  and an isolated invariant set  $\mathcal{S}_{01}$  satisfying  $p_0 \in \mathcal{S}_{01}$  and  $p_1 \in \mathcal{S}_{01}$ ; Result (2) There exists a heteroclinic connection between  $p_0$  and  $p_2$ ; and Result (3) There exists a heteroclinic connection between  $p_1$  and  $p_2$ . (Note that Results (2) and (3) sharpen Result (1).)

**To show Result (1):** We first propose three candidate isolating blocks, namely the block  $\mathcal{A}_{01}$ , which isolates the equilibria  $p_0$  and  $p_1$ , the block  $\mathcal{A}_2$ , isolating the equilibrium  $p_2$ , and  $\mathcal{A}_{012}$ , which isolates all three equilibria  $p_0$ ,  $p_1$ , and  $p_2$ .

- The candidate block  $\mathcal{A}_{01}$ , shown in Figure 3.9, is an ellipse centered at the origin, where the boundary of  $\mathcal{A}_{01}$  is parameterized by  $r : [0, 2\pi] \times (0, \pi) \rightarrow \partial\mathcal{A}_{01}$ , defined as

$$r(\varphi, \theta) = (a \cos \varphi \sin \theta, b \sin \varphi \sin \theta, c \cos \theta) , \quad \text{with} \quad a = 6/5, b = 3/10, c = 3/10$$

- The candidate block  $\mathcal{A}_2$ , shown in Figure 3.13, is a sphere centered at  $p_2 = (x_2, y_2, z_2) = (0, 1, -1)$ , with radius  $\rho = 1/5$ . The boundary of the block is parameterized using spherical coordinates  $r : [0, 2\pi] \times (0, \pi) \rightarrow \partial\mathcal{A}_2$ , however the boundary of the exit set  $\mathcal{A}_2^-$  intersects the “north pole” of the sphere if we use the standard parameterization. This can be remedied by rotating the standard parameterization, for example letting  $r$  take the form

$$r(\varphi, \theta) = \rho (\cos \varphi \sin(\theta - \pi/4) + x_2, \sin \varphi \sin(\theta - \pi/4) + y_2, \cos(\theta - \pi/4) + z_2)$$

- The candidate block  $\mathcal{A}_{012}$ , shown in Figure 3.12, is the sphere of radius  $\rho = 3/2$  centered at  $(x_{012}, y_{012}, z_{012}) = (0, 1/2, -1/2)$ , and the boundary of  $\mathcal{A}_{012}$  is parameterized by  $r : [0, 2\pi] \times (0, \pi) \rightarrow \partial\mathcal{A}_{012}$ , defined as

$$r(\varphi, \theta) = \rho (\cos \varphi \sin \theta + x_{012}, \sin \varphi \sin \theta + y_{012}, \cos \theta + z_{012})$$

Figure 3.9 shows the candidate block  $\mathcal{A}_{01}$  in the phase space. The boundary of the candidate has been shaded dark blue where the vector field (3.29) points outward from  $\mathcal{A}_{02}$ , and light blue where it points inward. The vector field is tangent to  $\mathcal{A}_{02}$  along the boundary between these shaded regions. The left panel of Figure 3.10 shows a numerical approximation of the exit set function  $u(p) = \langle f(p), \nu_p \rangle$  from Lemma 3.5.2 on the parametric domain  $\Omega = [0, 2\pi] \times (0, \pi)$ . Thus, one can imagine the patch shown in the left panel to wrap around the sphere defining  $\mathcal{A}_{01}$ , so that the lines  $\{0\} \times (0, \pi)$  and  $\{2\pi\} \times (0, \pi)$  are identified to form a meridian, and the entire line  $[0, 2\pi] \times \{\pi\}$  is the “north pole” of  $\mathcal{A}_{01}$ , while  $[0, 2\pi] \times \{0\}$  is the “south pole”. The right panel of Figure 3.10 shows a numerical approximation of the tangency test function  $v(p) = \langle Df(p)f(p), \nu_p \rangle - \mathbb{I}(\pi_p^\top f(p), \pi_p^\top f(p))$  from Lemma 3.5.3 on the parametric domain  $\Omega = [0, 2\pi] \times (0, \pi)$ . Again, one can imagine the patch shown in the right panel to wrap around the sphere defining  $\mathcal{A}_{01}$ , however in this case the tangency test is only relevant where  $u(p) = 0$ . An approximation to the level set

$N^0(\Omega, u)$  has been superimposed over the evaluation of  $v$  to help indicate regions on the boundary of the block where the flow is both tangent ( $u = 0$ ), and forms an internal tangency ( $v < 0$ ). We emphasize that Algorithm (IB) must be applied to the boundary of the block in order to guarantee that the points  $p \in \partial\mathcal{A}_{01}$  where  $u(p) = 0$  satisfy the condition that  $v(p) > 0$ , thereby establishing that 0 is a regular value of  $u$ , and that  $N^0(\Omega, u) \subset N^+(\Omega, v)$  (cf. Theorems 2.3.3 and 3.5.4).

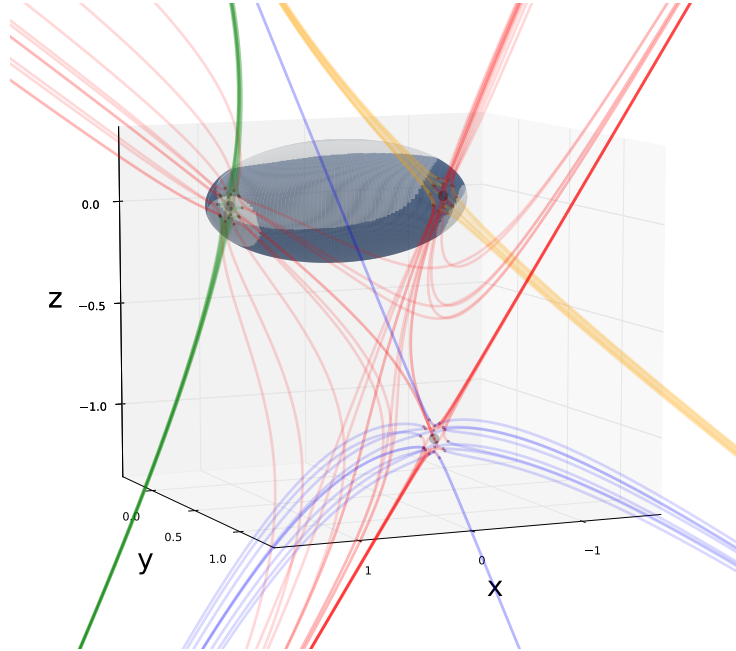
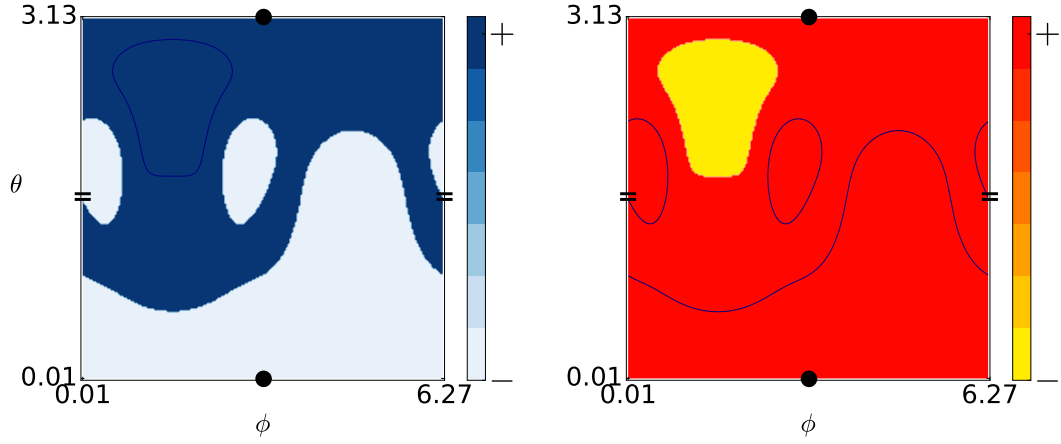


Figure 3.9: Several trajectories of Equation (3.29), along with the isolating block  $\mathcal{A}_{01}$ . Red trajectories are leaving their respective equilibria, and orange, green, and blue trajectories are traveling toward their respective equilibria.

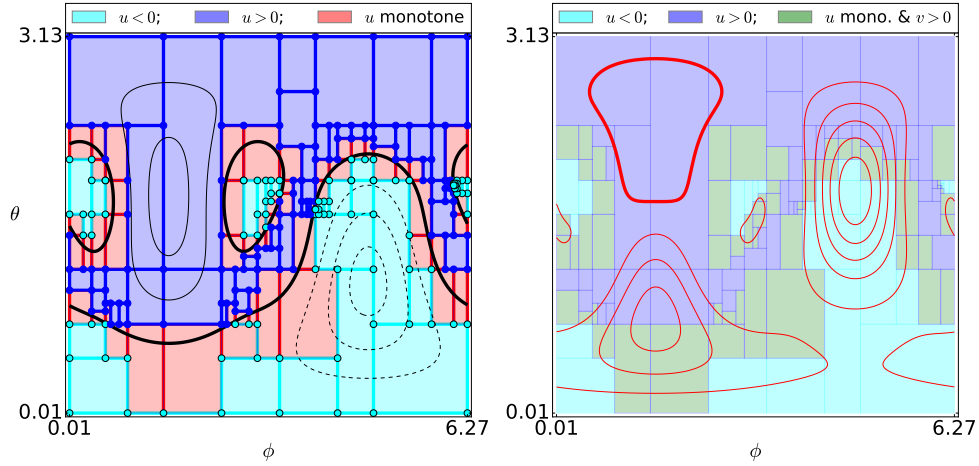
We are ready to apply Algorithm (IB) to each candidate block. The output of the algorithm applied to  $\mathcal{A}_{01}$  is shown in Figure 3.10. Algorithm (V) does not resolve  $N^0(\Omega, u)$  explicitly, but it does resolve rectangular subsets of  $\Omega$  on which  $u$  takes both positive and negative values (the monotone cells), and in the figure these cells are marked in red. The

right panel shows information from the successful completion of Algorithm (IB). Algorithm (IB) operates on cells  $R^n$  which are red on the left, and tests them for internal tangencies using  $v$  – if the cell  $R^n$  is red, and  $\inf[v(R^n)]$  is not bounded above zero, then  $R^n$  is divided and the resulting cells are submitted to (V). Green rectangles  $R^n$  in the right panel indicate that  $u$  takes both positive and negative values on  $R^n$ , and that  $\inf[v(R^n)] > 0$ , thus eliminating the possibility for internal tangencies on the portion of the block parameterized over  $R^n$ .





(a) Positive and negative regions of  $u$  and  $v$  over the domain  $\Omega = [0, 2\pi] \times (0, \pi)$ . The left panel shows the zero level set of  $v$  superimposed onto the plot of  $u$ . The right panel shows the zero level set of  $u$  superimposed onto the plot of  $v$ , and in this example it appears that  $N^0(\Omega) \subset \mathbb{N}^+(\Omega, v)$ .



(b) Validation that the candidate block  $\mathcal{A}_{01}$  is, indeed, an isolating block for Equation 3.29. The left panel shows all cells in `cmplx` constructed by Algorithm (V) applied to  $u$  over  $\Omega$ . The function  $u$  takes both positive and negative values on the red cells (the monotone cells in `cmplx`), and this is corroborated by the contour lines of  $u$  superimposed onto the colored cell complex. The right panel illustrates the work done by Algorithm (IB). Contours of  $v$  have been superimposed in red. In order to establish  $N^0(\Omega, u) \subset N^+(v)$ , Algorithm (IB) evaluates  $v$  on each red rectangle from the left, subdividing red rectangles if necessary. See Figure 3.17 for an example where these further subdivisions were necessary to establish  $N^0(\Omega, u) \subset N^+(v)$ .

Figure 3.10: The candidate block  $\mathcal{A}_{01}$  is an isolating block.

The successful completion of Algorithm (IB) on the candidate block  $\mathcal{A}_{01}$  allows us to use  $\mathcal{A}_{01}$  to compute the Conley index  $CH(\mathcal{S}_{01}) = H_*(\mathcal{A}_{01}, \mathcal{A}_{01}^-)$ , the Conley index of the

maximal invariant set  $\mathcal{S}_{01}$  contained within the interior of  $\mathcal{A}_{01}$ . The first step to computing  $H_*(\mathcal{A}_{01}, \mathcal{A}_{01}^-)$  is to submit **cmplx+**, the homotopy equivalent approximation to  $N^+(\Omega, u)$  produced by Algorithm (V), to the computational topology toolbox PHAT [6]. This step produces the Betti numbers of  $N^+(\Omega, u)$ , which allow us to create an accurate cubical representation of the pair  $(\mathcal{A}_{01}, \mathcal{A}_{01}^-)$ , which can then be sent to the program **homcubes**, from CHomP [10], to compute the relative homology. Figure 3.11 shows a cubical representation of  $\mathcal{A}_{01}$  and  $\mathcal{A}_{01}^- \subset \partial\mathcal{A}_{01}$ . The program **homcubes** computes the relative homology  $H_*(\mathcal{A}_{01}, \mathcal{A}_{01}^-)$ , which reveals the Conley index of  $\mathcal{S}_{01}$  to be

$$CH(\mathcal{S}_{01}) = (0, 0, \mathbb{Z}^2, 0, \dots)$$

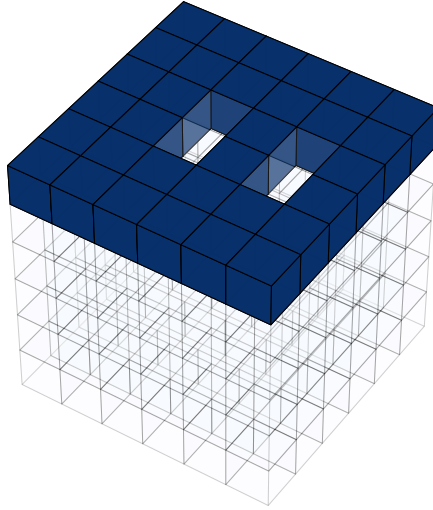


Figure 3.11: Cubical representation of  $\mathcal{A}_{01} \subset \mathbb{R}^3$ . The darkened cubes represent a set that has the same Betti numbers as  $\mathcal{A}_{01}^- \subset \partial\mathcal{A}_{01}$ . The program **homcubes** computes the relative homology  $H_*(\mathcal{A}_{01}, \mathcal{A}_{01}^-)$ , yielding  $H_*(\mathcal{A}_{01}, \mathcal{A}_{01}^-) = CH_*(\mathcal{S}_{01}) = (0, 0, \mathbb{Z}^2, 0, \dots)$ .

The candidate blocks  $\mathcal{A}_2$  and  $\mathcal{A}_{012}$  are shown positioned in the phase space in Figures 3.13 and 3.12, below. Algorithm (IB) applied to these candidate blocks is successful, and

the output of (IB) is shown in Figures 3.15 and 3.16. The Conley indices of  $\mathcal{S}_2$  and  $\mathcal{S}_{012}$  are computed precisely as above, resulting in

$$CH(\mathcal{S}_2) = (0, \mathbb{Z}, 0, 0, \dots)$$

$$CH(\mathcal{S}_{012}) = (0, 0, \mathbb{Z}, 0, \dots)$$

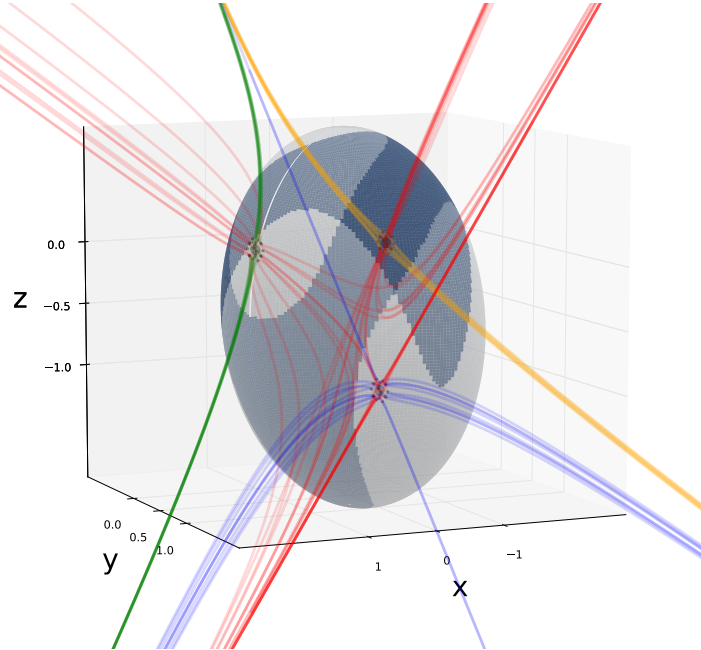


Figure 3.12: Several trajectories of Equation (3.29), along with the isolating block  $\mathcal{A}_{012}$  surrounding  $p_0$ ,  $p_1$ , and  $p_2$ . Red trajectories are leaving their respective equilibria, and orange, green, and blue trajectories are traveling toward their respective equilibria.

At this point we turn back to Equation 3.29, and combine information from Conley index with facts about the vector field 3.29 to obtain Result (1) There is at least one heteroclinic connection between  $p_2$  and an isolated invariant set  $\mathcal{S}_{01}$ . To see this, assume that  $\mathcal{S}_{01}$  and  $p_2$  comprise the maximal invariant set isolated by the block  $\mathcal{A}_{012}$ . By the

summation formula discussed in §3.3.4, we expect to have  $CH(\mathcal{S}_{012}) \simeq CH(\mathcal{S}_{01}) \oplus CH(\mathcal{S}_2)$ .

However, the homomorphism does not hold:

$$CH(\mathcal{S}_{012}) = (0, 0, \mathbb{Z}, 0, \dots)$$

$$\neq (0, 0, \mathbb{Z}^2, 0, \dots) \oplus (0, \mathbb{Z}, 0, 0, \dots) = CH(\mathcal{S}_{01}) \oplus CH(\mathcal{S}_2)$$

This immediately implies that  $\mathcal{S}_{012}$  contains more than  $\mathcal{S}_{01}$  and  $\mathcal{S}_2$ . This, together with the fact that 3.29 is a gradient system with three hyperbolic fixed points, the only other type of globally bounded orbits are heteroclinic orbits between these equilibrium solutions, therefore the maximal invariant set  $\mathcal{S}_{012}$  contains at least one heteroclinic orbit.

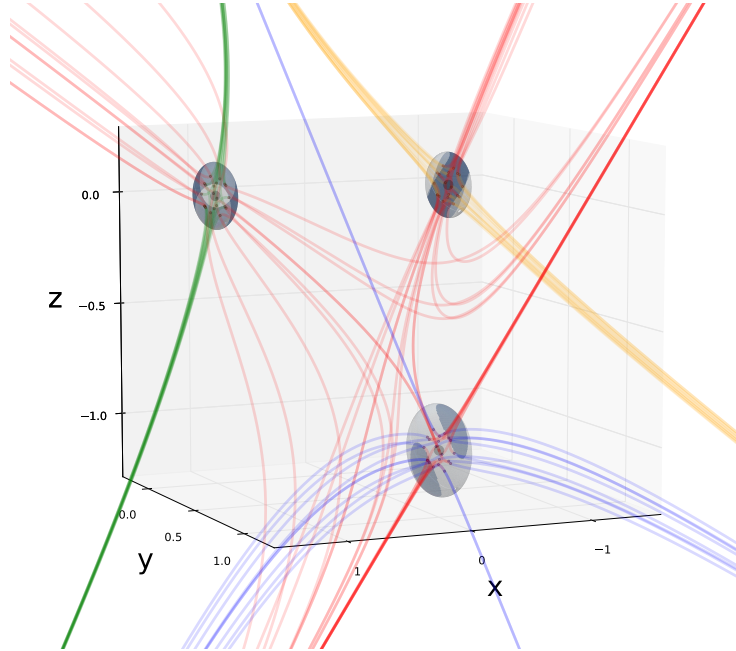


Figure 3.13: Trajectories of Equation (3.29), along with the isolating blocks  $\mathcal{A}_0$ ,  $\mathcal{A}_1$ , and  $\mathcal{A}_2$  individually surrounding  $p_0$ ,  $p_1$ , and  $p_2$ , respectively. Red trajectories are leaving their respective equilibria, and orange, green, and blue trajectories are traveling toward their respective equilibria.

**To show Results (2) and (3):** We will use  $\mathcal{A}_2$  from Result (1) and propose four new candidate isolating blocks, namely

- The candidate block  $\mathcal{A}_0$ , shown in Figure 3.13, is the sphere centered at  $p_0 = (x_0, y_0, z_0) = (-1, 0, 0)$ , with radius  $\rho = 3/20$ . The boundary of the block is parameterized using spherical coordinates  $r : [0, 2\pi] \times (0, \pi) \rightarrow \partial\mathcal{A}_2$ , however once again the boundary of the exit set  $\mathcal{A}_0^-$  intersects the “north pole” of the sphere if we use the standard parameterization. Therefore we let  $r$  take the form

$$r(\varphi, \theta) = \rho (\cos \varphi \sin(\theta - \pi/4) + x_0, \sin \varphi \sin(\theta - \pi/4) + y_0, \cos(\theta - \pi/4) + z_0)$$

- The candidate block  $\mathcal{A}_1$ , shown in Figure 3.13, is the sphere centered at  $p_1 = (x_1, y_1, z_1) = (1, 0, 0)$ , with radius  $\rho = 3/20$ , with boundary parameterized by

$$r(\varphi, \theta) = \rho (\cos \varphi \sin(\theta - \pi/4) + x_1, \sin \varphi \sin(\theta - \pi/4) + y_1, \cos(\theta - \pi/4) + z_1)$$

- The candidate blocks  $\mathcal{A}_{02}$  and  $\mathcal{A}_{12}$ , shown in Figure 3.14, are congruent 2-norm ellipsoids which are centered at the points  $(x_{02}, y_{02}, z_{02}) = (-1/2, 1/2, -1/2)$  and  $(x_{12}, y_{12}, z_{12}) = (1/2, 1/2, -1/2)$ , respectively. The parameterization of  $\partial\mathcal{A}_{02}$  is given by

$$r(\varphi, \theta) = \begin{pmatrix} 1/\sqrt{3} \\ 1/\sqrt{3} \\ -1/\sqrt{3} \end{pmatrix} a \sin \theta \cos \varphi + \begin{pmatrix} -1/\sqrt{2} \\ 1/\sqrt{2} \\ 0 \end{pmatrix} b \sin \theta \sin \varphi + \begin{pmatrix} -1/\sqrt{6} \\ -1/\sqrt{6} \\ -2/\sqrt{6} \end{pmatrix} c \cos \theta + \begin{pmatrix} x_{02} \\ y_{02} \\ z_{02} \end{pmatrix},$$

$$\begin{aligned}
r(\varphi, \theta) = & \begin{pmatrix} 1/\sqrt{3} \\ 1/\sqrt{3} \\ -1/\sqrt{3} \end{pmatrix} a \sin \theta \cos \varphi + \begin{pmatrix} -1/\sqrt{2} \\ 1/\sqrt{2} \\ 0 \end{pmatrix} b \sin \theta \sin \varphi \\
& + \begin{pmatrix} -1/\sqrt{6} \\ -1/\sqrt{6} \\ -2/\sqrt{6} \end{pmatrix} c \cos \theta + \begin{pmatrix} x_{02} \\ y_{02} \\ z_{02} \end{pmatrix},
\end{aligned}$$

and the parameterization of  $\partial\mathcal{A}_{12}$  is given by

$$\begin{aligned}
r(\varphi, \theta) = & \begin{pmatrix} -1/\sqrt{3} \\ 1/\sqrt{3} \\ -1/\sqrt{3} \end{pmatrix} a \sin \theta \cos \varphi + \begin{pmatrix} 1/\sqrt{2} \\ 1/\sqrt{2} \\ 0 \end{pmatrix} b \sin \theta \sin \varphi \\
& + \begin{pmatrix} 1/\sqrt{6} \\ -1/\sqrt{6} \\ -2/\sqrt{6} \end{pmatrix} c \cos \theta + \begin{pmatrix} x_{12} \\ y_{12} \\ z_{12} \end{pmatrix},
\end{aligned}$$

where  $a = 12/5$ , and  $b = c = 6/5$ .

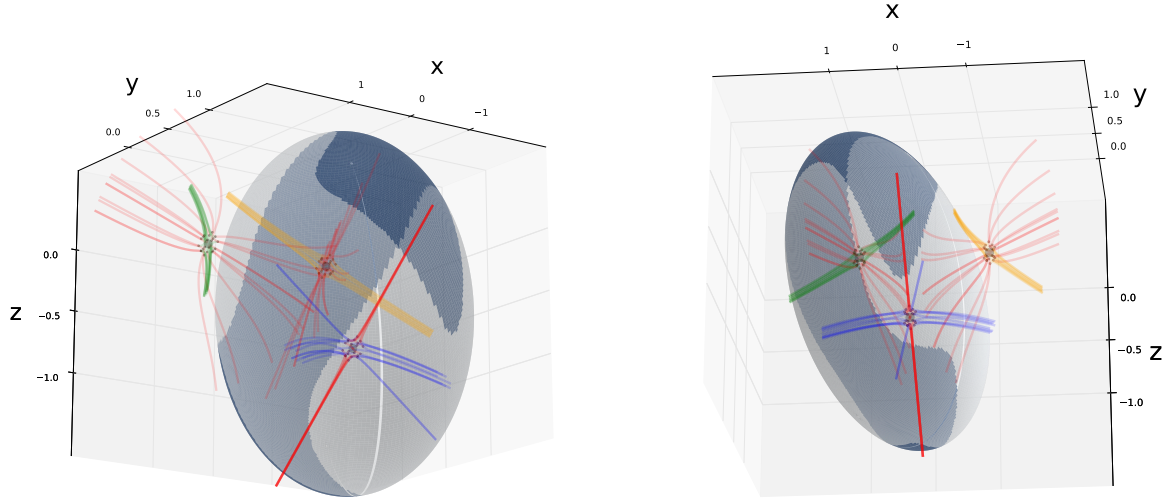


Figure 3.14: Trajectories of Equation (3.29), along with the isolating block  $\mathcal{A}_{02}$  (left) around  $p_0$  and  $p_2$ , and  $\mathcal{A}_{12}$  (right) around  $p_1$  and  $p_2$ .

Just as in Result (1), we first validate the new blocks using Algorithm (IB). The output of (IB) on the four new blocks is shown in Figures 3.18, 3.19, 3.17 and 3.20. Next we assume  $\mathcal{A}_{02}$  contains only  $\mathcal{S}_0$  and  $\mathcal{S}_2$ , the maximal invariant sets isolated by  $\mathcal{A}_0$  and  $\mathcal{A}_2$ , respectively. This assumption sets up the summation formula, which is immediately seen to fail. In particular,

$$CH(\mathcal{S}_{02}) = (0, 0, 0, 0, \dots)$$

$$\neq (0, 0, \mathbb{Z}, 0, \dots) \oplus (0, \mathbb{Z}, 0, \dots) = CH(\mathcal{S}_0) \oplus CH(\mathcal{S}_2), \quad \text{and}$$

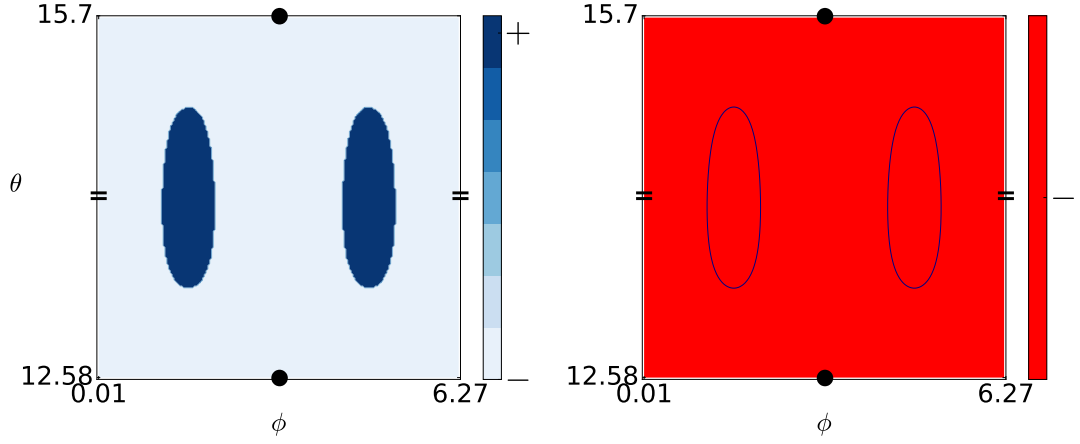
$$CH(\mathcal{S}_{12}) = (0, 0, 0, 0, \dots)$$

$$\neq (0, 0, \mathbb{Z}, 0, \dots) \oplus (0, \mathbb{Z}, 0, \dots) = CH(\mathcal{S}_1) \oplus CH(\mathcal{S}_2).$$

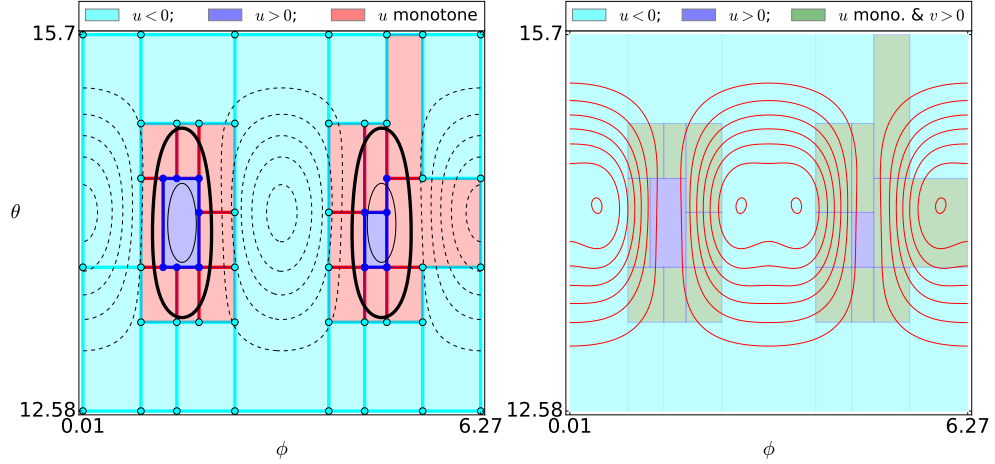
In this case we have that  $\mathcal{S}_{02}$  contains bounded invariant sets other than just the equilibria isolated by  $\mathcal{A}_0$  and  $\mathcal{A}_2$ , and similarly,  $\mathcal{S}_{12}$  contains more than just the equilibria in  $\mathcal{A}_1$  and  $\mathcal{A}_2$ . In each case, combining this Conley index information with the fact that (3.29) is a

gradient flow with only hyperbolic equilibria, we see that there is a heteroclinic connection between  $p_0$  and  $p_2$ , and another connection between  $p_0$  and  $p_2$ . This completes all results for this example, below are figures corresponding to the validations of the candidate isolating blocks used above.



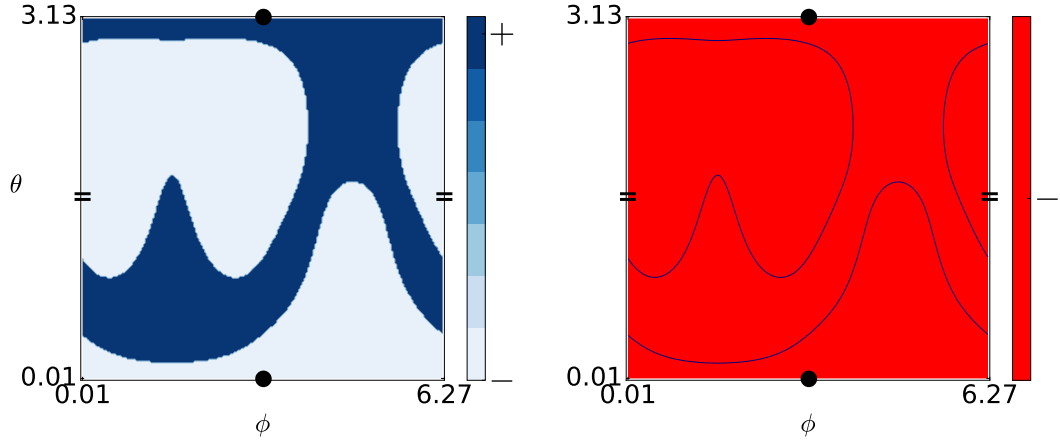


(a) Positive and negative regions of  $u$  and  $v$  over the domain  $\Omega = [0, 2\pi] \times (0, \pi)$ . The left panel shows the zero level set of  $v$  superimposed onto the plot of  $u$ . The right panel shows the zero level set of  $u$  superimposed onto the plot of  $v$ .

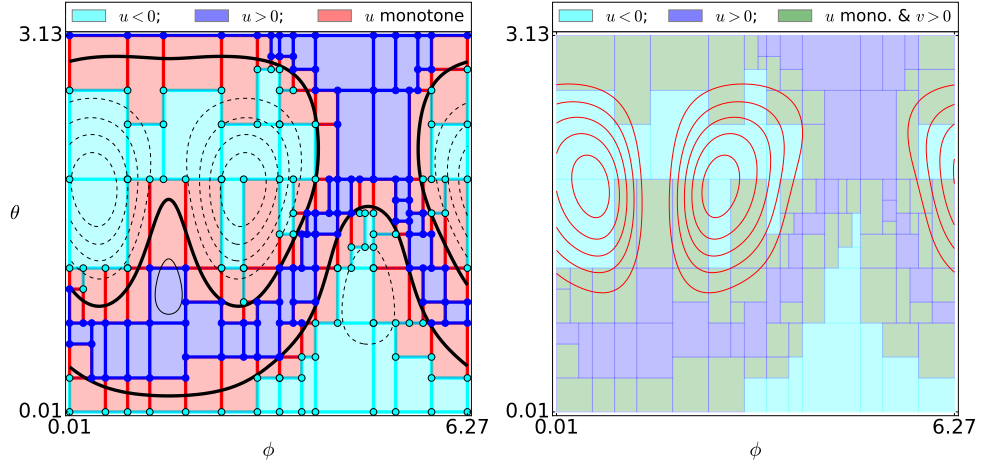


(b) Validation that the candidate block  $\mathcal{A}_2$  is, indeed, an isolating block for Equation 3.29. The color red is used in the left panel to indicate cells in `cmplx` where  $u$  takes both positive and negative values. This is emphasized by the contour lines of  $u$  superimposed onto the colored cell complex. The right panel illustrates the work done by Algorithm (IB). Contours of  $v$  have been superimposed in red. The tangency test function  $v$  was easily established as positive on all monotone cells from `cmplx`.

Figure 3.15: The candidate block  $\mathcal{A}_2$  is an isolating block.

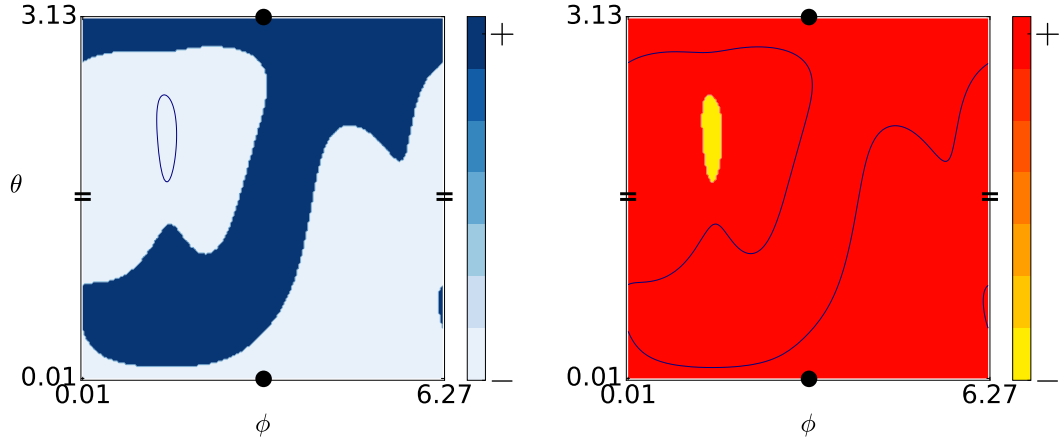


(a) Positive and negative regions of  $u$  and  $v$  over the domain  $\Omega = [0, 2\pi] \times (0, \pi)$ . The left panel shows the zero level set of  $v$  superimposed onto the plot of  $u$ . The right panel shows the zero level set of  $u$  superimposed onto the plot of  $v$ .

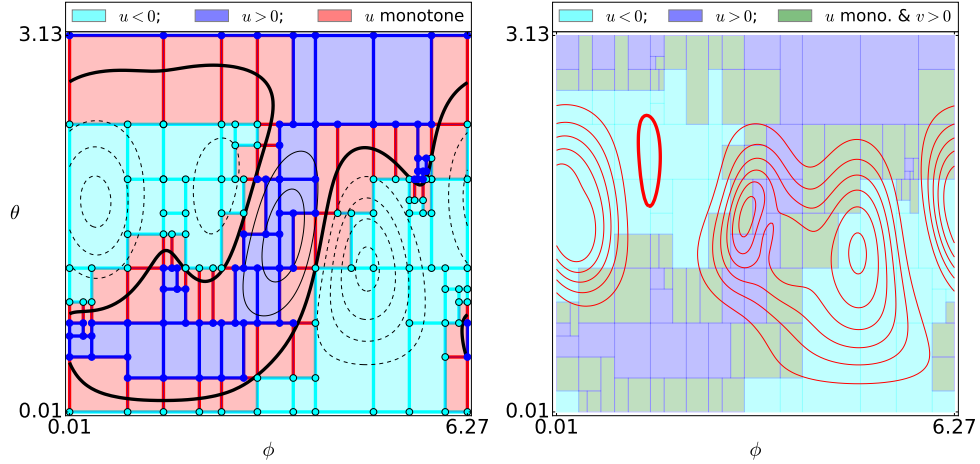


(b) Validation that the candidate block  $\mathcal{A}_{012}$  is, indeed, an isolating block for Equation 3.29. The color red is used in the left panel to indicate cells in `cmplx` where  $u$  takes both positive and negative values. This is emphasized by the contour lines of  $u$  superimposed onto the colored cell complex. The right panel illustrates the work done by Algorithm (IB). Contours of  $v$  have been superimposed in red. The tangency test function  $v$  was easily established as positive on all monotone cells from `cmplx`.

Figure 3.16: The candidate block  $\mathcal{A}_{012}$  is an isolating block.

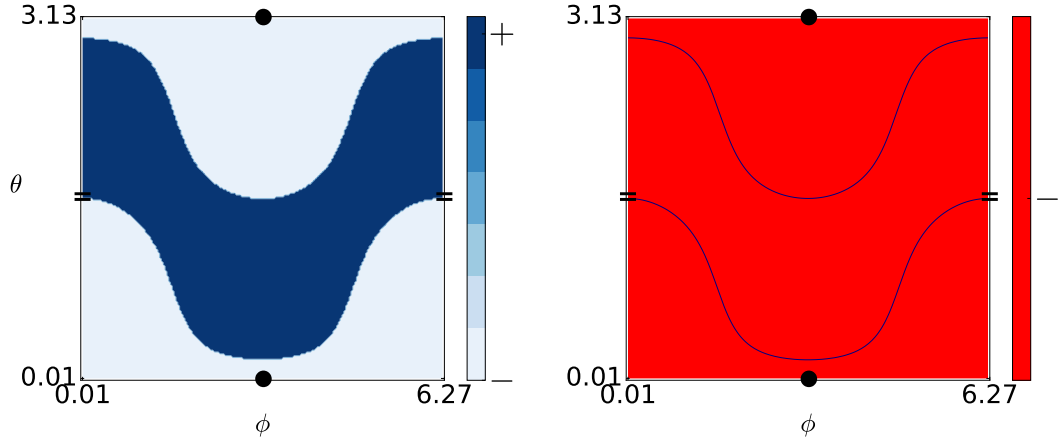


(a) Positive and negative regions of  $u$  and  $v$  over the domain  $\Omega = [0, 2\pi] \times (0, \pi)$ . The left panel shows the zero level set of  $v$  superimposed onto the plot of  $u$ . The right panel shows the zero level set of  $u$  superimposed onto the plot of  $v$ .

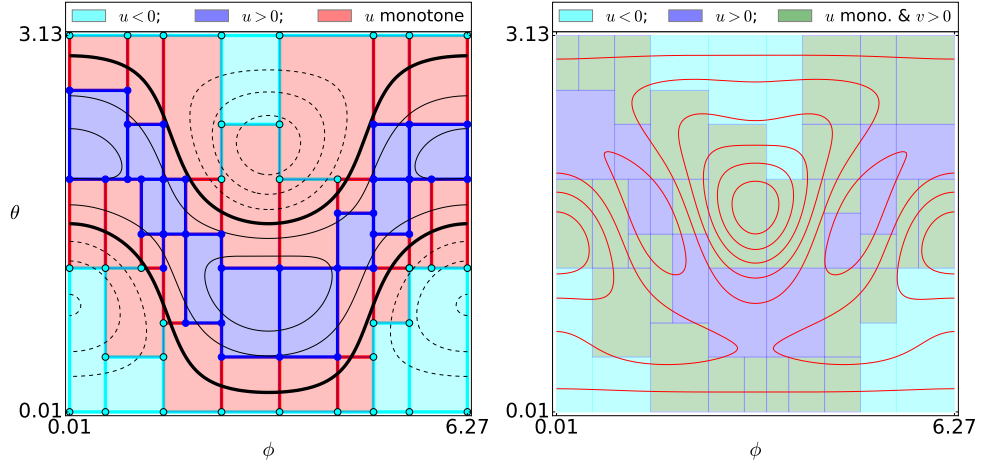


(b) Validation that the candidate block  $\mathcal{A}_{02}$  is, indeed, an isolating block for Equation 3.29. The right panel illustrates the work done by Algorithm (IB). It is apparent from this figure that the monotonicity information from  $u$  had to be tightened by (IB, step (b)) in order to establish the positivity of  $v$  in those regions (most notably, near the top left of the panel).

Figure 3.17: The candidate block  $\mathcal{A}_{02}$  is an isolating block.

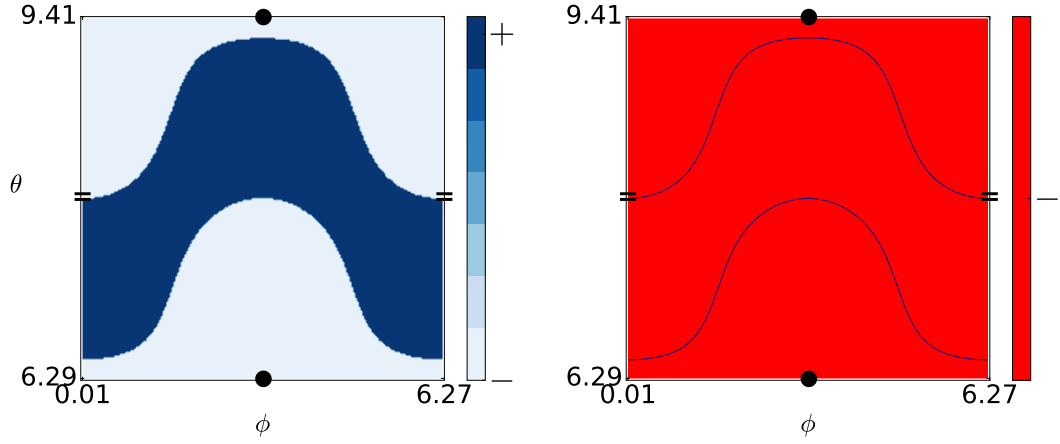


(a) Positive and negative regions of  $u$  and  $v$  over the domain  $\Omega = [0, 2\pi] \times (0, \pi)$ . The left panel shows the zero level set of  $v$  superimposed onto the plot of  $u$ . The right panel shows the zero level set of  $u$  superimposed onto the plot of  $v$ .

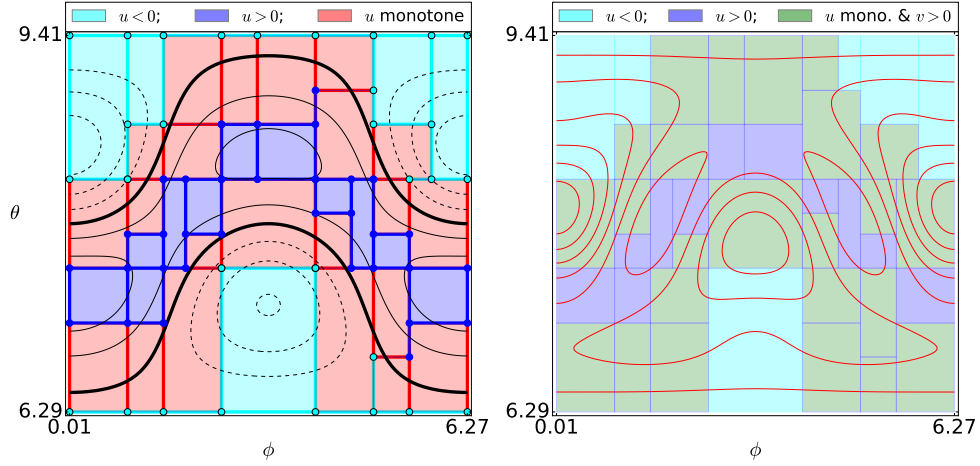


(b) Validation that the candidate block  $\mathcal{A}_0$  is, indeed, an isolating block for Equation 3.29. The color red is used in the left panel to indicate cells in `cmplx` where  $u$  takes both positive and negative values. This is emphasized by the contour lines of  $u$  superimposed onto the colored cell complex. The right panel illustrates the work done by Algorithm (IB). Contours of  $v$  have been superimposed in red.

Figure 3.18: The candidate block  $\mathcal{A}_0$  is an isolating block.

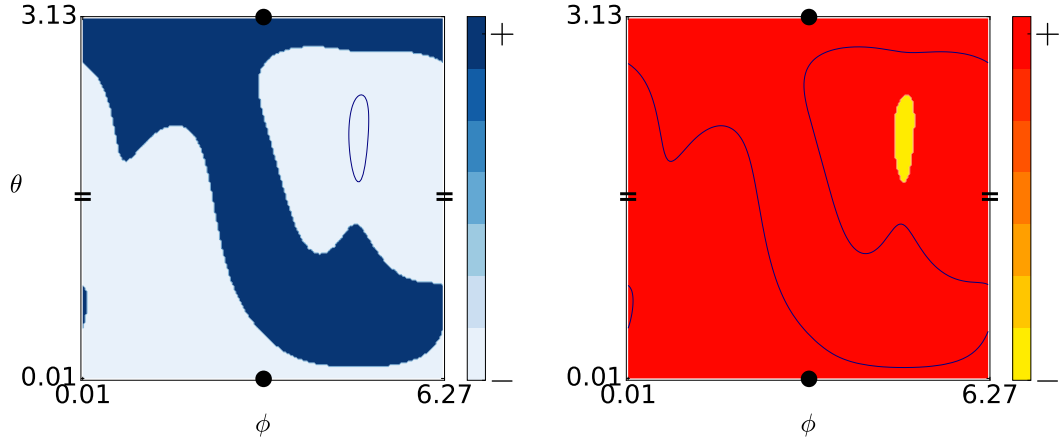


(a) Positive and negative regions of  $u$  and  $v$  over the domain  $\Omega = [0, 2\pi] \times (0, \pi)$ . The left panel shows the zero level set of  $v$  superimposed onto the plot of  $u$ . The right panel shows the zero level set of  $u$  superimposed onto the plot of  $v$ .

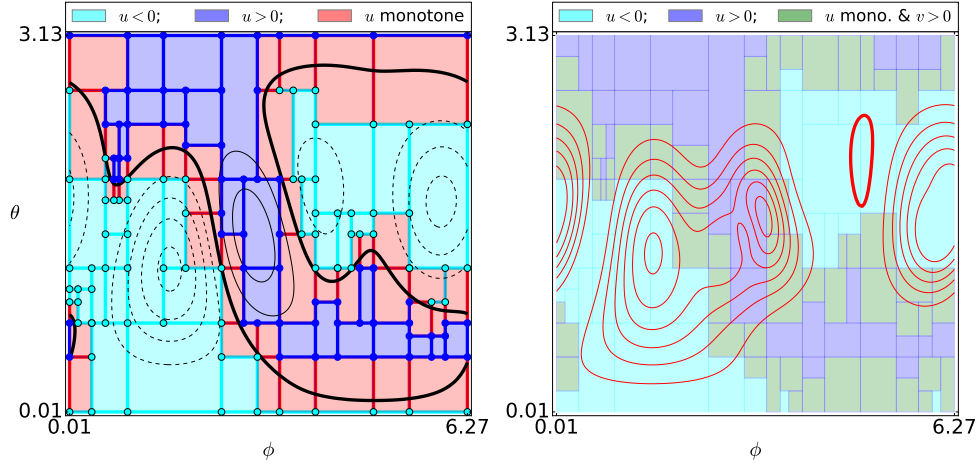


(b) Validation that the candidate block  $\mathcal{A}_1$  is, indeed, an isolating block for Equation 3.29. The color red is used in the left panel to indicate cells in `cmplx` where  $u$  takes both positive and negative values. This is emphasized by the contour lines of  $u$  superimposed onto the colored cell complex. The right panel illustrates the work done by Algorithm (IB). Contours of  $v$  have been superimposed in red.

Figure 3.19: The candidate block  $\mathcal{A}_1$  is an isolating block.



(a) Positive and negative regions of  $u$  and  $v$  over the domain  $\Omega = [0, 2\pi] \times (0, \pi)$ . The left panel shows the zero level set of  $v$  superimposed onto the plot of  $u$ . The right panel shows the zero level set of  $u$  superimposed onto the plot of  $v$ .



(b) Validation that the candidate block  $\mathcal{A}_{12}$  is, indeed, an isolating block for Equation 3.29. The color red is used in the left panel to indicate cells in `cmplx` where  $u$  takes both positive and negative values. This is emphasized by the contour lines of  $u$  superimposed onto the colored cell complex. The right panel illustrates the work done by Algorithm (IB). Contours of  $v$  have been superimposed in red.

Figure 3.20: The candidate block  $\mathcal{A}_{12}$  is an isolating block.

### 3.7.2 Asymptotic Behavior of Ground States

In [22], Hulshof & van der Vorst studied the asymptotic behavior of ground states of coupled semilinear Poisson equations. Their approach could reduce the problem to establishing the

existence of a certain heteroclinic orbit in a three-dimensional ordinary differential equation. This equation was later considered by Boczek et al. [8] as a test case for their polygonal flow approximations. In the following, we will show that our isolating block validation algorithm can be applied in this situation as well. We consider the ordinary differential equation

$$\begin{aligned}\dot{x} &= -x(x+1) - z, \\ \dot{y} &= y(2+6x-y) + 3x + z, \\ \dot{z} &= z(2-x+5y).\end{aligned}\tag{3.31}$$

This ordinary differential equation has equilibria at the points  $p_0 = (0, 0, 0)$  and  $p_1 = (-1, -1, 0)$ . Additionally, this equation has equilibria at  $(2, 0, -6)$ ,  $(0, 2, 0)$ ,  $(-1, -3, 0)$ , and  $(-3, -1, -6)$ . None of these will be relevant in the following, as they will lie outside all constructed isolating blocks.

**In this section we will show:** Result (1) The result in [8]: There exists a heteroclinic connection between  $p_0$  and  $p_1$ . Along the way we will observe how our procedure can still provide useful information, even when Algorithm (IB) fails.

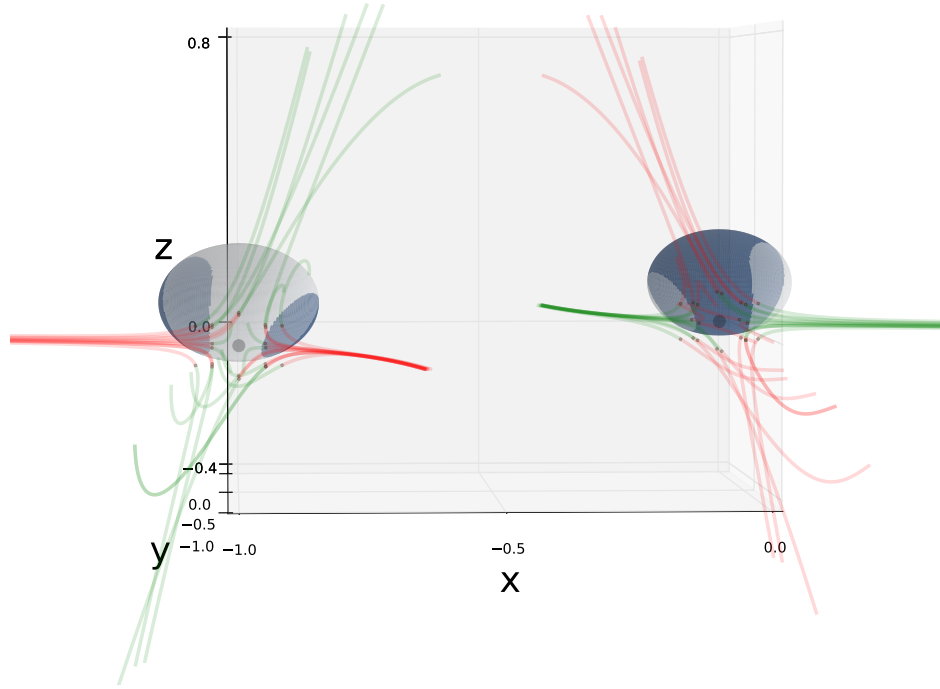


Figure 3.21: Trajectories of Equation (3.31), along with the isolating blocks  $\mathcal{B}_0$  and  $\mathcal{B}_1$ . Red trajectories are leaving their respective equilibria in forward time, and green trajectories are traveling toward their respective equilibria.

**To show Result (1):** As in the first example, finding isolating blocks around the equilibrium solutions is an easy task, we simply propose two spheres  $\mathcal{B}_0$  and  $\mathcal{B}_1$ , defined below. Finding an isolating block  $\mathcal{B}_{01}$  encompassing both  $p_0$  and  $p_1$ , as well as the anticipated heteroclinic orbit proves to be slightly more involved. As shown in [8], the orbit has the general shape of a parabola connecting the equilibria, and reaching almost to a height of 1. Thus, it seems reasonable to construct  $\mathcal{B}_{01}$  as the  $\rho$ -neighborhood of the parabolic space curve

$$\mathbf{r}(\theta) = \begin{pmatrix} \theta - 1 \\ \theta - 1 \\ 4h\theta(1 - \theta) + c \end{pmatrix} \quad \text{for } 0 \leq \theta \leq 1, \quad (3.32)$$

for suitable constants  $c$  and  $h$ , and with a suitable circular cross section of radius  $\rho$ . We



parameterize the surface of the tube in the following way. For  $0 \leq \theta \leq 1$  the standard Frenet-Serret frames are used to describe the circular cross section of  $\mathcal{B}_{01}$  with the plane through  $\mathbf{r}(\theta)$  and spanned by the unit binormal  $\mathbf{b} := (\mathbf{r}'(\theta) \times \mathbf{r}''(\theta)) / (\mathbf{r}'(\theta) \times \mathbf{r}''(\theta))$  and unit normal  $\mathbf{n}(\theta) := (\mathbf{b}(\theta) \times \mathbf{r}'(\theta)) / (\mathbf{b}(\theta) \times \mathbf{r}'(\theta))$  vectors at this point. In this way, the cylindrical surface is parameterized using  $0 \leq \theta \leq 1$  along the curve, and using  $0 \leq \varphi \leq 2\pi$  along the circular cross section. For  $-1/2 \leq \theta < 0$  and for  $1 < \theta \leq 3/2$  we use spherical coordinates to parameterize the spherical caps at the ends of  $\mathcal{B}_{01}$  in such a way that the equator of one cap matches the tubular cross section at  $\theta = 0$ , and the other at  $\theta = 1$ . With this discussion in mind, consider the following candidates:

- The candidate blocks  $\mathcal{B}_0$  and  $\mathcal{B}_1$ , shown in Figure 3.21, are the spheres of radius  $\rho = 3/20$ , centered at  $p_0 + (0, 0, 11/100) = (x_0, y_0, z_0) = (0, 0, 11/100)$  and  $p_1 + (0, 0, 11/100) = (x_1, y_1, z_1) = (-1, -1, 11/100)$ , respectively. Their parameterizations are the standard spherical parameterizations  $r : \Omega = [0, 2\pi] \times (0, \pi) \rightarrow \partial\mathcal{B}_k$ , for  $k = 0, 1$ .
- The candidate block  $\mathcal{B}_{01}$ , shown in Figure 3.22, being defined as the union of three manifolds with boundary, given by the parameterizations  $\gamma : \Omega = [0, 2\pi] \times [-0.5, 1.5] \rightarrow$

$\partial\mathcal{B}_{01}$ , defined as

$$\text{for } \theta \in [-0.5, 0] : \quad \gamma_-(\varphi, \theta) = \mathbf{r}(0) + \mathbf{n}(0) \rho \sin(\pi(\theta + 1.5)) \cos \varphi$$

$$+ \mathbf{b}(0) \rho \sin(\pi(\theta + 1.5)) \sin \varphi$$

$$+ \mathbf{r}'(0) \rho \cos(\pi(\theta + 1.5))$$

$$\text{for } \theta \in [0, 1] : \quad \gamma_0(\varphi, \theta) = \mathbf{r}(\theta) - \mathbf{n}(\theta) \rho \cos \varphi - \mathbf{b}(\theta) \rho \sin \varphi$$

$$\text{for } \theta \in [1, 1.5] : \quad \gamma_+(\varphi, \theta) = \mathbf{r}(1) + \mathbf{n}(1) \rho \sin(\pi(\theta + 0.5)) \cos \varphi$$

$$+ \mathbf{b}(1) \rho \sin(\pi(\theta + 0.5)) \sin \varphi$$

$$+ \mathbf{r}'(1) \rho \cos(\pi(\theta + 0.5))$$

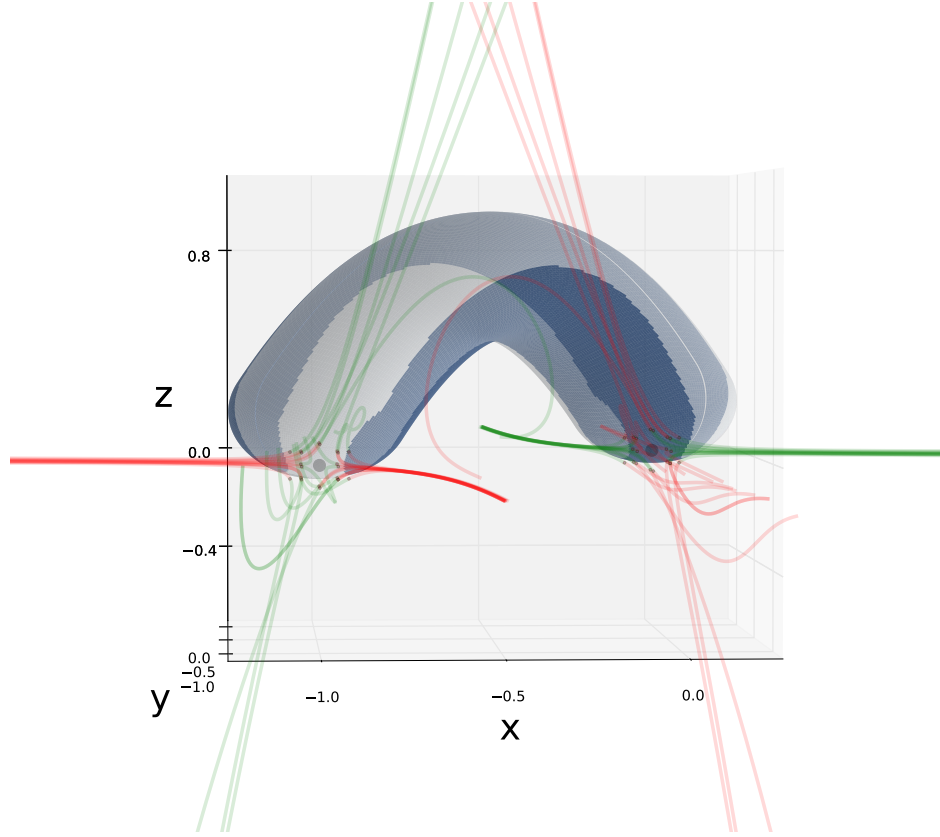


Figure 3.22: The tubular neighborhood  $\mathcal{B}_{01}$ . The boundary of this closed tube is parameterized as three smooth manifolds made up of the two spherical caps described by  $\gamma_+$  and  $\gamma_-$  above, and the parabolic section given by  $\gamma_0$ .

As a first attempt, we choose  $h = 1$ ,  $c = 0$ , and thickness  $\rho = 1/5$ . The corresponding exit set, and a plot of the tangency test function  $v$  are shown in the top row of Figure 3.23. Note that while the exit set would give  $\mathcal{B}_{01}$  a trivial Conley index, thus establishing the connecting orbit (since the sum  $CH(\mathcal{S}_0)$  and  $CH(\mathcal{S}_1)$  is not trivial, revisited below), it turns out that for these parameter values  $\mathcal{B}_{01}$  is not in fact an isolating block — the collection of tangencies of the flow on  $\mathcal{B}_{01}$  intersects the yellow region of internal tangencies, in particular  $N^0(\Omega, u) \cap N^{\leq 0}(\Omega, v) \neq \emptyset$ . Upon closer inspection one can see that this yellow region is located at the bottom bend of the tubular neighborhood, where the relatively high curvature of  $r(\theta)$  is larger than the curvature of the flow. Thus, in order to achieve an isolating

neighborhood one needs to decrease the curvature of  $r(\theta)$  at the bend, while still maintaining isolation of the heteroclinic orbit. This can be accomplished by decreasing  $h$ , while at the same time increasing  $c$  and possibly also  $\rho$ . More precisely, if we choose  $h = 1/2$ ,  $c = 1/5$ , and thickness  $\rho = 1/4$ , we obtain a tubular neighborhood  $\mathcal{B}_{01}$  whose exit set, along with the evaluation of tangency test function  $v$ , are shown in Figure 3.23. Applying the isolating block validation algorithm from Section 3.6 does indeed establish the new set as an isolating block with trivial Conley index which contains  $p_0$  and  $p_1$ , as seen in the bottom panel of 3.23. Since the equilibria have (Morse) indices 2 and 1, we have that

$$\begin{aligned} CH(\mathcal{S}_{01}) &= (0, 0, 0, \dots) \\ &\neq (0, 0, \mathbb{Z}, 0, \dots) \oplus (0, \mathbb{Z}, 0, \dots) \\ &= CH(\mathcal{S}_0) \oplus CH(\mathcal{S}_1), \end{aligned}$$

so the maximal invariant set in  $\mathcal{B}_{01}$  has to contain at least one additional orbit.

It remains to identify the additional part of the isolated invariant set as a connecting orbit. For this, one just has to note that in the quadrant  $2 - x + 5y > 0$  and  $z > 0$ , whose closure contains  $p_0$ , the  $z$ -component of the flow of (3.31) is strictly increasing, while in the quadrant  $2 - x + 5y < 0$  and  $z > 0$ , whose closure contains  $p_1$ , the  $z$ -component is strictly decreasing. It turns out that the part of the plane  $2 - x + 5y = 0$  in which the flow field of (3.31) is transverse to the plane with decreasing  $x$ - and  $y$ -coordinates contains a complete cross section of  $\mathcal{B}_{01}$ . In other words, the only possible additional full orbit in  $\mathcal{B}_{01}$  is a heteroclinic orbit which leaves  $p_0$  with increasing  $z$ -component until it traverses this plane, and then drops down towards  $p_1$ .

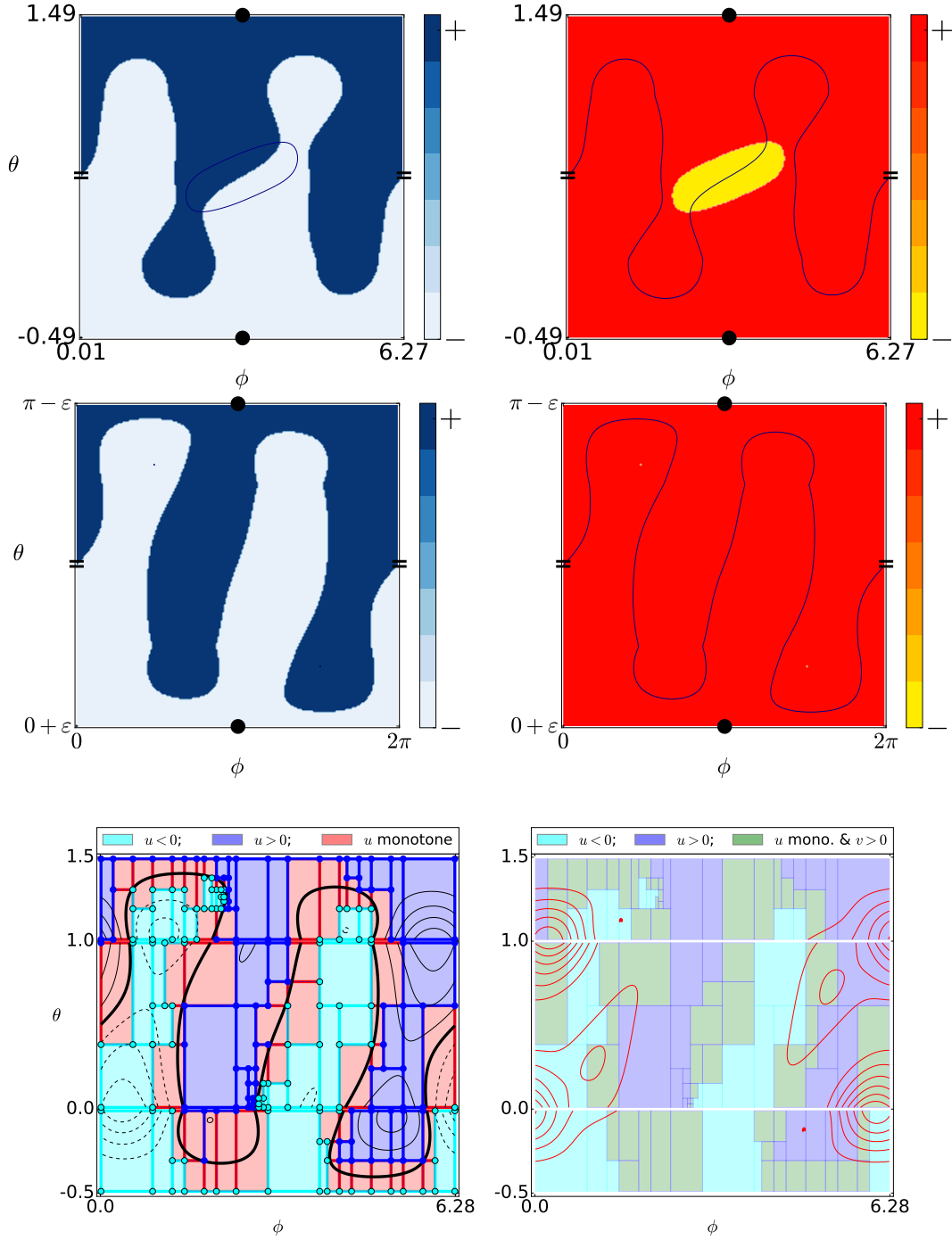
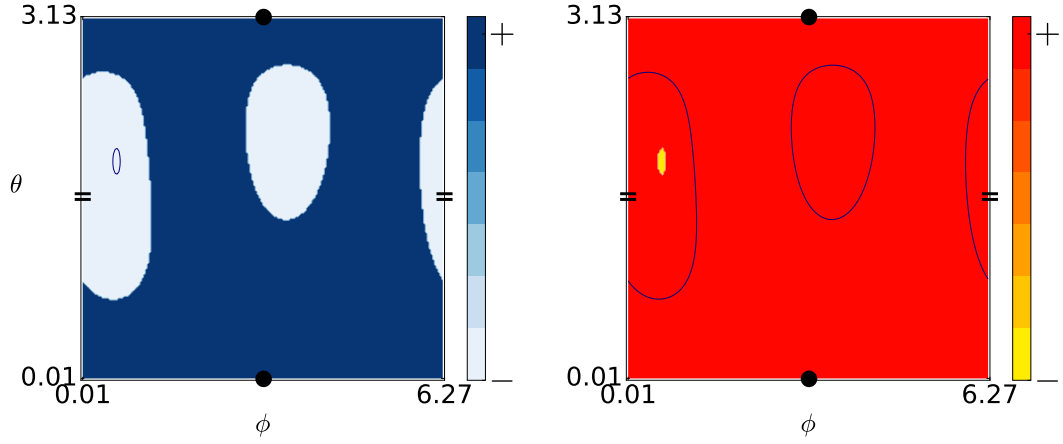
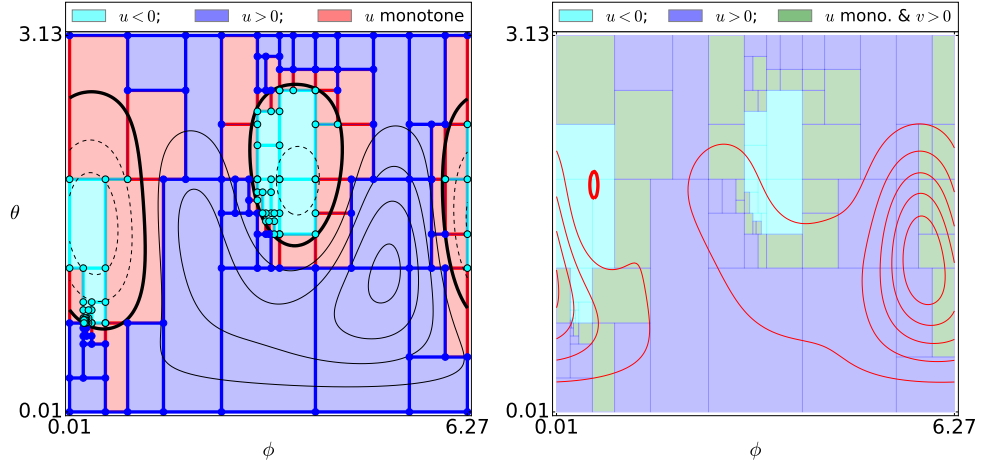


Figure 3.23: The top panel shows filled contour plots for the exit set and the tangency test function for a tubular neighborhood of the parabolic space curve (3.32) with  $h = 1$ ,  $c = 0$  and thickness  $\rho = 1/4$ . Since the boundary of the exit set intersects with the yellow region, there are internal tangencies — and this neighborhood is not an isolating block. The middle row shows a corrected tubular neighborhood, with  $h = 1$  and  $c = 0$  and thickness  $\rho = 1/5$ . The bottom row illustrates a successful application of the validation algorithm (IB) applied to  $\partial\mathcal{B}_{01}$ , defined piecewise over the domains  $\Omega_- = [0, 2\pi] \times (-1.5, 0)$ ,  $\Omega_0 = [0, 2\pi] \times (0, 1)$ , and  $\Omega_+ = [0, 2\pi] \times (1, 1.5)$ .

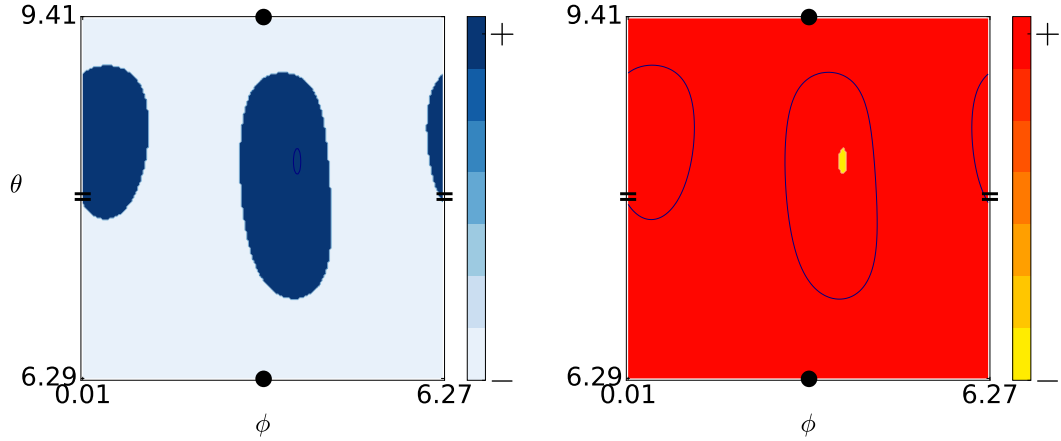


(a) Positive and negative regions of  $u$  and  $v$  over the domain  $\Omega = [0, 2\pi] \times (0, \pi)$ . The left panel shows the zero level set of  $v$  superimposed onto the plot of  $u$ . The right panel shows the zero level set of  $u$  superimposed onto the plot of  $v$ .

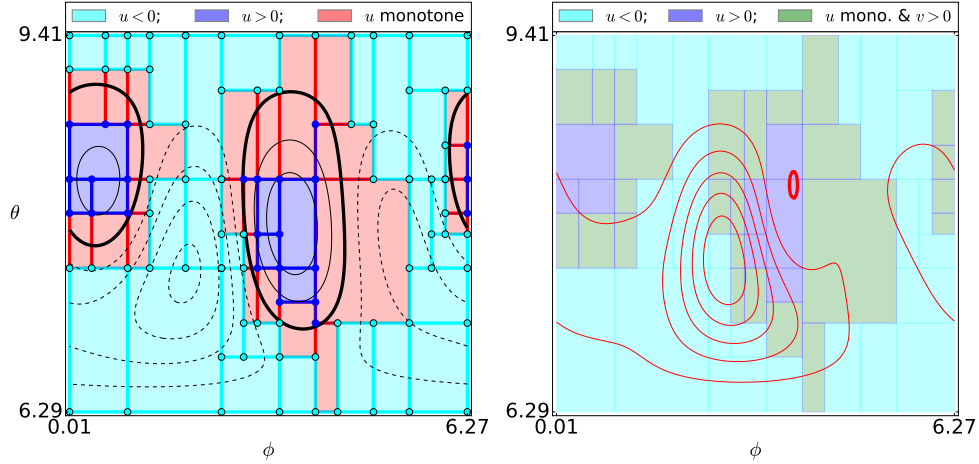


(b) Validation that the candidate block  $\mathcal{B}_0$  is, indeed, an isolating block for Equation 3.31. The color red is used in the left panel to indicate cells in `cmplx` where  $u$  takes both positive and negative values. This is emphasized by the contour lines of  $u$  superimposed onto the colored cell complex. The right panel illustrates the work done by Algorithm (IB). Contours of  $v$  have been superimposed in red.

Figure 3.24: The candidate block  $\mathcal{B}_0$  is an isolating block.



(a) Positive and negative regions of  $u$  and  $v$  over the domain  $\Omega = [0, 2\pi] \times (0, \pi)$ . The left panel shows the zero level set of  $v$  superimposed onto the plot of  $u$ . The right panel shows the zero level set of  $u$  superimposed onto the plot of  $v$ .



(b) Validation that the candidate block  $\mathcal{B}_1$  is, indeed, an isolating block for Equation 3.31. The color red is used in the left panel to indicate cells in `cmplx` where  $u$  takes both positive and negative values. This is emphasized by the contour lines of  $u$  superimposed onto the colored cell complex. The right panel illustrates the work done by Algorithm (IB). Contours of  $v$  have been superimposed in red.

Figure 3.25: The candidate block  $\mathcal{B}_1$  is an isolating block.

### 3.7.3 A Planar Hopf Bifurcation

Our final example is concerned with an essentially planar system undergoing a Hopf bifurcation. The planar version of this example was considered in the work of Eberlein &

Scheurle [18]. Since our focus is the study of three-dimensional flows, we instead consider the system

$$\begin{aligned}\dot{x} &= \lambda x + y - x^3, \\ \dot{y} &= -x + \lambda y, \\ \dot{z} &= 5z,\end{aligned}\tag{3.33}$$

which is obtained from [18, p. 396] by adding an unstable  $z$ -direction. This system depends on a real parameter  $\lambda$ , and we are interested in the dynamics of (3.33) as  $\lambda$  increases through zero.

The origin is an equilibrium for (3.33), which is unstable with (Morse) index 1 for  $\lambda < 0$ , and unstable with index 3 for  $\lambda > 0$ . As  $\lambda$  increases through zero, the linearization of (3.33) at the origin has a pair  $\lambda \pm i$  of complex eigenvalues which cross the imaginary axis with nonzero speed — hence triggering a Hopf bifurcation.

**In this section we will show:** Result (1) For  $\lambda = -1/10$ , the Conley index on each of two concentric spheres,  $\mathcal{C}_1$  and  $\mathcal{C}_2$ , around the origin corresponds to an index-1 hyperbolic fixed point, as expected; and Result (2) Equation (3.33) undergoes a Hopf bifurcation as  $\lambda$  moves from  $-1/10$  to  $1/10$ . In particular, for  $\lambda = 1/10$ , the block  $\mathcal{C}_2 \setminus \mathcal{C}_1$  captures a periodic orbit denoted by  $\mathcal{S}_{21}$ , and there exists at least one connecting orbit from the now-unstable equilibrium at the origin to  $\mathcal{S}_{21}$ .



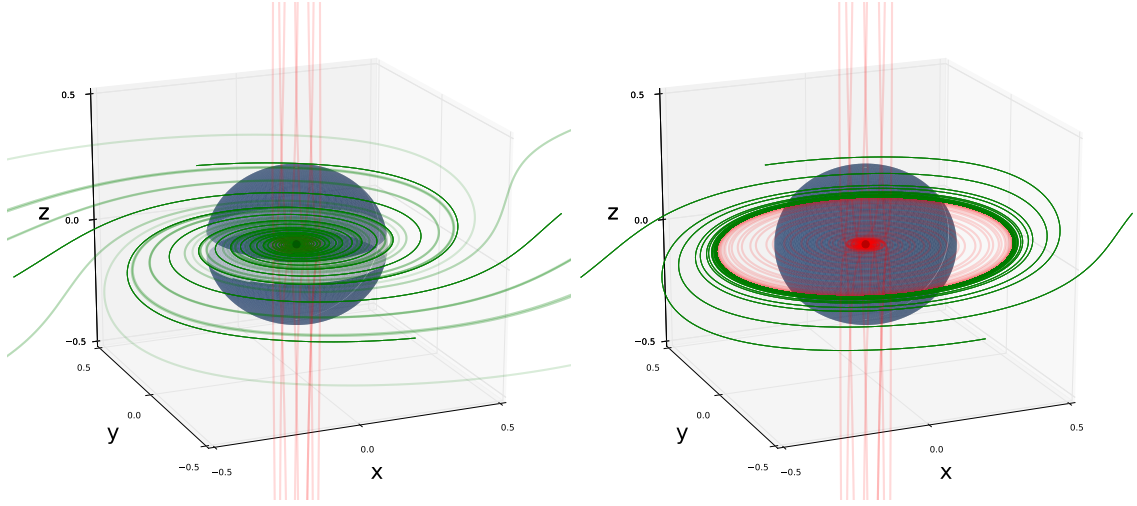


Figure 3.26: Trajectories of Equation (3.33) for  $\lambda = -1/10$  (left), and  $\lambda = 1/10$  (right). Red lines are moving away from the origin, and green lines are moving toward the origin. The small sphere  $C_1$  around the origin is a valid isolating block for (3.33) with  $\lambda = -1/10$ . The same sphere is a valid isolating block for (3.33) with  $\lambda = 1/10$ , however it must fail to be in isolating neighborhood at some value  $\lambda \in (-1/10, 1/10)$  due to the different topological type of  $C_1^-$  for  $\lambda = \pm 1/10$ .

**To show Result (1):** ( $\lambda = -1/10$ ) We first propose two candidate isolating blocks isolating the origin.

- The candidate block  $C_1$ , shown for  $\lambda = -1/10$  in the left panel of Figure 3.26, is a ball of radius  $3/10$  centered at the origin. The boundary of  $C_1$  is parameterized using the usual spherical coordinates  $r : \Omega = [0, 2\pi] \times (0, \pi) \rightarrow \partial C_1$ .
- The candidate block  $C_2$  is an ellipsoid centered at the origin, shown for  $\lambda = -1/10$  in left panel of Figure 3.27, with major axes rotated around the  $z$ -axis. We use the parameterization  $r : \Omega = [0, 2\pi] \times (0, \pi)$ , given by

$$r(\varphi, \theta) = \begin{pmatrix} 1/\sqrt{5} \\ 2/\sqrt{5} \\ 0 \end{pmatrix} a \sin \theta \cos \varphi + \begin{pmatrix} -2/\sqrt{5} \\ 1/\sqrt{5} \\ 0 \end{pmatrix} b \sin \theta \sin \varphi + \begin{pmatrix} 0 \\ 0 \\ 1 \end{pmatrix} c \cos \theta,$$

where  $a = 3$ , and  $b = c = 2$ .

Our validation algorithm can be applied to both neighborhoods  $\mathcal{C}_1$  and  $\mathcal{C}_2$ , and it confirms both as isolating blocks when  $\lambda = -1/10$ . The validations are illustrated in Figures 3.28 and 3.29.

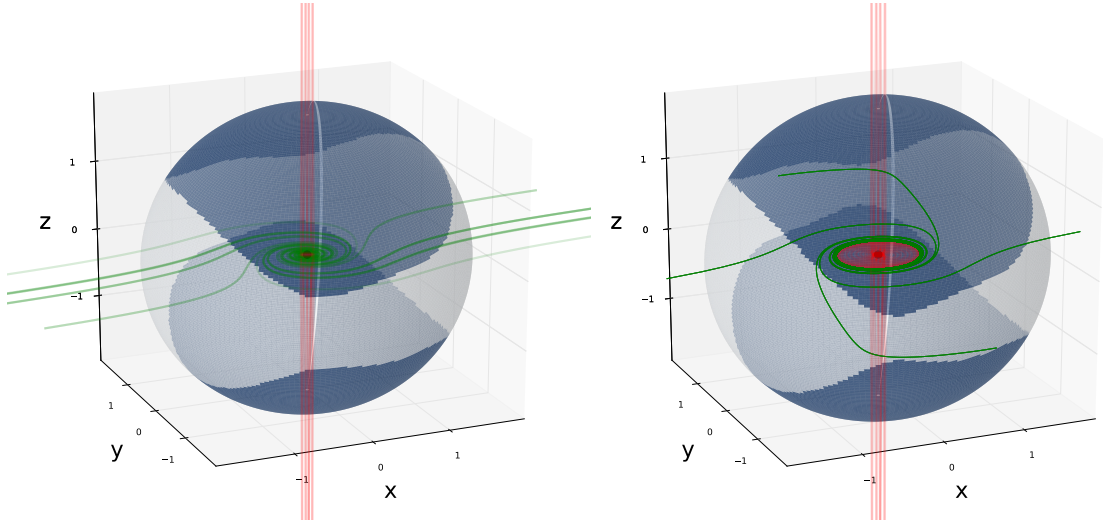


Figure 3.27: Trajectories of Equation (3.33) for  $\lambda = -1/10$  (left), and  $\lambda = 1/10$  (right). Red lines are moving away from the origin, and green lines are moving toward the origin. The sphere  $\mathcal{C}_2$  around the origin is larger than  $\mathcal{C}_1$  in Figure 3.26, and  $\mathcal{C}_2$  is a valid isolating block for (3.33) with  $\lambda = -1/10$ . The same sphere is a valid isolating block for (3.33) with  $\lambda = 1/10$ , and in fact, the topological type of the exit set  $\mathcal{C}_2^-$  is the same for both parameter values.

The Conley indices of the maximal invariant sets  $\mathcal{S}_1$  and  $\mathcal{S}_2$  are simply  $CH(\mathcal{S}_1) = CH(\mathcal{S}_2) = (0, \mathbb{Z}, 0 \dots)$ , corresponding to (Morse) index-1 hyperbolic equilibria.

**To show Result (2):** ( $\lambda = 1/10$ ) Our validation algorithm still can be applied successfully to both  $\mathcal{C}_1$  and  $\mathcal{C}_2$  from above, however the configuration of the exit set on  $\mathcal{C}_1$  has changed (cf. Figures 3.28 and 3.30). For  $\lambda = 1/10$  in Equation 3.33, the exit set function  $u$  turns out to be strictly positive on  $\Omega = [0, 2\pi] \times (0, \pi)$ , so the resulting grid contains only one rectangle, and step (IB2) in the validation algorithm completes without any evaluation of

the tangency test function  $v$ . This can be observed in Figure 3.30 For the isolating block  $\mathcal{C}_2$ , its exit set is shown in dark blue in the upper left image of Figure 3.31.

These images show that while the homological Conley index of the isolating block  $\mathcal{C}_2$  remains unchanged as  $\lambda$  moves through zero, the Conley index computed using  $\mathcal{C}_1$  is now

$$CH_*(\mathcal{S}_1) \simeq (0, 0, 0, \mathbb{Z}, 0, \dots) ,$$

which is the expected Conley index of a (Morse) index 3 unstable equilibrium. Of course, this equilibrium is the origin which is contained in  $\mathcal{C}_1$ . We would like to point out that in contrast to the case  $\lambda < 0$ , in the present case the differential equation (3.33) has the additional equilibria  $\pm \left( \sqrt{\lambda + 1/\lambda}, \sqrt{1/\lambda + 1/\lambda^3}, 0 \right)$  for  $\lambda > 0$ . Yet, for the present choice of  $\lambda = 1/10$ , one can easily verify that these additional equilibrium solutions lie outside the isolating blocks  $\mathcal{C}_1$  and  $\mathcal{C}_2$ .

We now combine this Conley index information with some observations about the vector field (3.33) to obtain a computer-assisted proof of the existence of a Hopf bifurcation for  $\lambda \in [-1/10, 1/10]$ . From our above discussion of the equilibrium solutions we see that both  $\mathcal{C}_1$  and  $\mathcal{C}_2$  only contain one equilibrium, namely the origin — and as  $\lambda$  increases from  $-1/10$  to  $1/10$  no other equilibria enter these isolating blocks. Thus, the index change implies the bifurcation of an invariant set which has to touch  $\partial\mathcal{C}_1$  for some  $\lambda$ -value strictly between  $-1/10$  and  $1/10$ . But we can say even more at  $\lambda = 1/10$ . Since the surface  $\partial\mathcal{C}_1$  consists only of exit points, as shown in Figure 3.26, it is straightforward to construct the isolating block  $\mathcal{C} := \overline{\mathcal{C}_2 \setminus \mathcal{C}_1}$ , and use this to compute the homological Conley index

$$CH(\mathcal{S}) = H_*(\mathcal{C}, \mathcal{C}^-) \simeq (0, \mathbb{Z}, \mathbb{Z}, 0, 0, \dots) .$$

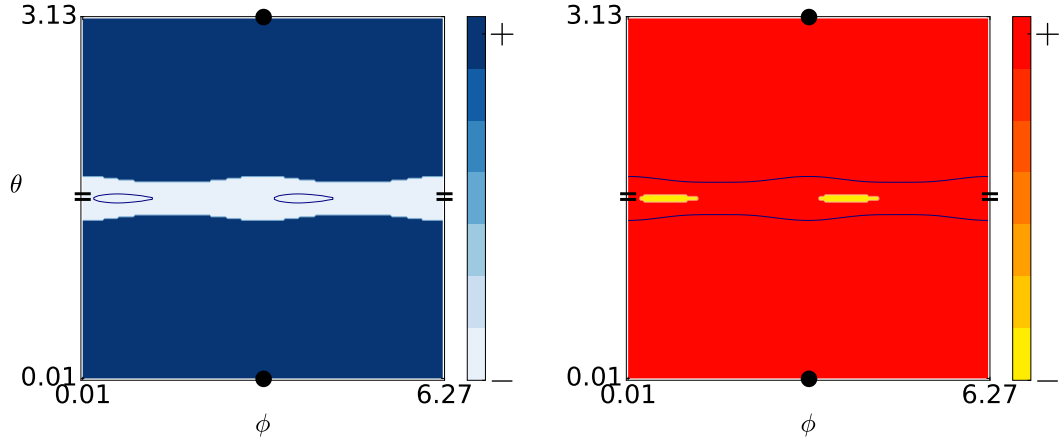
This index is non-trivial, and therefore the interior of  $\mathcal{C} = \overline{\mathcal{C}_2 \setminus \mathcal{C}_1}$  contains a maximal isolated invariant set  $\mathcal{S} \neq \emptyset$ . As discussed earlier, the set  $\mathcal{S}$  cannot contain any equilibria. Furthermore, due to the form of (3.33), every globally bounded invariant set has to be

contained in the  $x$ - $y$ -plane. But then the Poincaré-Bendixson theorem implies that  $\mathcal{S}$  has to contain a periodic orbit. Note that this is consistent with the above Conley index information, as the index is that of an unstable periodic orbit with two-dimensional unstable manifold. Finally, due to

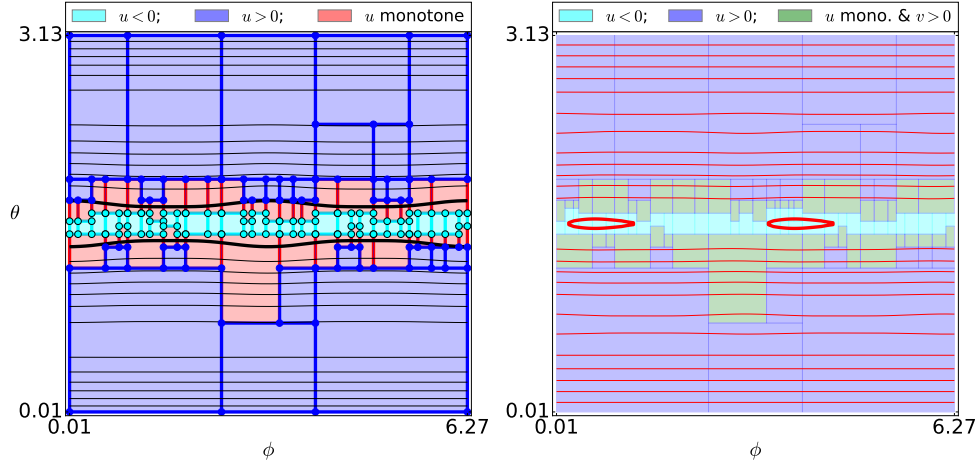
$$CH_*(\mathcal{S}_2) = (0, \mathbb{Z}, 0, \dots)$$

$$\neq (0, 0, 0, \mathbb{Z}, 0, \dots) \oplus (0, \mathbb{Z}, \mathbb{Z}, 0, \dots) = CH_*(\mathcal{S}_1) \oplus CH_*(\mathcal{S}),$$

there has to be at least one connecting orbit from the unstable origin to the isolated invariant set  $\mathcal{S}$ .

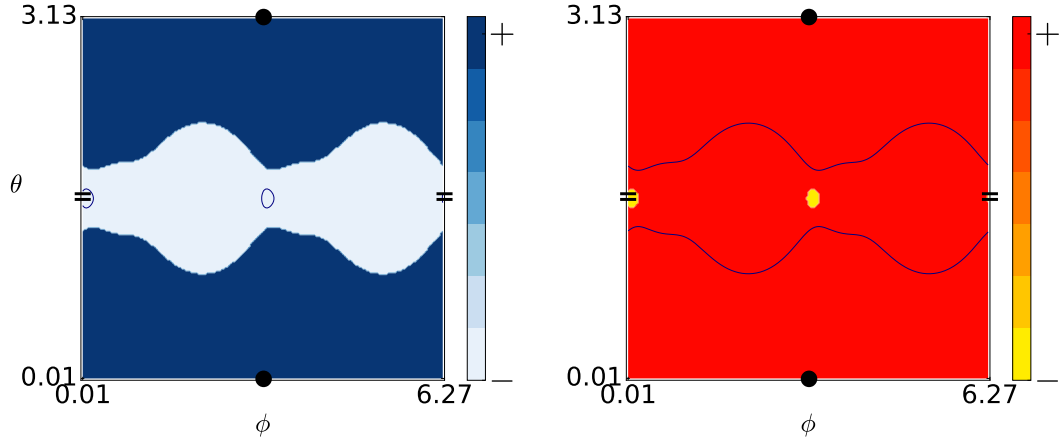


(a) Positive and negative regions of  $u$  and  $v$  over the domain  $\Omega = [0, 2\pi] \times (0, \pi)$ . The left panel shows the zero level set of  $v$  superimposed onto the plot of  $u$ . The right panel shows the zero level set of  $u$  superimposed onto the plot of  $v$ .

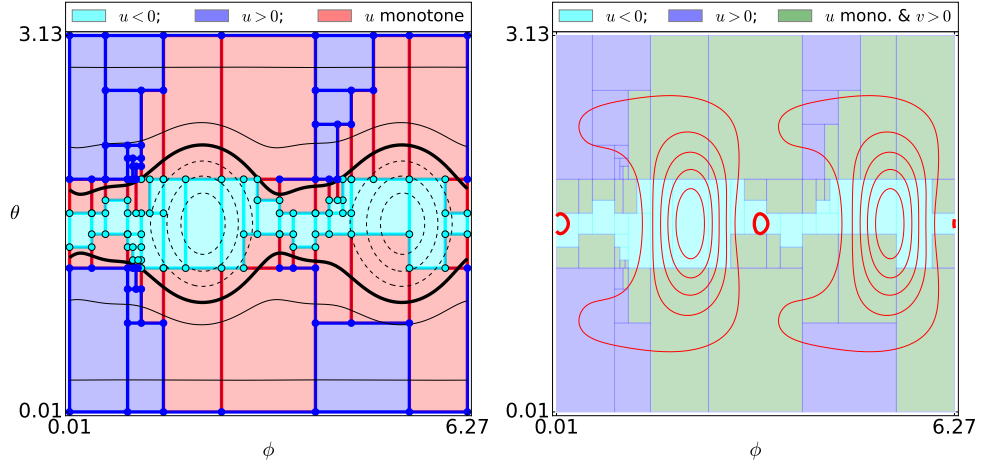


(b) Validation that the candidate block  $\mathcal{C}_1$  is, indeed, an isolating block for Equation 3.29 with  $\lambda = -1/10$ . The color red is used in the left panel to indicate cells in `cmplx` where  $u$  takes both positive and negative values. This is emphasized by the contour lines of  $u$  superimposed onto the colored cell complex. The right panel illustrates the work done by Algorithm (IB). Contours of  $v$  have been superimposed in red.

Figure 3.28: The candidate block  $\mathcal{C}_1$  is an isolating block.

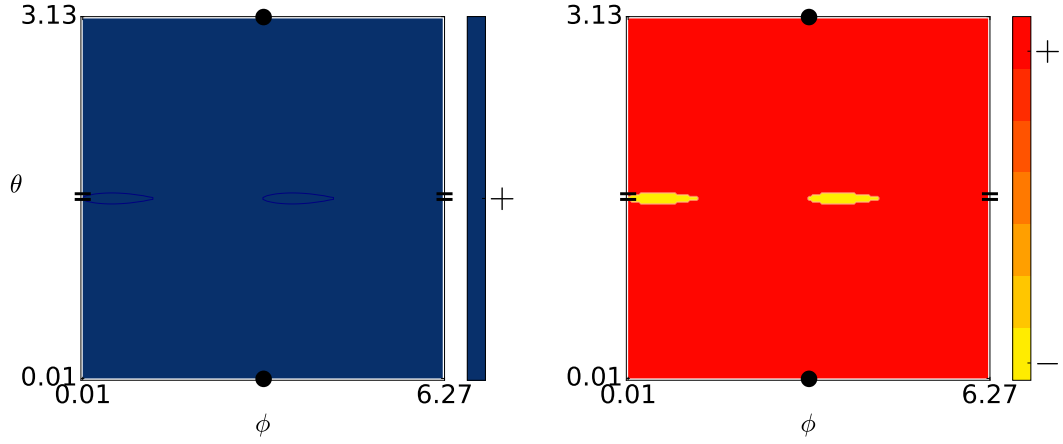


(a) Positive and negative regions of  $u$  and  $v$  over the domain  $\Omega = [0, 2\pi] \times (0, \pi)$ . The left panel shows the zero level set of  $v$  superimposed onto the plot of  $u$ . The right panel shows the zero level set of  $u$  superimposed onto the plot of  $v$ .

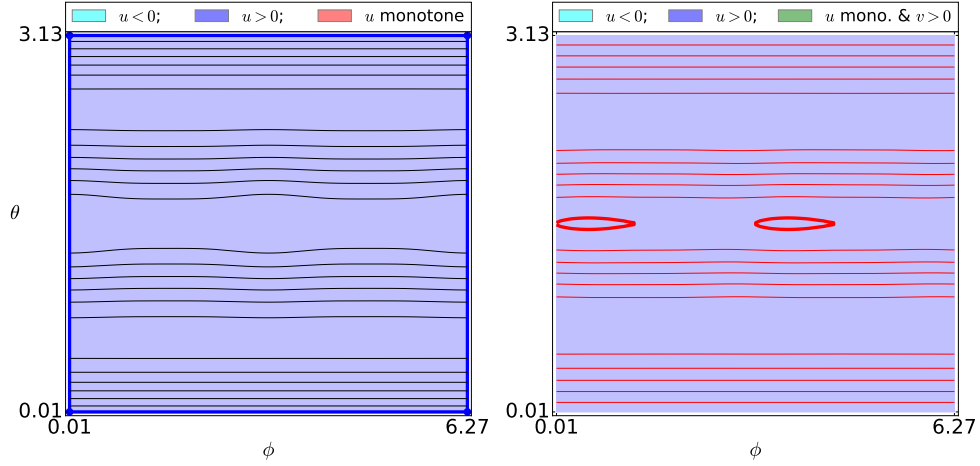


(b) Validation that the candidate block  $\mathcal{C}_2$  is, indeed, an isolating block for Equation 3.29 with  $\lambda = -1/10$ . The color red is used in the left panel to indicate cells in `cmplx` where  $u$  takes both positive and negative values. This is emphasized by the contour lines of  $u$  superimposed onto the colored cell complex. The right panel illustrates the work done by Algorithm (IB). Contours of  $v$  have been superimposed in red.

Figure 3.29: The candidate block  $\mathcal{C}_2$  is an isolating block.

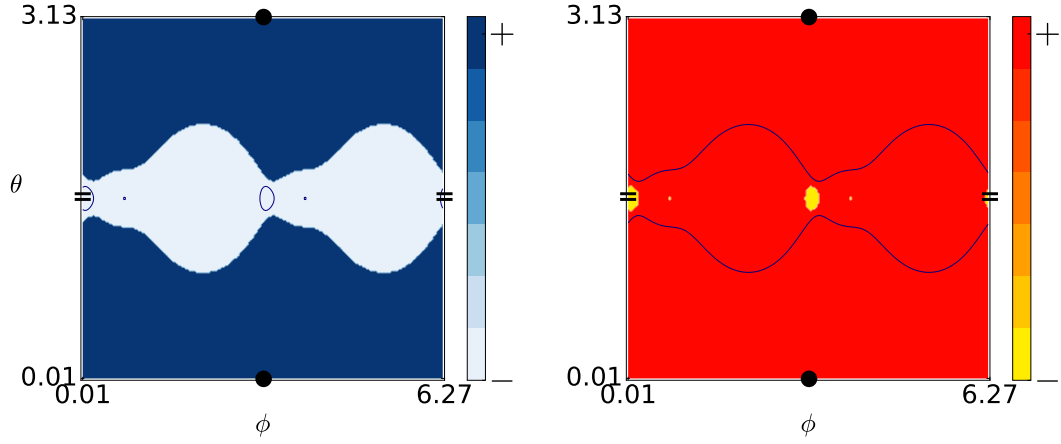


(a) Positive and negative regions of  $u$  and  $v$  over the domain  $\Omega = [0, 2\pi] \times (0, \pi)$ . The left panel shows the zero level set of  $v$  superimposed onto the plot of  $u$ . The right panel shows the zero level set of  $u$  superimposed onto the plot of  $v$ .

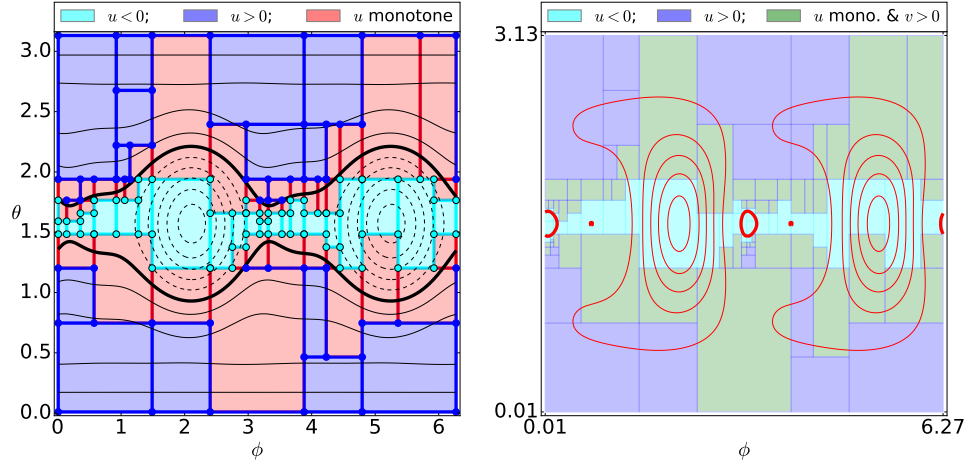


(b) Validation that the candidate block  $\mathcal{C}_1$  is, indeed, an isolating block for Equation 3.29 with  $\lambda = 1/10$ . In fact, the function  $u$  from Lemma 3.5.2 which characterizes the exit set  $\partial\mathcal{C}_1^- \subset \partial\mathcal{C}_1$  is positive on the entire parametric domain  $\Omega = [0, 2\pi] \times (0, \pi)$ . The output of Algorithm (V) is the single two-cell, its four edges and four vertices, shown in blue in the left panel. The solid color of the right panel indicates that no steps beyond (IBa) were required in Algorithm (IB).

Figure 3.30: The candidate block  $\mathcal{C}_1$  is an isolating block.



(a) Positive and negative regions of  $u$  and  $v$  over the domain  $\Omega = [0, 2\pi] \times (0, \pi)$ . The left panel shows the zero level set of  $v$  superimposed onto the plot of  $u$ . The right panel shows the zero level set of  $u$  superimposed onto the plot of  $v$ .



(b) Validation that the candidate block  $\mathcal{C}_2$  is, indeed, an isolating block for Equation 3.29 with  $\lambda = 1/10$ . The color red is used in the left panel to indicate cells in `cmplx` where  $u$  takes both positive and negative values. This is emphasized by the contour lines of  $u$  superimposed onto the colored cell complex. The right panel illustrates the work done by Algorithm (IB). Contours of  $v$  have been superimposed in red.

Figure 3.31: The candidate block  $\mathcal{C}_2$  is an isolating block.



## Concluding Remarks

In the following paragraphs we revisit some challenges that arose during the course of this research, and leave some remarks for possible next steps.

The superlevel set approximation algorithm in Chapter 2 is developed in what we consider to be quite general terms. The collapse criteria only require monotonicity along a single direction on the top-dimensional cell, and the collapse itself is built through a recurrence relation, making use of monotonicity information acquired at each dimension of the rectangular cell complex. Furthermore, the subdivision of the domain is non-uniform. Together, we believe these features provide a perfect compromise between conceptual simplicity and computational efficiency. The alternative is to aim for some purely topological collapse criterion, and achieve even fewer subdivisions of the domain.

One feature of our approach that we did not take full advantage of is the flexibility provided by taking nonuniform subdivisions of the domain  $\Omega$ . Even with our golden ratio subdivision strategy, it is possible that a vertex  $R^0$  may land in  $\Omega$  at a place where the interval range enclosure  $[u(R^0)]$  cannot be bounded away from zero. This causes the current implementation of the algorithm to fail. The much better strategy is to keep the previous instance of the cell complex data structure so the algorithm can recover from the poor choice which created  $R^0$ . Uniform subdivisions cannot recover from this because there are no options at this point. Nonuniform subdivisions permit any number of alternative subdivisions to be tried, one of which may position  $R^0$  in a better place in  $\Omega$ , and allow the algorithm to continue. We do not foresee any technical challenge to handling this exception in the code.

With regard to constructing candidate isolating blocks for flows in  $\mathbb{R}^n$ , our current efforts have been restricted to systems in  $\mathbb{R}^3$  even though the theory holds for arbitrary finite dimensions. Additionally, obtaining parameterizations for smooth manifolds in  $\mathbb{R}^n$  which satisfy some geometric conditions is a significant technical challenge. In some contexts, these challenges have been met by following flows expressed as geometric partial differential equations in order to evolve hypersurfaces using deforming finite element meshes. In this procedure one typically constructs an energy functional defined for a codimension one smooth manifold  $\mathcal{M}$ , where the energy penalties arise from local geometric properties of the manifold – for example,  $J(\mathcal{M}) := \int_{\mathcal{M}} (H(s) - c_0(s))^2 ds$ , where  $H(s)$  is the mean curvature at  $s \in \mathcal{M}$ ,  $c_0(s)$  defines a preferred curvature, and  $ds$  is the surface measure on  $\mathcal{M}$ . The minimization of this energy (in some Banach space) from some initial manifold  $\mathcal{M}_0$  generates a family of manifolds,  $\mathcal{M}_t$  for  $t > 0$ , which evolve to bring the surface into agreement with  $c_0(s)$ . See [16] for examples of how to take the first variation, or ‘shape derivative’, of such functionals, and [4], [3], and [5] for examples of finite element simulation strategies for evolving surfaces under geometric constraints.

Recall that our candidate isolating block  $\mathcal{B} \subset \mathbb{R}^n$  has a codimension one smooth manifold  $\partial\mathcal{B}$  as boundary, parameterized through  $r : \Omega \subset \mathbb{R}^{n-1} \rightarrow \partial\mathcal{B}$ ,  $u, v : \partial\mathcal{B} \rightarrow \mathbb{R}$  are smooth functions which depend on geometric data computed on  $\partial\mathcal{B}$ , and that we must rigorously establish the condition  $N^0(\Omega, u) \subset N^{>0}(\Omega, v)$  (along with the regularity of zero for  $u$ ) in order to establish the candidate as an isolating block. Because this is a local condition on the boundary of the block, it is plausible that one may start with a somewhat arbitrary candidate and deform it in such a way as to satisfy the condition. An expression such as  $e^{-u^2}e^{-v}$  is mostly concentrated near zero for  $u$ , and is positive and large where  $v < 0$ , meaning that evolving the boundary of a candidate block by driving  $\int_{\partial\mathcal{B}} e^{-u(s)^2} e^{-v(s)} ds$  toward a minimum may have a chance to settle into a configuration that satisfies  $N^0(\Omega, u) \subset N^{>0}(\Omega, v)$ . Technical difficulties will arise with calling Algorithm (V) on the finite element mesh which represents the manifold due to the fact that the mesh is only a polyhedral

approximation to  $\partial\mathcal{B}$ , so that  $u := \langle f(p), \nu_p \rangle$  is not defined along any edge or at vertex of the mesh since  $\nu_p$  is not well defined there. Additionally, in order to use interval arithmetic the domain must permit rectangular subdivisions, hence the finite element mesh must be rectangular, but efficient finite element meshes are merely quadrilateral. We point the interested reader to the open source finite element library `deal.ii` at [www.dealii.org](http://www.dealii.org), [2], and set this exploration aside for now.

## Index

- $\alpha$ -level set, 6
- $\alpha$ -sublevel set, 6
- $\alpha$ -superlevel set, 6
- $k$ -cell, 22
- $k$ -skeleton, 22
- `cmplx+`, 24
- `cmplx`, 24
- Algorithm (IB), *see* Isolating Block Validation Algorithm
- Algorithm (V), *see* Superlevel Set Validation Algorithm
- automatic differentiation, 18
- backward orbit, 55
- bifurcation, 64
- boundary, 22
- bounded invariant set, 55
- Brouwer degree, 56, 66
- candidate isolating block, 68, 77
- cell complex, *see* rectangular cell complex
- characteristic map, 22
- co-boundary, 22
- collapsing, 32, 42
- computer-assisted proof, 17, 68, 89
- Conley index, 59, 63, 83
- continuation, 64
- critical point, 11
- critical value, 11
- cubical representation, 84, 95
- CW complex, *see* rectangular cell complex
- deformation retract, 12
- deformation retraction, 12
- degenerate (rectangle), 21
- dimension (of a cell complex), 22
- dual number, 18
- dynamical system, 53
- edge, 22
- exit set, 35, 58, 70
- external tangency, 69, 72
- flow, 42, 53, 65
- forward orbit, 55
- global flow, 54
- homological Conley index, *see* Conley index
- homotopy, 12
- homotopy equivalence, 12
- index (of a critical point), 11

index pair, 59  
 internal tangency, 58, 69, 72  
 interval, 16  
 interval arithmetic, 17, 85  
 interval range enclosure, 17  
 invariant set, *see* bounded invariant set  
 isolated invariant set, 57, 63, 89  
 isolating block, 58, 62, 63, 65, 87  
 Isolating Block Validation Algorithm, 86  
 isolating neighborhood, 57  
  
 level set, *see*  $\alpha$ -level set  
  
 maximal invariant set, 57  
 Morse theory, 14  
  
 negative sublevel set, 69  
 negatively invariant, 55  
 non degenerate (rectangle), 22  
 nonuniform subdivision, 25  
 numerically rigorous, 16  
  
 one-parameter family, 64  
 orbit, 55  
 orthogonal projection, 69, 78  
 outward normal vector, 69  
  
 parameterization (of isolating block), 79  
 phase space, 53  
 pointed topological space, 59  
 positive superlevel set, 69  
 positively invariant, 55  
  
 rectangle, 21  
 rectangular cell complex, 22  
 Regular Interval theorem, 14  
 Regular Level Set theorem, 13  
 regular point, 11  
 regular value, 11, 26  
 relative homology, 59  
 rigorous, *see* numerically rigorous  
 rigorous numerical integration, 52  
  
 Sard's theorem, 11  
 second fundamental form, 70, 78  
 Simple  $n$ -dimensional Rectangular Cell Complex, 23  
 Skelboe, 26  
 solution, *see* orbit  
 strong deformation retract, 62  
 strong deformation retraction, 12, 62  
 subadditive, 17  
 subcomplex, 22  
 sublevel set, *see*  $\alpha$ -sublevel set  
 summation formula, 64  
 superlevel set, *see*  $\alpha$ -superlevel set  
 Superlevel Set Validation Algorithm, 27, 86  
 surrogate cell, *see* Simple  $n$ -dimensional Rectangular Cell Complex  
  
 tangent space, 69

validation of  $n$ -dimensional cell, 25

vertex, 22

Ważewski set, 35, 62

Ważewski theorem, 35, 62

Ważewski property, 63

zero level set, 69

## Bibliography

- [1] Herbert Amann. *Ordinary differential equations: an introduction to nonlinear analysis*, volume 13. Walter de Gruyter, 1990.
- [2] W. Bangerth, T. Heister, L. Heltai, G. Kanschat, M. Kronbichler, M. Maier, and B. Turcksin. The `deal.II` library, version 8.3. *Archive of Numerical Software*, 4(100):1–11, 2016.
- [3] John W. Barrett, Harald Garcke, and Robert Nürnberg. On the parametric finite element approximation of evolving hypersurfaces in  $\mathbb{R}^3$ . *Journal of Computational Physics*, Vol. 227:4281–4307, 2008.
- [4] John W. Barrett, Harald Garcke, and Robert Nürnberg. Parametric approximation of Willmore flow and related geometric evolution equations. *SIAM Journal on Scientific Computing*, Vol. 31(1):225–253, 2008.
- [5] Sören Bartels. *Numerical methods for nonlinear partial differential equations*. Springer, 2015.
- [6] Ulrich Bauer, Michael Kerber, Jan Reininghaus, and Hubert Wagner. Phat–persistent homology algorithms toolbox. In *Mathematical Software–ICMS 2014*, pages 137–143. Springer, 2014.
- [7] Erik Boczko. *Polygonal Approximation for Flows*. PhD thesis, Georgia Institute of Technology, 2002.
- [8] Erik Boczko, William D. Kalies, and Konstantin Mischaikow. Polygonal approximation of flows. *Topology and its applications*, Vol. 154:2501–2520, 2007.

- [9] Glen E. Bredon. *Topology and Geometry*. Springer, 1993.
- [10] CHomP. Computational Homology Project. *Software available at* <http://chomp.rutgers.edu>, 2013.
- [11] Gregory S. Cochran, Thomas Wanner, and Paweł Dłotko. A Randomized Subdivision Algorithm for Determining the Topology of Nodal Sets. *SIAM Journal on Scientific Computing*, 35(5):B1034–B1054, 2013.
- [12] Charles Conley. *Isolated Invariant Sets and the Morse Index*. American Mathematical Society, Providence, R.I., 1978.
- [13] Charles Conley and Robert Easton. Isolated invariant sets and isolating blocks. *Transactions of the American Mathematical Society*, 158(1):35–61, July 1971.
- [14] Paweł Dłotko, Tomasz Kaczynski, Marian Mrozek, and Thomas Wanner. Coreduction homology algorithm for regular CW-complexes. *Discrete & Computational Geometry*, 46(2):361–388, 2011.
- [15] Manfredo P do Carmo. *Riemannian geometry*, 1992.
- [16] Günay Doğan and Ricardo H. Nochetto. First variation of the general curvature-dependent surface energy. *European Series in Applied and Industrial Mathematics: Mathematical Modeling and Numerical Analysis*, 46:59–79, 2012.
- [17] Dominik Eberlein. *Topologische Methoden zur Analyse dynamischer Systeme*. PhD thesis, Technische Universität München, 2004.
- [18] Dominik Eberlein and Jürgen Scheurle. Algorithmic computation of the Conley index. *Journal of Difference Equations and Applications*, Vol. 12(3-4):385–398, 2006.
- [19] R Hammer, U Hocks, Kulisch, M, and Ratz. *C++ Toolbox for Verified Scientific Computing-Theory, Algorithms and Programs: Basic Numerical Problems*. Springer-Verlag New York, Inc., 1995.



- [20] Allen Hatcher. *Algebraic Topology*. Cambridge University Press, 2001.
- [21] Morris W Hirsch. Differential topology, volume 33 of graduate texts in mathematics, 1994.
- [22] Josephus Hulshof and Robertus van der Vorst. Asymptotic behaviour of ground states. *Proceedings of the American Mathematical Society*, 124(8):2423–2431, 1996.
- [23] Jonathan Jaquette and Miroslav Kramar. On  $\epsilon$  approximations of persistence diagrams. *Mathematics of Computation*, TO APPEAR, 2016.
- [24] Tomasz Kaczynski, Konstantin Mischaikow, and Marian Mrozek. *Computational Homology*. Springer, 2004.
- [25] Efthimios Kappos. The Conley index and global bifurcations. I. Concepts and theory. *International Journal of Bifurcation and Chaos*, Vol. 5(4):937–953, 1995.
- [26] John M Lee. *Smooth manifolds*. Springer, 2003.
- [27] William S Massey. *A basic course in algebraic topology*, volume 127. Springer Science & Business Media, 1991.
- [28] John Willard Milnor. *Morse theory*. Princeton University Press, 1963.
- [29] Konstantin Mischaikow and Marian Mrozek. Conley index. *Handbook of dynamical systems*, 2:393–460, 2002.
- [30] Nedialko S Nedialkov and Kenneth R Jackson. *The design and implementation of an object-oriented validated ODE solver*. Kluwer Academic Publishers, 2002.
- [31] Helmut Ratschek and Jon Rokne. *Geometric Computations with Interval and New Robust Methods: Applications in Computer Graphics, GIS and Computational Geometry*. Harwood Publishing, 2003.

- [32] S.M. Rump. INTLAB - INTerval LABoratory. In Tibor Csendes, editor, *Developments in Reliable Computing*, pages 77–104. Kluwer Academic Publishers, Dordrecht, 1999. <http://www.ti3.tuhh.de/rump/>.
- [33] Sarah Day and William D. Kalies and Thomas Wanner. Verified homology computations for nodal domains. *SIAM Journal on Multiscale Modeling & Simulation*, 7(4):1695–1726, 2009.
- [34] Arthur Sard et al. The measure of the critical values of differentiable maps. *Bull. Amer. Math. Soc*, 48(12):883–890, 1942.
- [35] Joel Smoller. *Shock Waves and Reaction-Diffusion Equations*. Springer-Verlag, New York, second edition, 1994.
- [36] Thomas Stephens and Thomas Wanner. Rigorous validation of isolating blocks for flows and their Conley indices. *SIAM Journal on Applied Dynamical Systems*, 13(4):pp. 1847–1878, 2014.
- [37] Victor A Toponogov. *Differential geometry of curves and surfaces*. Springer, 2006.
- [38] Thomas Wanner. Topological analysis of the diblock copolymer equation. In Yasumasa Nishiura and Motoko Kotani, editors, *Mathematical Challenges in a New Phase of Materials Science*. Springer Proceedings in Mathematics and Statistics, 2016.

## Curriculum Vitae

Thomas Stephens usually measures five feet and ten inches tall. He is the grateful possessor of two eyes, one nose, and a mouth. Thomas spent many years believing that the doctoral degree in Mathematics would come with a free guide to The Knowledge of the Universe, and has recently found out that this is not the case. Nevertheless, he will presently finish this biography of himself, and step out into the world with an invigorated appreciation for all things to which mathematics does not pertain – but especially for those things to which mathematics *does* pertain.